IEEE Access
Multidisciplinary | Rapid Review | Open Access Journal

Received June 16, 2021, accepted June 27, 2021, date of publication July 7, 2021, date of current version July 21, 2021.

Digital Object Identifier 10.1109/ACCESS.2021.3095346

A Tutorial on 3GPP Initial Cell Search: Exploring a Potential for Intelligence Based Cell Search

SEUNGHWAN WON[1], (Senior Member, IEEE), AND SANG WON CHOI[2], (Member, IEEE)
[1]Department of Electrical and Electronic Engineering, University of Southampton Malaysia (UoSM), Iskandar Puteri, Johor 79200, Malaysia
[2]Department of Electronic Engineering, Kyonggi University, Suwon-si, Gyeonggi-do 13557, Republic of Korea

Corresponding author: Sang Won Choi (swchoi20@kyonggi.ac.kr)

This work was supported by Institute of Information & communications Technology Planning & Evaluation (IITP) grant funded by the Korea government (Ministry of Science and ICT, MSIT) (No. 2021-0-01024, Standard technology development and its international standardization for mission-critical smart mobility services based on 5G+) as well as partly by a grant from R&D program of the Fundamental Research Grant Scheme funded by Malaysia's Ministry of Higher Education (FRGS/1/2015/TK04/USMC/02/2).

ABSTRACT This tutorial guides the reader through the open literature on the aspect of Initial Cell Search (ICS) in both Code Division Multiple Access (CDMA) and Orthogonal Frequency Division Multiple Access (OFDMA) systems perspectives with a special focus on the DownLink (DL), where the ICS represents the very first operational stage of commercial mobile station modem's always-on mobility. There is no comprehensive up-to-date tutorial of the ICSs encompassing 3G, 4G, and 5G systems. Hence, we review the ICS-related operations which have been proposed for Wideband CDMA (W-CDMA), Time Division-Synchronous CDMA (TD-SCDMA), Long Term Evolution Frequency Division Duplex (LTE-FDD), and Time Division LTE (TD-LTE) from the point of view of 3rd Generation Partnership Project (3GPP) standard and implementation. In the case of TD-SCDMA, there is no in-depth literature illustrating the details of ICS. Therefore, this tutorial aims to fill the related gap in the literature. As an evolution from the operational systems, we also shed light on the ICS being employed in New Radio (NR) system operating at sub-6 GHz and provide insight into interesting and challenging technical issues in millimeter-Wave spectrum bands, which is an ultimate foundation to be deployed in the full-scale NR system. Furthermore, we exemplify entire cell search operations over diverse spectrum bands and elucidate intelligent ways of designing multi-mode mobile station modem in a systematic manner. A taxonomy diagram also classifies three main targets constituting ICS procedures in 3G, 4G, and 5G systems. It is expected that this tutorial is beneficial not only for academic researchers but also for practical modem development engineers.

INDEX TERMS Initial cell search, LTE-FDD, multi-mode mobile station modem, new radio, Millimeter-wave, synchronization, TD-LTE, TD-SCDMA, W-CDMA.

I. INTRODUCTION

Code Division Multiple Access (CDMA) based mobile communication systems and their evolutions have been widely advocated by the 3rd Generation Partnership Project (3GPP). Consequently, the progress of CDMA has led to the 3G systems [1], [2], namely the Wideband CDMA (W-CDMA) [1] and the Time Division Synchronous CDMA (TD-SCDMA) [2] operating models. Then, the Orthogonal Frequency Division Multiplexing Access (OFDMA) based Long Term Evolution (LTE) and their derivatives have been specified by 3GPP for the 4G systems [3]. Nowadays, 5G systems, referred to as New Radio (NR), have been released under the auspices of the 3GPP standardization activities [4]–[8]. In the above-mentioned 3G, 4G, and 5G systems, the very first operational stage of mobile communication systems is an Initial Cell Search (ICS) procedure, initiated by the User Equipment (UE)[1] in order to achieve both the appropriate time and frequency synchronizations as well as to detect a particular cell ID.

For structural understanding on Initial Access (IA),[2] a top-down architecture of this tutorial is visualized in Fig. 1,

The associate editor coordinating the review of this manuscript and approving it for publication was Derek Abbott.

[1]In 3GPP terminology, UE is equivalent to mobile station.

[2]In addition, we also would like to direct the attention of those readers, who wish to delve into further detail, to some excellent tutorial papers such as [10]–[14] amongst others.

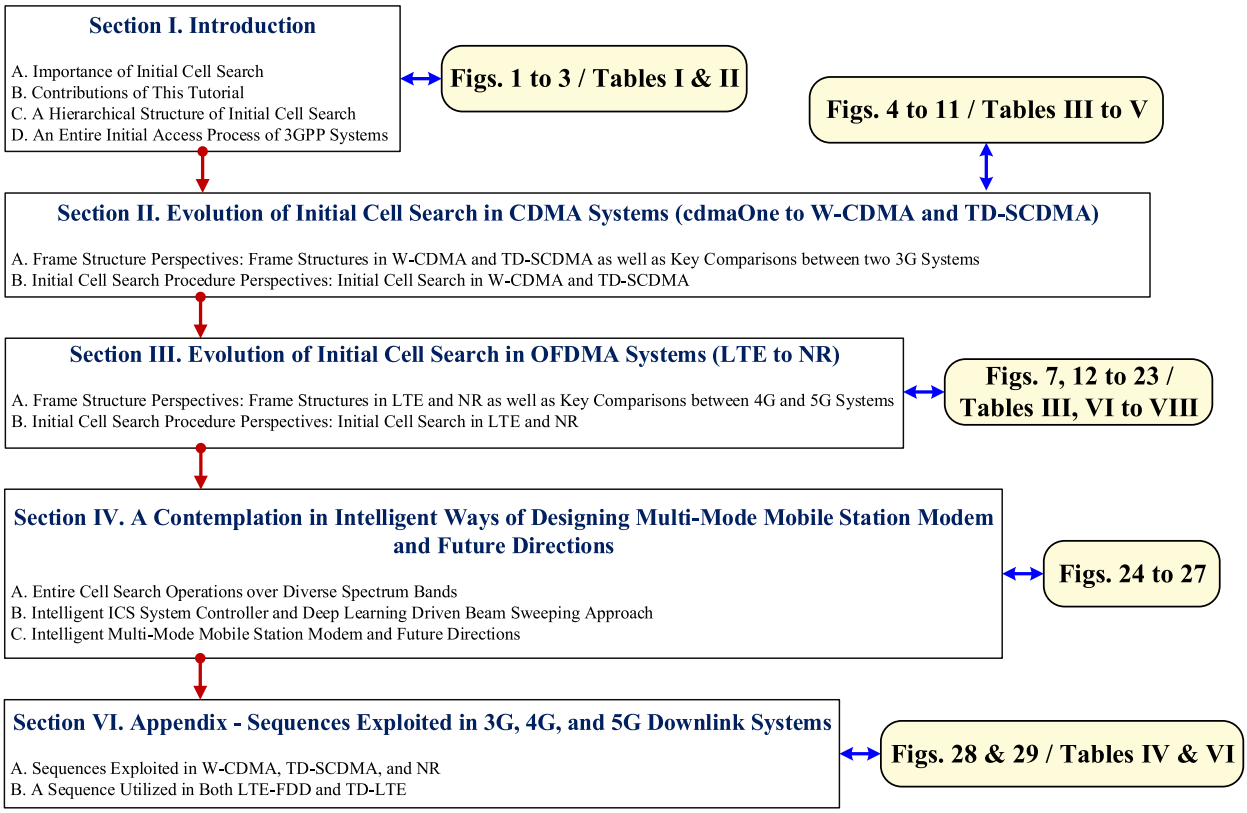

FIGURE 1. Overall structure of this tutorial manifesting key topics associated with the corresponding figures and tables.

where the structure indicates IAs of two representative systems adopted in 3GPP standardization as well as all the relevant figures and tables are manifested together.

Fig. 2 specifies a hierarchical structure of cell search and an entire IA process of 3GPP systems in both DownLink (DL) and UpLink (UL), aligned with the philosophy articulated through 3GPP target cell search [9]. More explicitly, the IA procedure in DL constitutes both ICS and the following cell selection as well as system information reception, where ICS represents a specific cell search procedure operating at physical layer level. In the forthcoming Sections II and III, full details of ICS scenarios are portrayed in 3G (CDMA systems) as well as 4G and 5G (OFDMA systems), respectively. Specifically, the ICS stages of 3G/4G/5G mobile communication systems are (1) to acquire coarse correct timing of a reference path among the incoming multi-path signals received in the DL, (2) to carry out the initial frequency offset compensation based on the path chosen in (1), and finally derive a serving cell ID before commencing normal communication procedures. Hence, the ICS procedure in the DL is the very first operation of commercial mobile station modem's always-on mobility that has to be performed, as soon as the UE is turned on. To illustrate it a little bit further, the ICS operation is conducted by processing an unmodulated and predefined pilot signal or preamble being transmitted periodically, which is broadcast over the entire cell. There are two main issues constituting (1) very wide uncertainty region in the DL, for example which may correspond to an entire radio-frame duration and (2) high initial frequency offset substantially deviated from an exact carrier frequency locked on. Those two main factors lead to two-dimensional enormous search space of the ICS procedure. In order for us to lead explicit presentation, Fig. 3 visualizes three groups (Figs. 7 & 12, Figs. 8, 10, & 13, and Figs. 9, 11, 21, 22, & 23) to categorize a hierarchical structure of entire ICS flow and a taxonomy diagram to classify three major operations, namely (1) Timing synchronization, (2) Frequency synchronization, and (3) Code/Cell identification, which form pivotal ICS procedures in 3G, 4G, and 5G systems. It is noted that subframe in TD-SCDMA, half radio-frame in LTE, and SS burst set in NR are set to 5 ms. However, each mode has a completely different terminology to express the same time period. Accordingly, in our taxonomy diagram, three terminologies are exploited separately to comply with 3GPP's convention. Further details of all mentioned in the taxonomy diagram will be elucidated in Sections II and III.

For the sake of minimizing the entire cell search complexities, hierarchical cell search procedures have been proposed and adopted in all the systems mentioned in [4], [7], [8], [15]–[19]. After ICS, which is invoked for the initial synchronization with a potential serving cell, the Target Cell Search (TCS) is used for finding adjacent cells required for

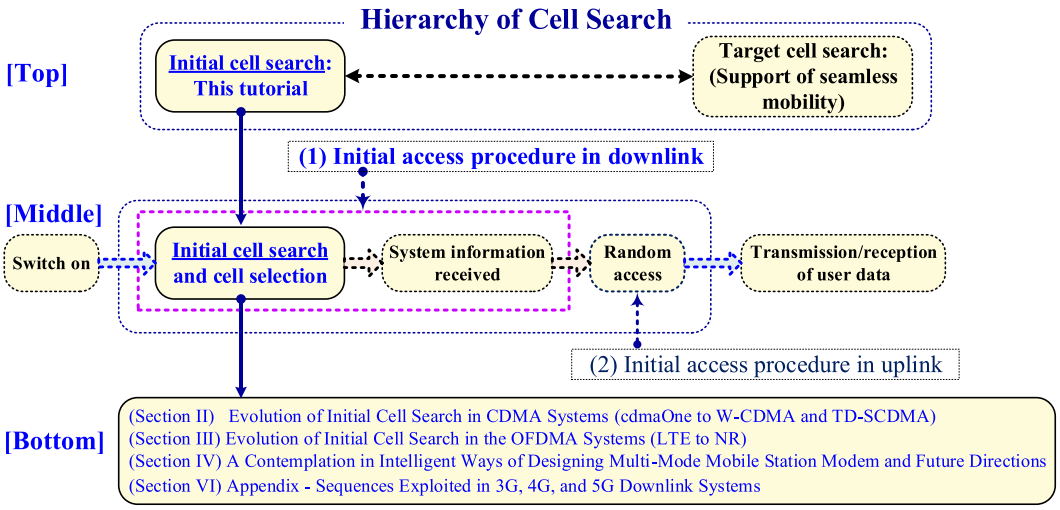

FIGURE 2. Hierarchical structure of cell search and the corresponding entire initial access process of 3GPP systems in both downlink and uplink.

potential handovers [9], [20]. This tutorial paper focuses mainly on the ICS in the idle mode UE, which is operated in 3G, 4G, and 5G systems.[3] Even though substantial research efforts have been devoted to concrete detection schemes exploited for ICS algorithms at each stage of the entire ICS flow [10], [17], [18], [21]–[25], there is a paucity of in-depth studies in the open literature providing a review of all the ICS procedures and scenarios employed in practical mobile station modems satisfying 3GPP specifications for 3G, 4G, and 5G systems, which is also very beneficial for readers to review the existing standards in a systematic manner and to gain an insightful view on the future communication systems. Table 1 depicts an overall investigation of cell searches for 3G, 4G, and 5G through two decades.

Main contribution of this tutorial is to provide essential guidelines for understanding IA by clarifying two decades of a journey for ICS through 3G, 4G, and 5G. Specifically, by contemplating not only fundamental principles for beginners but also essential implementation factors for practical modem engineers, we elaborate key issues for comprehending the underlying principles of the ICS. One aspect is details of the radio-frame structure including the basic understanding of diverse sequences and their key properties, which is described in Appendix. Another aspect is associated with the ICS procedure itself in the time- and frequency domains. In each step of the ICS procedure, role of the step is demystified and then how the entire ICS procedure flows are also visualized through 3G, 4G, and 5G in terms of the time and frequency-domain approaches. Accordingly, we shed light on how the ICS works in the sense of the theoretic view, which can be beneficial for beginners in this area. Secondly, we devote our passion to shedding light on the aspects of modem implementation especially for practical modem engineers. For stable and reliable operation of the ICS, we introduce main challenging technical issues to be considered with feasible approaches encompassing new beam operation in ICS, which is more useful especially at millimeter-Wave (mmW) spectrum bands in NR [4]–[7], [19]. Lastly, with the aid of Fig. 24, we introduce a sketch of entire cell search operations over diverse spectrum bands for beyond 5G communication systems. Conceptual diagrams of both intelligent ICS system controller and deep learning driven beam sweeping approach are also demystified by Figs. 25 and 26, respectively. Moreover, a macroscopic view on intelligent multi-mode mobile station modem and future directions are illustrated based on Fig. 27.

This tutorial is organized as follows: We enlighten the evolution of IA in the CDMA systems by portraying the ICS operations of the W-CDMA and the TD-SCDMA systems in Section II. In Section III, as another evolution of IA during the two decades, we consider the progress of IA by virtue of ICS operations of the LTE and the NR systems. A contemplation in intelligent ways of designing multi-mode mobile station modem and future directions is elucidated in Section IV. Throughout Sections II, III, and IV, for enhancing the understanding of IA and its evolution in CDMA and OFDMA systems, we look into the IA in the perspectives of radio-frame structures and the corresponding ICS procedures in conjunction with major technical issues, which are inevitably confronted for commercial mobile station modem implementation. Our conclusions are provided in Section V with Appendix summarizing the main characteristics of the synchronization sequences employed in W-CDMA, TD-SCDMA, LTE, and NR [28]–[35]. Table 2 provides a complete list of acronyms employed for the tutorial.

[3]Radio resource control protocol constitutes idle and connected modes [9].

TABLE 1. A concise comparison of our study with the existing relevant papers.

Relevant Paper	Year	Key Topic	Main Issues Addressed
Wang *et al.* [21]	2000	Cell search in W-CDMA	ICS procedures of W-CMDA system have been discussed with some simulation results.
Tsai *et al.* [11]	2007	Cell search in LTE	ICS procedures of LTE like system have been discussed at preliminary stage of LTE standardization.
Won *et al.* [12]	2009	Initial and post-initial code acquisition	Both initial and post-initial acquisition schemes in the Multiple-Input Multiple-Output (MIMO)-aided direct-sequence CDMA DL system have been analyzed.
Won *et al.* [10]	2012	Initial synchronization of direct sequence systems	Initial synchronization in MIMO and cooperative-aided single- and multi-carrier CDMA as well as direct sequence-ultra wideband DL systems has been tutorialed.
Won *et al.* [13]	2012	Synchronization of noncoherent MIMO systems	Initial synchronization of noncoherent MIMO DL systems with the aid of information-theoretic features has been guided.
Shen *et al.* [20]	2012	Neighboring cell search	A general framework for neighboring cell search in LTE systems has been established to derive sufficient signal metrics under various channel conditions and propose cell search algorithms based on it.
Won *et al.* [14]	2014	Synchronization issues in relay-aided cooperative MIMO networks	Initial synchronization of multihop relay-aided cooperative noncoherent MIMO DL systems experiencing multi-path fading channels has been characterized.
Soleimani *et al.* [26]	2019	IA for mmW 5G systems with hybrid beamforming	A particular online method to gain directions of arrival statistics has been proposed to reduce the average IA time at mmW aided 5G systems.
Omri *et al.* [27]	2019	Synchronization procedure in 5G NR systems	ICS procedure and some challenges in 5G NR systems have been analyzed.
Won *et al.* [9]	2020	Three decades of 3GPP TCS through 3G, 4G, and 5G	All the TCS procedures of W-CDMA, TD-SCDMA, LTE-FDD, TD-LTE, and NR operating particularly at mmW spectrum bands have been detailed in a comprehensive manner.
This tutorial	2021	ICS procedures of standardized 3G, 4G, and 5G DL systems	Full details of ICS procedures of W-CDMA, TD-SCDMA, Long Term Evolution Frequency Division Duplex (LTE-FDD), Time Division LTE (TD-LTE), and NR operating at both sub-6 GHz and mmW spectrum bands are tutorialed in a consistent manner.

TABLE 2. List of essential acronyms.

Acronym	Definition	Acronym	Definition
3GPP	3rd Generation Partnership Project	PCI	Physical-layer Cell-Identity
CDMA	Code Division Multiple Access	P-CCPCH	Primary Common Control Physical CHannel
CP	Cyclic Prefix	P-CPICH	Primary Common PIlot CHannel
DC	Direct Current	PDSCH	Physical Downlink Shared CHannel
DL	DownLink	PLMN	Public Land Mobile Network
DMRS	DeModulation Reference Signal	$\text{PSC}^{(1)}$	Primary Scrambling Code
DwPTS	Downlink Pilot Time Slot	$\text{PSC}^{(2)}$	Primary Synchronization Code
EDGE	Enhanced Data rates for GSM Evolution	P-SCH	Primary Synchronization CHannel
FFT	Fast Fourier Transform	PSS	Primary Synchronization Signal
FR	Frequency Range	RAT	Radio Access Technology
GP	Guard Period	RB	Resource Block
GPRS	General Packet Radio Service	RE	Resource Element
GSM	Global System for Mobile communications	RI	Root Index
IA	Initial Access	RRC	Radio Resource Control
ICS	Initial Cell Search	RS	Reference Signal
LAA	Licensed Assisted Access	SIB	System Information Block
LTE	Long Term Evolution	SS	Synchronization Signal
LTE-FDD	LTE Frequency Division Duplex	SSC	Secondary Synchronization Code
LTE-U	LTE Unlicensed	S-SCH	Secondary Synchronization CHannel
MIB	Master Information Block	SSS	Secondary Synchronization Signal
MIMO	Multiple-Input Multiple-Output	TCS	Target Cell Search
mmW	millimeter-Wave	TD-LTE	Time Division LTE
NPBCH	New radio Physical Broadcast CHannel	TD-SCDMA	Time Division Synchronous CDMA
NPSS	New radio Primary Synchronization Signal	TS	Time Slot
NR	New Radio	UE	User Equipment
NSSS	New radio Secondary Synchronization Signal	UL	UpLink
OFDM	Orthogonal Frequency Division Multiplexing	UpPTS	Uplink Pilot Time Slot
OFDMA	Orthogonal Frequency Division Multiple Access	USIM	Universal Subscriber Identity Module
OVSF	Orthogonal Variable Spreading Factor	W-CDMA	Wideband CDMA
PBCH	Physical Broadcast CHannel	ZC	Zadoff-Chu

II. EVOLUTION OF INITIAL CELL SEARCH IN THE CDMA Systems (cdmaOne TO W-CDMA AND TD-SCDMA)

In this Section, based on Figs. 1, 2, and 3 as well as the corresponding cell search's hierarchical structure and detailed taxonomy classification articulating three major targets of ICS scenarios in W-CDMA and TD-SCDMA systems, we present the detailed physical channel structures used in the ICS scenarios of two 3G CDMA systems, followed

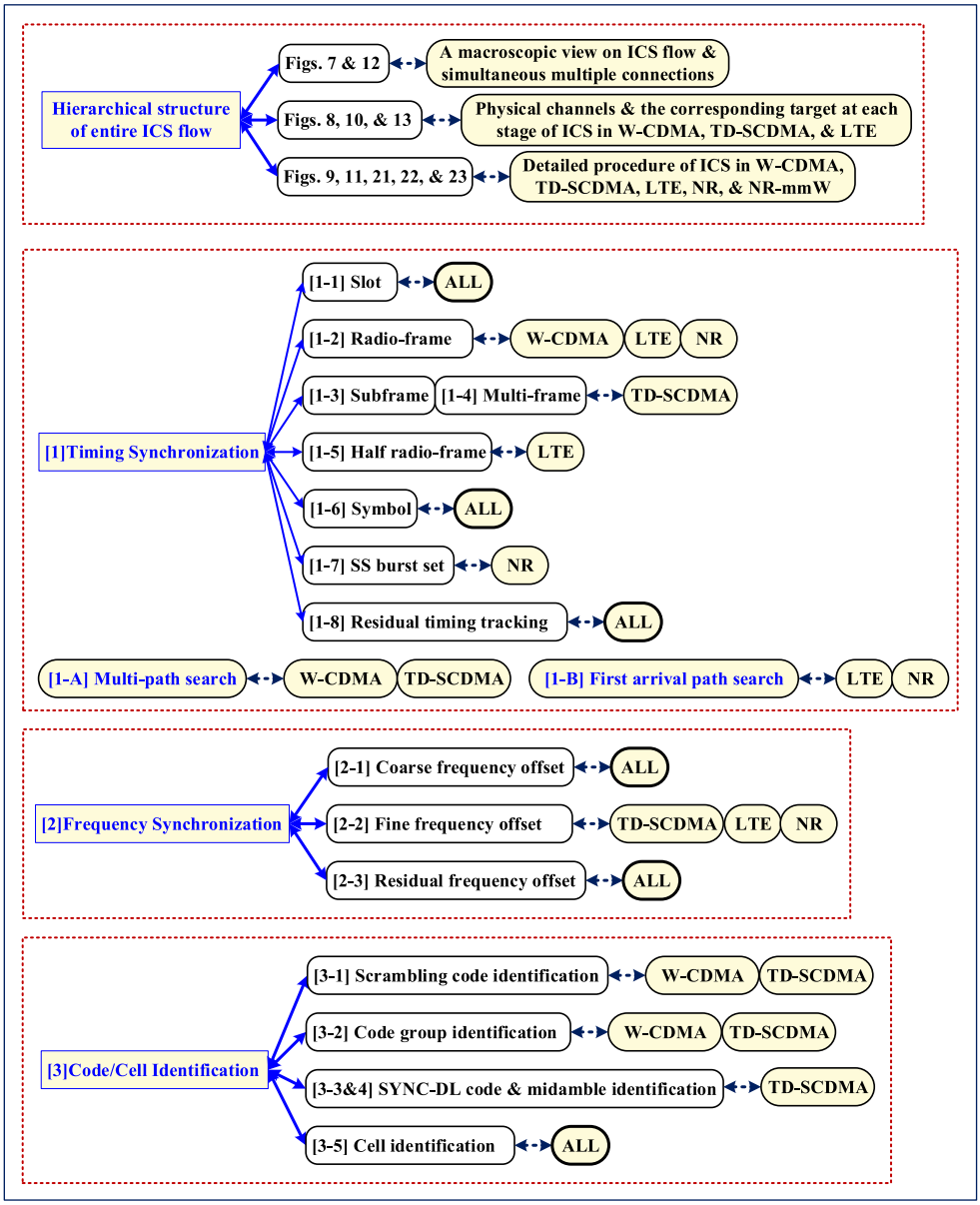

FIGURE 3. Hierarchical structure of entire initial cell search flow with the corresponding figures and taxonomy of three main operations constituting initial cell search procedures in 3G, 4G, and 5G systems.

by detailed feature comparisons. Then, full details of the ICS scenarios are illustrated, which are further visualized in Figs. 4 to 11 and portrayed in Tables 3 to 5.

A. RADIO-FRAME STRUCTURE PERSPECTIVE

1) KEY COMPARISONS BETWEEN TWO 3G SYSTEMS

For the sake of clarifying main features of two 3G systems, we provide a digest of W-CDMA and TD-SCDMA with specific emphasis given on the transmitted signals' structures, which determines two 3G systems' ICS and TCS design philosophies. More explicitly, the upper part of Fig. 4 visualizes the power spectra of the time- and frequency-domains' signal waveforms related to (1) OFDMA (LTE), (2) cdmaOne (Interim Standard-95), (3) TD-SCDMA, and (4) W-CDMA DL [1], [2], [13]. Let us focus on three CDMA families. The first commercial CDMA system referred to as cdmaOne (a.k.a. Interim Standard-95) became a 2G mobile telecommunications standard leveraging characteristics of basic CDMA principles, where only PN code having a fixed code length has been exploited [29], [36]. When contemplating time-domain comparisons for those three cases, cdmaOne has a longer chip duration of 1000.0 ns, while two 3GPP siblings manifest relatively shorter chip durations. More explicitly, chip durations of W-CDMA and TD-SCDMA are set to 260.4 ns and 781.25 ns, respectively, where the latter has three times longer than that of W-CDMA counterpart. It is noted that the chip duration of each CDMA system is inversely propor-

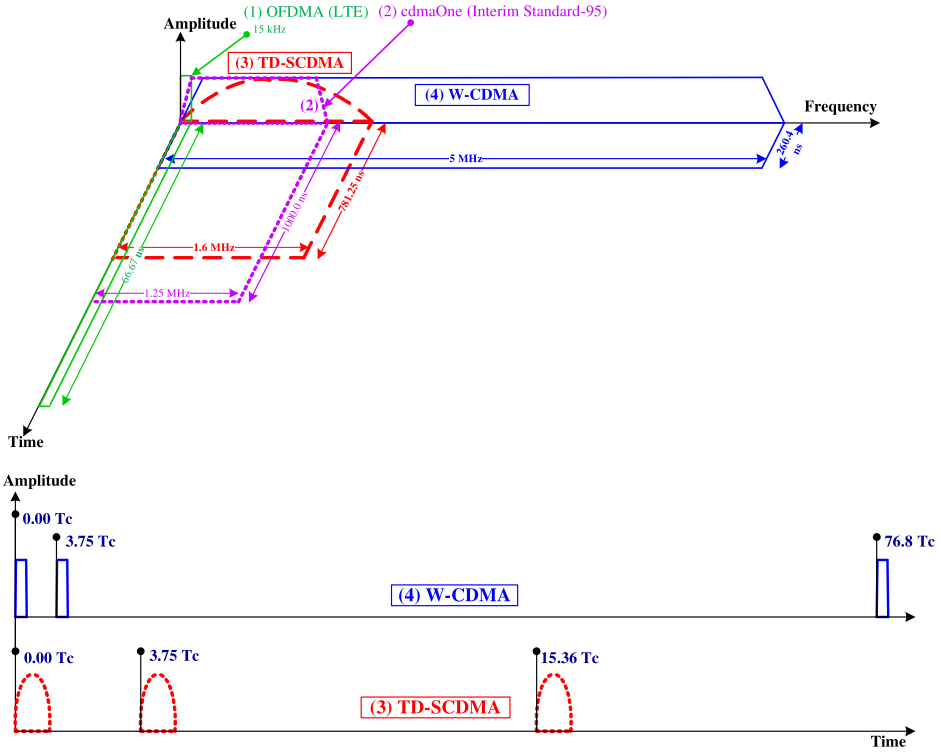

FIGURE 4. Power spectra of signal waveforms in the time- and frequency-domains associated with (1) OFDMA (LTE), (2) cdmaOne (Interim Standard-95), (3) TD-SCDMA, and (4) W-CDMA DL as well as an exemplification of multi-path channel comparison of W-CDMA and TD-SCDMA.

tional to the bandwidth allocated. Accordingly, a bandwidth of cdmaOne occupies relatively narrower channel bandwidth of 1.25 MHz. Those of W-CDMA and TD-SCDMA occupy 5 MHz and 1.6 MHz, respectively. Furthermore, an optional mode of TD-SCDMA is capable of supporting three-carrier transmission by employing three separate channel bandwidths in frequency-domain, which can be a realization of multi-carrier direct sequence CDMA.

On the other hand, an evolution of cdmaOne to W-CDMA illustrates an exemplification of a single carrier direct sequence CDMA having wider channel bandwidth. Then, the lower part of Fig. 4 portrays how a multi-path fading channel model of W-CDMA is different from the corresponding counterpart of TD-SCDMA. To illustrate it a little bit further, the multi-path fading channel model has been designed for testing the receiver under very high multi-path delay spread environments. Such a scenario is referred to as an extreme case being very infrequently encountered in real situation. However, the model can be exploited for testing the receiver performances under worst-case scenarios. Also, it elucidates that three paths having equal power gain are scattered over a predefined chip duration in time-domain [37]–[39]. Specifically, a case of W-CDMA has the third path positioned at 76.8 chip durations leading to substantial receiver performance degradation owing to its extremely wide multi-path span. Similarly, that of TD-SCDMA also has the third path located at 15.36 chip durations. However, its multi-path span is relatively shorter than that of W-CDMA. Accordingly, the multi-path channels' scatteredness of W-CDMA having shorter chip duration and wider bandwidth is predominant over that of TD-SCDMA. It is also noted that three times higher time-domain resolution of W-CDMA leads to more richness of the multi-paths having diverse delay spreads. Based on the aforementioned, ICS issues of all the CDMA families put much emphasis on the timing synchronization portrayed in Fig. 3. On the other hand, owing to the existence of inherently embedded cyclic prefix per symbol as exemplified in Figs. 14 and 15, the timing synchronization induced issues of all the OFDMA families are relatively easier than the CDMA counterparts. Instead, in order to guarantee the strict orthogonal multiplexing in frequency domain, ICS issues of all the OFDMA families focus their attention on the frequency synchronization visualized in Fig. 3.

2) FRAME STRUCTURE IN W-CDMA

Fig. 5 illustrates four physical channel structures of W-CDMA DL systems employed for ICS procedure scenario, namely Primary Synchronization CHannel (P-SCH), Secondary Synchronization CHannel (S-SCH), Primary Common Pilot CHannel (P-CPICH), and Primary Common Control Physical CHannel (P-CCPCH) [1], [21], [22]. Both P-SCH and S-SCH are referred to as synchronization channels, which are transmitted simultaneously. For the sake of identifying cells in W-CDMA DL systems, 512 Primary Scrambling Codes ($PSCs^{(1)}$) are generated based on truncated ($2^{18} - 1$) Gold sequences, which fit to a single

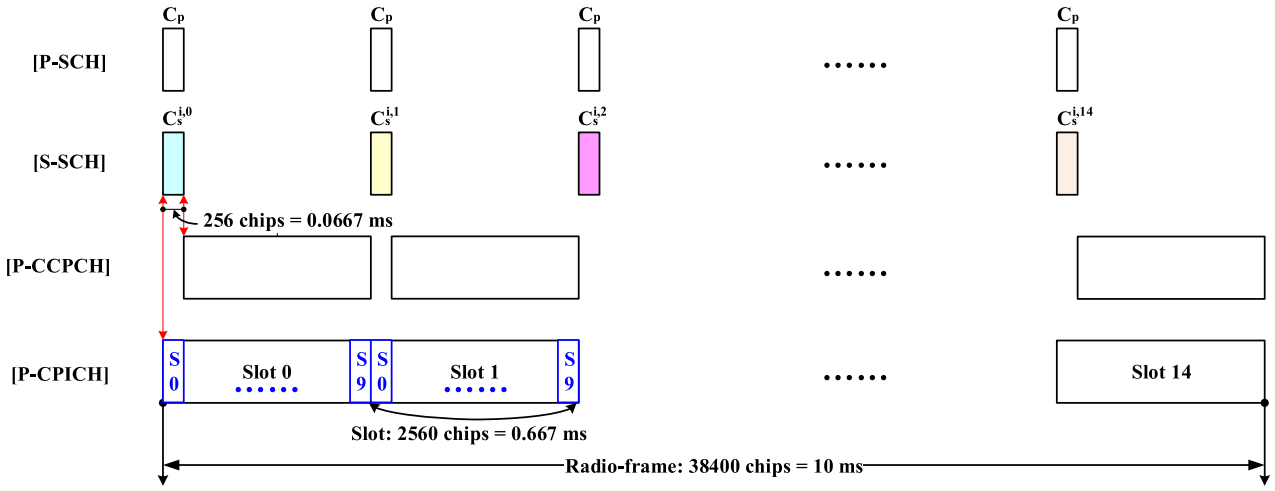

FIGURE 5. Radio-frame structure used in cell search scenarios of W-CDMA DL.

radio-frame period constituting 38400 chips for the chip rate of 3.84 Mchips per sec. These codes are partitioned into 64 groups having eight PSCs$^{(1)}$ in each group to enhance the performance of hierarchical cell search. A specific PSC$^{(1)}$ is assigned to an individual cell as well as exploited to scramble both P-CCPCH and P-CPICH. Fig. 5 visualizes the slot and radio-frame formats of these physical channels. Each radio-frame of 38400 chips (equivalent to 10 ms) is partitioned into 15 slots, which of each constitutes 2560 chips (equal to 0.667 ms). It is noted that both P-SCH and S-SCH have only a 10 percentage duty cycle. To elaborate it a little bit further, the synchronization channel is only transmitted during the first symbol (equivalent to 256 chips) of each slot. Hence, during the remaining portion of each slot the P-CCPCH is transmitted, where the P-CCPCH is a fixed rated DL physical channels having a spreading factor of 256 exploited to carry cell specific information.

P-CPICH is also a fixed rated DL physical channel having a spreading factor of 256 to carry a predefined bit pattern. Each slot of the P-CPICH constitutes ten pilot symbols, where each symbol is spread by a particular spreading code of all ones having a length of 256 chips and the pilot symbols are scrambled by a specific PSC$^{(1)}$ dedicated to each cell. As illustrated in Fig. 5, ($S0$,...,$S9$) represent the ten symbols constituting each slot. A particular spreading sequence of the P-CPICH is chosen from the set of Orthogonal Variable Spreading Factor (OVSF) codes,[4] maintaining mutual orthogonality among the P-CPICH and the other DL physical channels spread by diverse OVSF codes. All symbols are also modulated by Quadrature Phase Shift Keying and the bit pattern of the pilot symbols is recognized after the radio-frame boundary is detected [1], [21], [22], [40]. It is worth noting that neither the P-SCH nor S-SCH is scrambled by any PSC$^{(1)}$. Rather than using the OVSF codes, the P-SCH constitutes the Primary Synchronization Code (PSC$^{(2)}$) having a length 256 chips transmitted during the first symbol of every slot. As portrayed in Fig. 5, the PSC$^{(2)}$ C_p of P-SCH is common to all the existing cells in the W-CDMA systems and exploited to select the slot boundary of the most appropriate cell. The PSC$^{(2)}$ is referred to as a generalized Golay sequence and has good aperiodic autocorrelation property [40], [41]. The S-SCH consists of 15 Secondary Synchronization Codes (SSCs) having a length 256 chips also transmitted during the first symbol of every slot. The 15 SSCs are repeatedly transmitted every radio-frame to designate one of 64 scrambling code groups and also to determine the start point of each radio-frame together. Individual SSC $C_s^{i,j}$ is selected from a set of different 16 orthogonal codes, where $i = 0, \ldots, 63$ and $j = 0, \ldots, 14$ represent the group number of PSCs$^{(1)}$ and the slot number, respectively. The S-SCH sequence is generated by employing a cyclically permutable code. The code is a set of codewords such that each codeword is non-cyclic shift of another and a particular codeword has distinct cyclic shift within a specific period, which may be selected as a subset of M-ary Reed-Solomon (n, k) codes, where n is set to the number of slots in a radio-frame. $M^{(k-1)}$ cyclically permutable codewords exist in the M-ary (n, k) Reed-Solomon codes. Specifically, in case of W-CDMA DL systems, 64 S-SCH sequences are chosen from (15, 3) Reed-Solomon codes and the sequences are represented as ($C_s^{i,0}$,...,$C_s^{i,14}$) as illustrated in Fig. 5 [21], [22], [40]. It is also noted that the SSC is mutually orthogonal to the PSC$^{(2)}$ as well as both PSC$^{(2)}$ and SSC are transmitted in parallel as visualized in Fig. 5. For further details of the sequences exploited in W-CDMA, refer to Appendix.

3) RADIO-FRAME STRUCTURE IN TD-SCDMA

Fig. 6 visualizes a hierarchical radio-frame structure of TD-SCDMA DL systems, exploited for all the cell search scenarios. Here, minimum frequency bandwidth required is set to 1.6 MHz and its corresponding chip duration is 781.25 ns, which is three times longer than W-CDMA chip duration.

[4]For a definition of the OVSF codes, refer to Appendix.

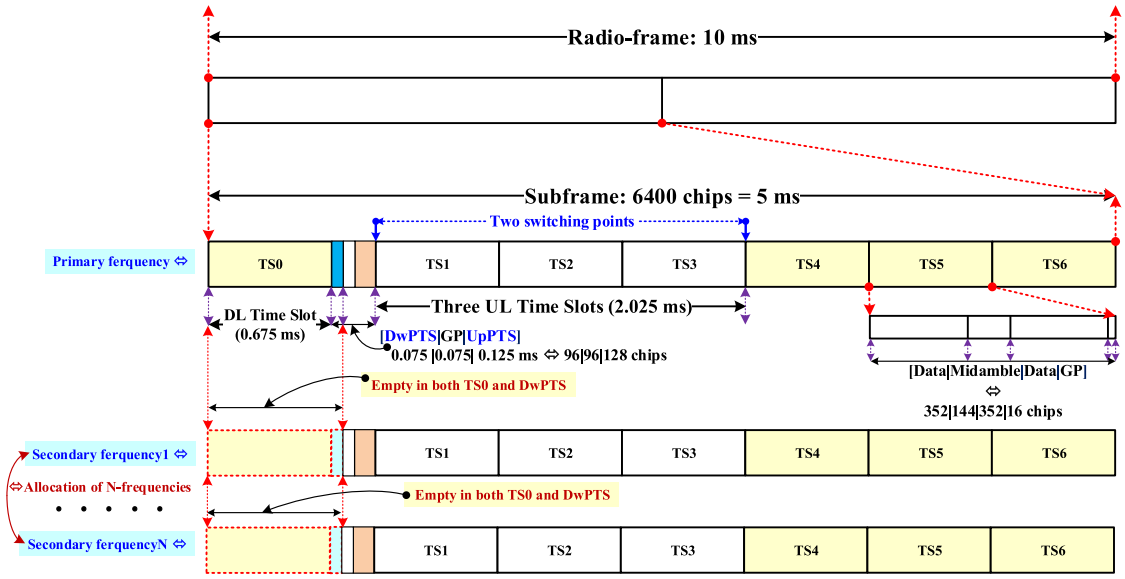

FIGURE 6. Radio-frame structure exploited in cell search scenarios of TD-SCDMA DL, where [DwPTS|GP|UpPTS] corresponds to three special time slots and [Data|Midamble|Data|GP] represents all the components of each time slot.

A radio-frame comprises two subframes, equivalent to 10 ms. A single subframe period having $T_{sf} = 6400$ chips for the chip rate 1.28 M chips per sec comprises seven time slots and three special time slots, which corresponds to 5 ms. More explicitly, as portrayed in Fig. 6, each of the time slots has a length $T_{slot} = 864$ chip duration, equivalent to 0.675 ms and three special time slots known as Downlink Pilot Time Slot (DwPTS), Guard Period (GP), and Uplink Pilot Time Slot (UpPTS) correspond to 96, 96, and 160 chips, respectively. These three chip durations also correspond to 0.075, 0.075, and 0.125 ms, respectively. Furthermore, each time slot consists of two data symbol fields of having 352 chips each, a midamble of 144 chips. The midamble of 144 chips is structured from one out of 128 basic midamble sequences having a length of 128 chips each, generated based on m-sequences, where the GP of 16 chips has been determined to avoid multi-path induced interferences [43]. It is noted that the UL-DL configurations having 5 ms DL-to-UL switch-point periodicity is exploited in TD-SCDMA as shown in Fig. 6. Specifically, if the switch time is set to 5 ms, there are two switching points per subframe. The first time slot denoted as Time Slot0 (TS0) and DwPTS are always reserved for DL transmission. Similarly, UpPTS and the time slot immediately following UpPTS such as time slot 1 are also reserved for UL transmission. For the sake of performing all the possible cell searches, we are interested in two physical channels in TS0, namely two P-CCPCHs and DwPTS exploited in TD-SCDMA, where the location of two P-CCPCHs is fixed in the TS0 and the first two code channels having a spreading factor of 16 are always assigned to these two P-CCPCHs, respectively. Here, a physical channel is allocated and transmitted in a specific time slot of TD-SCDMA. Each physical channel also constitutes two data symbol fields, a midamble, and a GP. Several channels can be transmitted simultaneously from one transmitter. Therefore, the data symbol fields must exploit different OVSF channelization codes, however the same scrambling code is shared by all the channels. It is also worth noting that P-CCPCH has beacon characteristics to support a reference for all the possible measurement purposes.

DwPTS comprises a GP of 32 chips and SYNC-DL code of 64 chips which is one of 32 distinguishable SYNC-DL codes. Here, the SYNC-DL code is generated based on Gold-sequence, neither scrambled nor spread. The DwPTS is capable of distinguishing 32 code groups. It is also noted that the DwPTS is transmitted with a constant power level to cover an entire cell. A specific constant phase pattern is also contemplated in the SYNC-DL code for each subframe. The value of phase shift is one of 45, 135, 225, or 315 degrees. As another resource for the cell search, midambles assigned to active users in the same time slot of a single cell are generated by cyclic shifts of a single basic midamble code. The midambles are beneficial in a sense that channel impulse response can be estimated from it, which enhances the detection performance effectively through coherence detection. Given the midamble code index, according to the parameter K_{CELL}, up to K_{CELL} users can be allocated maximally. The k-th midamble sequence becomes the $(K_{CELL} - k)\cdot W$ shifted version of the original concatenated midamble sequence, where a set of $1 \leq k \leq K_{CELL}$ and W represents a predetermined shift value in which the channel impulse response is no longer than W chips. It is noted that the TS0 in each subframe has a fixed allocation of $K_{CELL} = 8$ and at least the first midamble shift should be allocated, which can be typically employed to estimate not only timing and frequency offsets but also multi-path positions. Among four different midamble

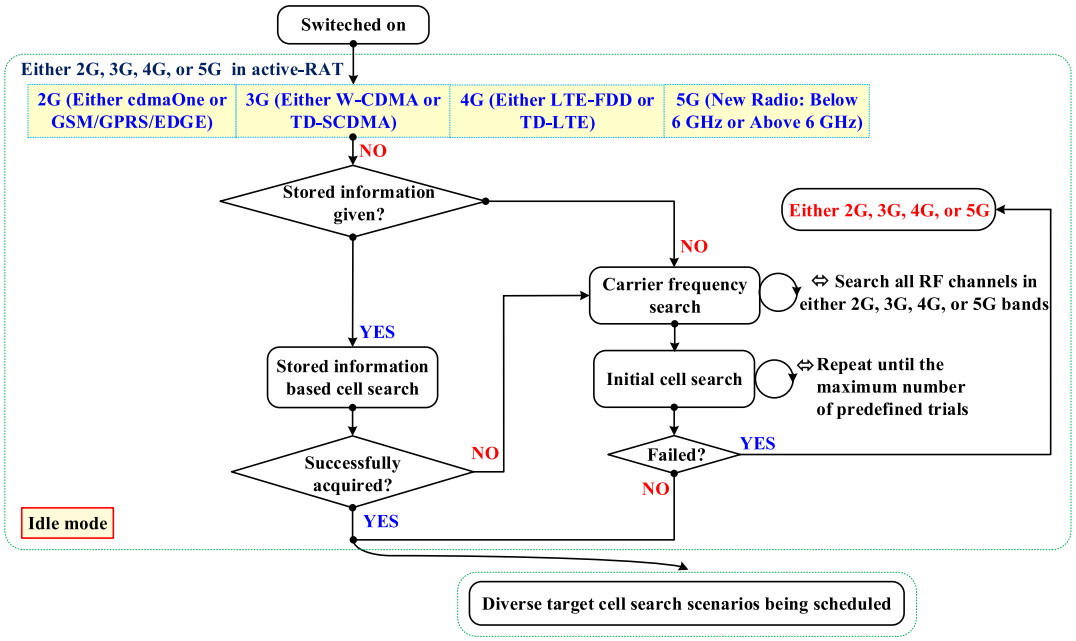

FIGURE 7. A macroscopic view on initial cell search flow used in 2G, 3G, 4G, or 5G systems.

allocation schemes, default midamble allocation is used for P-CCPCH, based on a fixed association between midambles and channelization codes [43]. An individual SYNC-DL code corresponds to a group of four distinct basic midamble codes, which is a part of 128 non-overlapping midamble codes ranging from 0 to 127. A basic midamble code is directly related to a corresponding scrambling code, which is one out of 128 codes ranging from 0 to 127 as elucidated in a table manifesting a distinct relationship among the SYNC-DL sequences, the scrambling codes and the midamble codes for each code group [41]. A scrambling code identifies a particular TD-SCDMA cell as in W-CDMA cell.

Up to now, the details of the TD-SCDMA radio-frame and channel structures have been illustrated in single frequency network. Now, let's introduce its generalization referred to as N-frequency network, which is the current commercial network deployed in China as a mandatory feature. In the N-frequency network, all the existing carriers in a single cell are identified by a single cell ID. When the cell is configured, only a single carrier is established as a primary frequency and the rest is considered as the secondary frequencies 1 to N as visualized in Fig. 6. All the existing carriers are also established based on the same midamble code ID and scrambling code ID. More explicitly, the midamble parts in different carriers have the same basic midamble code utilized in the primary frequency [43]. The N-frequency cell must have a unified UL and DL switching point among all the existing carriers. To illustrate it a little bit further, the switching point configuration on the secondary frequencies is exactly the same as that on the primary frequency. All the existing control channels such as P-CCPCHs are only established on the primary frequency as well as both TS0 and DwPTS on any secondary frequency are not assigned by the network. Accordingly, all the cell search operations are performed on the primary frequency under the current N-frequency configuration [43], [44]. For further details of the sequences employed in TD-SCDMA, refer to Appendix.

B. INITIAL CELL SEARCH PROCEDURE PERSPECTIVE

The ICS procedure constitutes initial timing recovery, initial frequency offset compensation, and finally cell ID detection. For W-CDMA and TD-SCDMA, there is some change in the cell identification in the sense that the hierarchical search for the cell ID is utilized. In case of the timing recovery, the adoption of matched filter leveraging the correlation characteristics of predefined synchronization sequences has been considered for the first step of ICS procedures. For the frequency offset estimation, there exists a remarkable difference between W-CDMA and TD-SCDMA owing to the distinguishing sequence transmission. More specifically, as illustrated in Fig. 5, the employment of continuous P-CPICH transmission in W-CDMA is capable of simplifying the frequency offset compensation, which is very similar to that of cdmaOne [29], [36]. Hence, a simple one-shot frequency offset estimator is sufficient in realistic mobile environments. On the other hand, Fig. 6 highlights sparseness of periodic synchronization preambles' transmission in TD-SCDMA. The feature makes multi-step aided approach only guarantee reliable target performances. Fig. 7 manifests a macroscopic view on ICS flow exploited in active-radio access technology mode of 2G, 3G, 4G, or 5G systems, where 2G system usually consists of cdmaOne, Global System for Mobile communications (GSM)/General Packet Radio Service (GPRS)/Enhanced Data rates for GSM Evolution

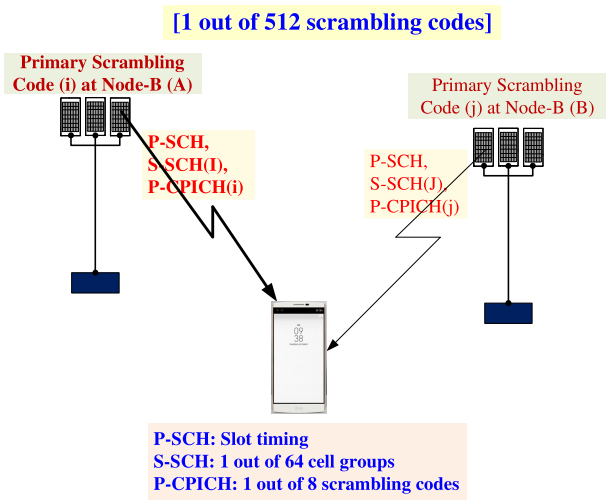

FIGURE 8. Physical channels and the corresponding target at each stage of initial cell search in W-CDMA, where Node-B (A) is assumed to be a serving cell and all related information is highlighted in bold type.

(EDGE). Even if a UE has a priority to start at either 2G, 3G, 4G, or at 5G, we assume that 3G mode (either W-CDMA or TD-SCDMA) has its top priority to initiate. Regarding the ICS procedure in either 4G or 5G systems, either mode will have its top priority to commence. As soon as a UE is turned on, ICS procedure in idle mode commences based on previously stored information such as carrier frequency, Cell ID, and so on. If the trial is not available or failed, carrier frequency search embarks on searching all 3G radio frequency channels in the 3G bands and on finding candidates of possible frequency bands available. Then, after the successful completion of the ICS procedure, diverse TCS procedures will be activated to support seamless handovers [9]. Let us delve into details of ICS procedures in both W-CDMA and TD-SCDMA systems.

1) INITIAL CELL SEARCH IN W-CDMA

In order to reduce the complexity of entire cell search, both W-CDMA and TD-SCDMA have adopted hierarchical cell search procedure to acquire scrambling codes employed for distinguishing cells in both W-CDMA and TD-SCDMA systems [21], [22], [40], [41]. A brief procedure of finding one out of 512 PSCs$^{(1)}$ is portrayed in Fig. 8, where detection of P-SCH indicates acquisition of slot boundary as well as detection of S-SCH represents acquisitions of both radio-frame boundary and one out of 64 scrambling code groups. Then, the employment of P-CPICH is finally to achieve PSC$^{(1)}$ dedicated to a serving cell, namely one out of eight PSCs$^{(1)}$. Here, three stage-aided ICS is inevitable for achieving the best possible overall ICS performance, which harmonizes detection probability, miss-detection probability, false alarm probability, and mean acquisition time optimally [10], [11], [14] as well as especially at least as a verification mode, the third stage should be contemplated in the perspective of mobile station modem implementation. Table 3 demonstrates

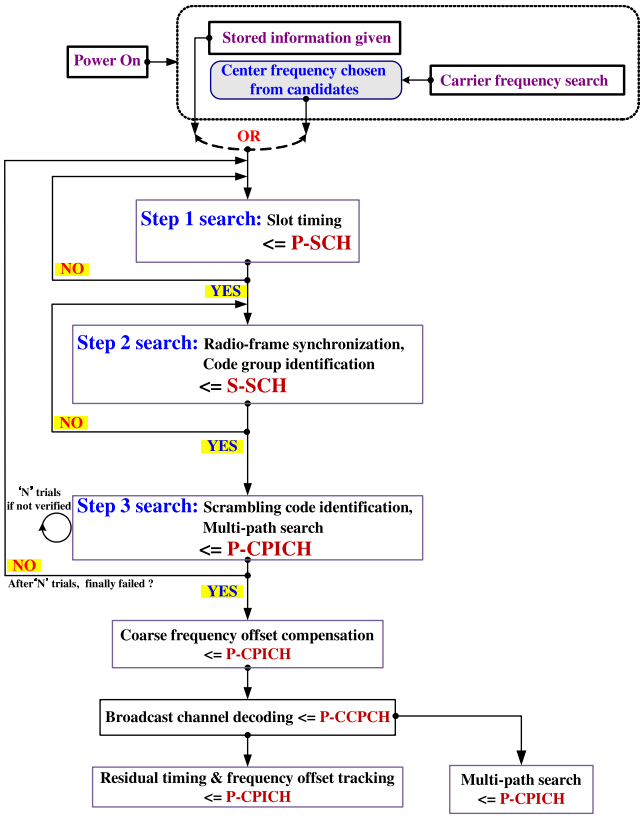

FIGURE 9. Detailed procedure of initial cell search in W-CDMA constituting three steps and the following frequency offset compensation.

entire search spaces of ICS scenarios with commonly used detection algorithms when W-CDMA, TD-SCDMA, LTE-FDD, TD-LTE, or NR is in active-Radio Access Technology (RAT), where PSS and NPSS represent primary synchronization signal and new radio primary synchronization signal, respectively as well as the number of NR symbols is changed based on a scaling numerology having N = 1, 2, 8, or 16. To elaborate it a little bit further, maximal time duration of W-CDMA is set to 0.67 ms owing to its periodic P-SCH transmission. If the number of samples per chip is set to two,[5] the number of hypotheses in the time-domain becomes 5120. Accordingly, finding a start point of peaky signal over the entire search space plays a pivotal role in ICS procedure. Finally, concise processing complexities of four 3GPP systems in Table 3 are determined as the search space times the multiple codes, namely W-CDMA: 5120, TD-SCDMA: 409600·32, LTE: 28800·3, and NR: 115200·N·3. Now, let us investigate the details of the ICS.

Fig. 9 illustrates the details of the entire ICS procedure in W-CDMA systems, where the ICS procedure constitutes three steps as a realization of the hierarchical ICS. On each selected carrier achieved by carrier frequency search, which is illustrated in Figs. 7 and 9, the ICS procedure moves

[5]When testing two hypotheses per chip, it is capable of reducing the corresponding signal-to-interference plus noise loss to 0.91 dB [29], [45], [46].

TABLE 3. Entire search spaces of initial cell search scenarios in W-CDMA, TD-SCDMA, LTE-FDD, TD-LTE, and NR.

	Max. time duration	Search space	Multiple codes	Typical Algorithm (Common)
W-CDMA	0.67 ms	5120 hypotheses	1 P-SCH	· Noncoherent Energy Detection
TD-SCDMA	5.0 ms	409600 hypotheses	32 SYNC-DLs	· Full Search
LTE-FDD&TD-LTE	5.0 ms	28800 hypotheses	3 PSSs	· Threshold optimization
NR	20.0 ms	115200 · N hypotheses	3 NPSSs	· Memory overhead consideration

TABLE 4. A Comparison of sequences exploited.

	W-CDMA	TD-SCDMA
Scr. code	Gold seq.	Gold seq.
Step1	P-SCH (Hier. Golay seq.)	DwPTS (Gold seq.)
Step2	S-SCH (Reed-Solomon code)	Midamble (m-seq.)
Step3	P-CPICH (OVSF code)	DwPTS & Midamble

into the step 1 search stage. During the step 1 search procedure of Fig. 9, slot timing is only acquired by using a single-matched filter dedicated to the PSC$^{(2)}$. Step 2 search stage commences by correlating the received signal of S-SCH with all the 16 SSCs in parallel and then accumulates all the resultant S-SCH correlations over multiple slots with the aid of the 64 Reed-Solomon codewords exploited, each codeword having 15 candidates of radio-frame boundaries. The entire number of hypotheses is determined as 960, which consists of 64 codewords times 15 locations of each radio-frame [21], [22], [40]. Hence, after 15 SSCs' sequences have been achieved, the transmitted S-SCH sequence is determined by comparing the estimated sequence with all the possible 960 S-SCH sequences. If an S-SCH sequence is attained within minimum distance from the sequence received, the S-SCH sequence is contemplated as being detected. Received PSC$^{(2)}$ is also exploited for estimating channel state information to perform coherent detection in the step 2 search stage.

Then, the step 3 search procedure conducts scrambling code identification, where P-CPICH is correlated with eight PSCs$^{(1)}$ in the identified code group. Additional role of the step 3 search finds meaningful multi-paths available. After the three step aided ICS procedure has been completed, the employment of continuous P-CPICH is readily to compensate for coarse frequency offset, followed by broadcast channel decoding to read cell-specific broadcast information. Table 4 compares sequences exploited for ICS procedures of W-CDMA and TD-SCDMA, where Scr. code, seq., and Hier. Golay represent scrambling code, sequence, and Hierarchical Golay, respectively. As scrambling codes distinguishing and identifying serving cell(s) from adjacent ones, Gold sequence is chosen for both 3G systems. On the other hand, sequences utilized in each step are entirely different between two 3G systems. Further details of the sequences used in W-CDMA are provided in Appendix. Table 5 summarizes ICS procedure comparisons for W-CDMA and TD-SCDMA with some noticeable algorithm design issues. Owing to inherently contrasting features of both frequency and time division duplexes, details of all the three steps are quite different between two 3G systems.

Until step 3 of the ICS procedure in two CDMA families is complete, mobile station cannot receive any key system information. Hence, the employment of multiple antenna aided transmission is extremely limited. It can be known as blind ICS procedure having very limited cell information such as a list of carrier frequencies to be searched, spectrum bandwidth, and so on. More explicitly, in case of W-CDMA system, one P-SCH code and predefined S-SCH codes can alternately be transmitted by exploiting a single transmit antenna for each slot in the time-switched transmit diversity mode [1]. In the configuration of the ICS procedure, both step 1 and step 2 enable to obtain the time switched transmit diversity gain. However, during step 3 search, mobile station is able to receive only one P-CPICH channel. Accordingly, no transmit diversity gain can be used for enhancing detection performance of step 3 search.

In a realistic situation, a UE usually receive P-CCPCH signals from several mobile network service providers. For the sake of identifying a predetermined mobile network, the UE will proceed to acquire Master Information Block (MIB), which finds a matched network. More explicitly, the UE is capable of acquiring multiple MIBs from all nearby Node-Bs indicating base stations at both intra- and inter-carrier frequencies. According to the order of cell powers measured, the UE tries to check whether the identity gained from received MIB is matched to that stored in the Universal Subscriber Identity Module (USIM) card of the UE until found, where MIB on P-CCPCH is broadcast by each Node-B and encompasses key system information such as the Public Land Mobile Network (PLMN) ID, PLMN List (if necessary), PLMN types to be supported, and scheduling information for the other System Information Blocks (SIBs) to perform the following mandatory operations [47]. After that, whenever normal communication starts, the UE moves into the connected mode. Depending on data services, a state of the UE moves back to the idle mode or keeps staying in the connected mode. In the connected mode, both residual timing error and residual frequency offset compensations are required to maintain a best possible radio link continuously.

2) INITIAL CELL SEARCH IN TD-SCDMA

A brief ICS procedure in TD-SCDMA systems is illustrated in Fig. 10. Specifically, detection of SYNC-DL code start position exhibits acquisition of subframe boundary while 1 out of 32 SYNC-DL codes is also obtained simultaneously. It is noted that slot boundary can be readily derived from the subframe boundary. Then, cell identification is accomplished by detecting midamble code index, which chooses

TABLE 5. Initial cell search procedure comparisons for W-CDMA and TD-SCDMA.

	W-CDMA	TD-SCDMA	Algorithm Design Issues
Step 1	Slot boundary	Subframe & slot boundaries and SYNC-DL code identification	·Frequency offset compensation can start in TD-SCDMA ·Memory overhead due to full search
Step 2	Radio-frame boundary and code group identification	Midamble and scrambling code identifications	·Multi-path search can start in TD-SCDMA
Step 3	Scrambling code identification and multi-path search	Multi-frame boundary	·Coherent detection becomes feasible by considering estimation of channel state information.

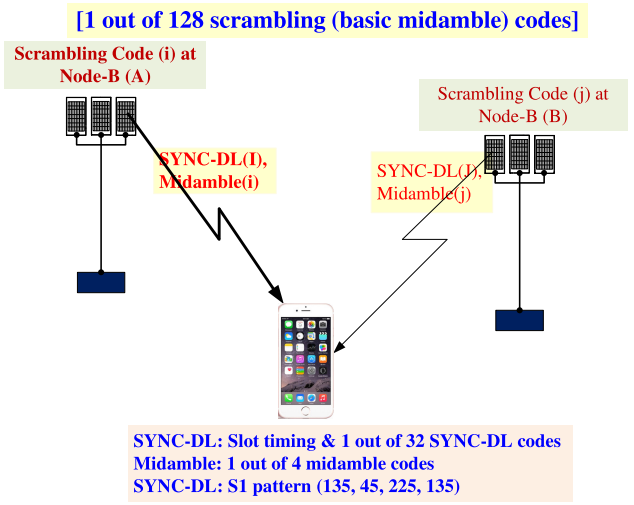

FIGURE 10. Codes and the corresponding target at each stage of initial cell search in TD-SCDMA, where Node-B (A) is assumed to be a serving cell and all related information is highlighted in bold type.

one out of four feasible midamble codes in each code group. Detection of a particular midamble code also leads to finding one out of 128 scrambling codes dedicated to a serving cell. Finally, multi-frame boundary is acquired exploiting specific S1 phase pattern of SYNC-DLs over four consecutive subframes to detect the existence of the P-CCPCH. As portrayed in Table 3, maximal time uncertainty duration of TD-SCDMA is set to 5 ms owing to its periodic DwPTS transmission. If the number of samples per chip is set to two, the number of hypotheses in the time-domain becomes 12800 [29], [45], [46]. However, when contemplating 32 SYNC-DL codes together, the entire number of the hypotheses is finally 409600 owing its two-dimensional search space. The number is 80 times more than that of W-CDMA. Accordingly, the entire ICS performance in TD-SCDMA becomes more critical than that in W-CDMA.

Now, let us investigate the details of the ICS procedure. Fig. 11 illustrates the details of the entire ICS procedure in TD-SCDMA systems, where the ICS procedure constitutes three steps as a realization of the hierarchical ICS. On each selected carrier achieved by carrier frequency search, which is illustrated in Figs. 7 and 11, the ICS procedure moves into the step 1 search stage [48]. During the step 1 search procedure of Fig. 11, joint detection of slot and subframe timings as well as identification of SYNC-DL code index may be realized by using a bank of matched filters dedicated to all the existing SYNC-DLs at the cost of high complexity. Otherwise, in order to reduce the complexity of the step 1 searcher, two-stage aided step 1 searcher have been considered with degraded detection performance. Namely, the 1st and 2nd stages represent signal edge detection scheme based on 5 ms search duration and matched filters on reduced search space, respectively [49], [50]. Here, the 1st stage constitutes selection of the power ratio metric to detect SYNC-DL start position and detection of roughly estimated start position of SYNC-DL.

By exploiting received midamble in TS0, step 2 search stage detects a midamble code index, which becomes the scrambling code index automatically via a predetermined mapping rule between the midamble code index and the scrambling code index. Given the estimated SYNC-DL code index obtained from the step 1 searcher, only four possible midamble code indexes exist on the candidates. For the sake of improving its detection performance, refined multi-path positions should be considered, which can be implemented using either time- or frequency-domain correlation, where the frequency-domain correlation can be implemented using efficient Fast Fourier Transform (FFT) [51]. Hence, during the step 2 search, multi-path searcher should be activated to find meaningful and refined multi-paths, which will be exploited for enhancing the step 2 searcher performance. It is noted that the multi-path searcher is capable of employing more resource, namely SYNC-DL and midamble in TS0 simultaneously to increase its multi-path detection performance. For achieving reliable timing and cell identification in the ICS procedure [16], the existing initial frequency offset should be compensated in an appropriate manner. For example, coarse frequency offset compensation for minimizing the existing initial frequency offset is practicable when the detected SYNC-DL code index and slot boundary are leveraged [23], [24].

Unlike that in W-CDMA, along with the time-domain synchronization, two stage aided coarse frequency offset compensation approach as a frequency-domain synchronization can be accomplished simultaneously as depicted in Fig. 11. Depending on the timing of the time-domain synchronization, either coarse or fine frequency offset compensation is activated. Specifically, the coarse frequency offset compensation scheme can be performed by leveraging the information of SYNC-DL code index attained from the step 1 searcher.

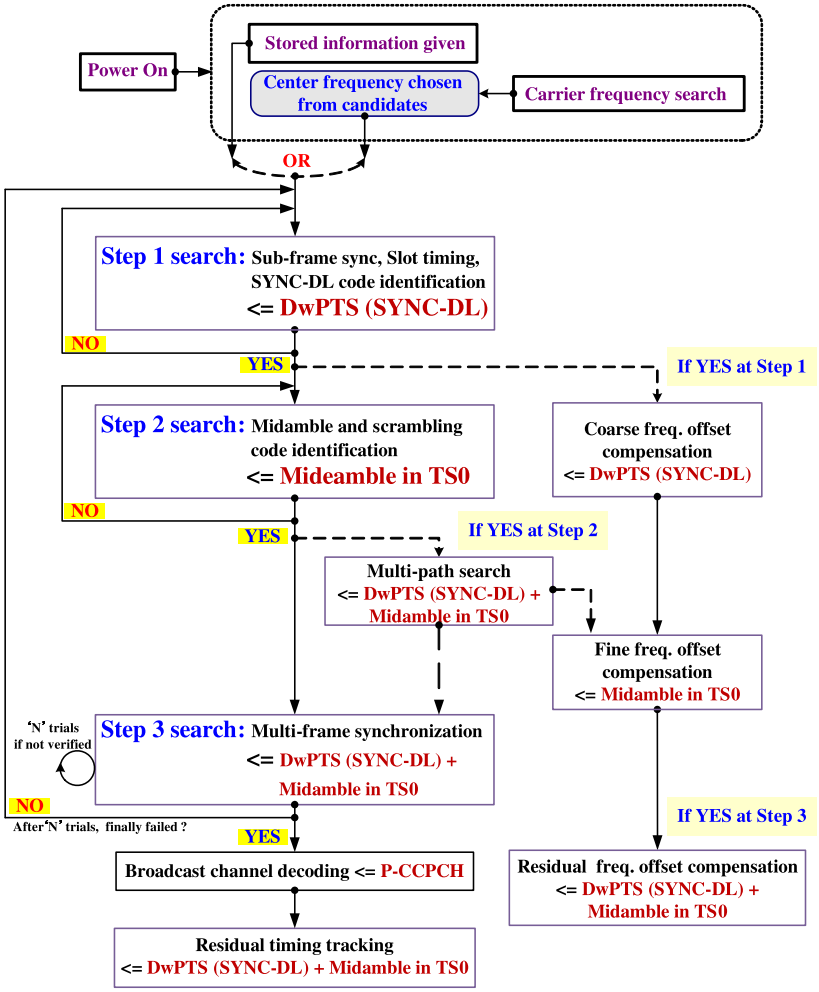

FIGURE 11. Detailed procedure of initial cell search in TD-SCDMA constituting three steps and relevant frequency offset compensations, where TS0 represents time slot zero.

Furthermore, the fine frequency offset estimation can also be activated using the midamble code index gained from the step 2 searcher. Basically, a midamble sequence having 128 chip duration twice longer than a SYNC-DL sequence is cyclic shifted with a chip length of 16. This makes more effective and sophisticated frequency-domain synchronization schemes possible. The enhancement is further capable of increasing the detection performance of the time-domain synchronization completed in the step 1 search stage. Typical algorithms of these frequency offset compensation schemes may be differential methods or maximum likelihood estimation [23], [24], [51]. In short, a main role of the frequency offset compensation accelerates timing synchronization and cell identification with the known side-information such as timing and scrambling code ID. It is noteworthy that timing synchronization and frequency offset estimation are processed in parallel as visualized in Fig. 11. As time goes on, dynamic range of the residual frequency offset is usually diminished with the aid of the attained side-information.

Then, the step 3 search procedure is followed to achieve multi-frame synchronization exploiting other side-information such as midamble code index and subframe boundary. TD-SCDMA provides a peculiar radio-frame structure in a sense that a constant phase pattern is allocated over consecutive positions of SYNC-DL sequence. Each subframe in TD-SCDMA systems has its own phase pattern over SYNC-DL sequence [41]. More explicitly, four successive phases referred to as phase quadruple of the SYNC-DL are employed to determine the existence of the P-CCPCH in the following four consecutive subframes also called the multi-frame. In case that its presence is decided, the next following subframe becomes the starting point of the multi-frame. The SYNC-DL sequence is Quadrature Phase Shift Keying modulated, whose phases constitutes 45, 135, 225, and 315 degrees. Two phase quadruples indicate S1 being a series of 135, 45, 225, and 135 degrees as well as S2 being another series of 315, 225, 315, and 45 degrees, respectively, which also correspond to the existence and non-existence of P-CCPCH in the next four consecutive subframes, respectively [41], [43].

Once the cell is identified, channel estimation using the cell ID is feasible so that coherent detection for the multi-frame synchronization can be accomplished [52]. By using each subframe's own phase pattern and coherent detection with

the detected cell ID, the multi-frame boundary is acquired and is followed by broadcast channel decoding just after the step 3 search as illustrated in Fig. 11. When the start point of the multi-frame boundary is found, residual frequency offset compensation should be activated to reduce further residual frequency offset by utilizing both SYNC-DL and midamble sequences in TS0. It is also capable of guaranteeing stable channel decoding performance. After the successful broadcast channel decoding, residual timing tracking commences by further decreasing residual timing error by employing both SYNC-DL and midamble in TS0. Finally, both the residual frequency offset and timing error are within the target range. Otherwise, rather than performing the step 3 search stage portrayed above, a simple method may consider the employment of sliding broadcast channel decoding for conducting multi-frame start position detection and broadcast channel decoding simultaneously. However, it can sometimes require very high computational complexity and lengthy decoding time owing to an excessive number of broadcast channel decoding trials. Similar to W-CDMA, DwPCH can be transmitted at each sub-frame having a predefined antenna pattern configuration. More explicitly, only step 1 enables to achieve the time switched transmit diversity gain owing to complete difference of synchronization channel structures of two CDMA families. No transmit diversity gain can be exploited for improving detection performances of both step 2 and step 3 search procedures. Sequences used for ICS procedure of TD-SCDMA are summarized in Table 4. Further details of the sequences are also given in Appendix. It is worth noting that summarized ICS procedures for W-CDMA and TD-SCDMA are compared in Table 5.

In case of the timing recovery and(/or) cell identification failure in the present step, taking back to the previous step is a reasonable strategy in general to enhance detectability and minimize entire cell search time simultaneously. However, when broadcast channel decoding failure does happen, going back to very initial step such as carrier frequency search might be an appropriate choice as visualized in Fig. 7, because detectability of broadcast channel decoding step is sufficiently higher than basic detection performance owing to the robustness of channel decoding. Thus, in case of the broadcast channel decoding failure, it is highly likely to have performed an ICS procedure in a wrong carrier frequency band rather than the decoding failure itself. Continuous management for reducing residual frequency offset is also beneficial to have high detection performance, which ultimately results in decreasing entire cell search time. Similar to that in W-CDMA, after the above-mentioned is complete, with the aid of system information obtained from successive broadcast channel decoding based on the detected radio-frame boundary, UE moves into the connected mode. The details of the procedure have already been illustrated in the ICS procedure of W-CDMA above. In the connected mode, both the residual timing error and frequency offset compensations are required for maintaining a best possible radio link continuously [51].

Before finalizing the mandatory feature in TD-SCDMA network, we introduce how the N-frequency network and its ICS procedure are related in brief. As visualized in Fig. 6, only a single carrier is established as the primary frequency and the rest is configured as the secondary frequencies 1 to N. All the existing control channels such as P-CCPCHs in TS0 and DwPTS are only configured on the primary frequency. On the other hand, as portrayed in Fig. 6, on any secondary frequency those durations are empty [43], [44]. When a UE camps on a serving cell, at first it tries to listen to the primary frequency to get broadcast messages. After the ICS is successfully performed, a particular UE is allocated to a specific frequency among all the possible ones depending on the radio resource availability in the N-frequency network. In case of the handover procedure, the UE will directly synchronize the primary frequency of the target cell, where the primary frequency may be different from that of the current serving cell. It is noted that two different cells can have the same SYNC-DL code index. Hence, the step 2 search completes the cell identification as well. In this case, there is a possibility that each multi-path position for the SYNC-DL sequences corresponds to a separate midamble sequence. An identification of individual cell is also distinguishable from other cells by employing the multi-path searcher [43], [51]. Accordingly, the exploitation of both the step 2 searcher and the multi-path searcher boosts the cell identification capability.

C. SUMMARY AND LESSONS LEARNED

In Section II, by employing a concise depiction of cdmaOne, W-CDMA, and TD-SCDMA based on the synchronization signals' structures of Fig. 4, we have proceeded by offering profound insight into the following three key findings:

- The chip duration of each CDMA system is inversely proportional to the bandwidth allocated.
- An evolution of cdmaOne to W-CDMA illustrates an exemplification of a single carrier direct sequence CDMA having wider channel bandwidth. On the other hand, an optional mode of TD-SCDMA is capable of supporting three-carrier transmission by exploiting three separate channel bandwidths in frequency-domain, which can be a realization of multi-carrier direct sequence CDMA.
- The multi-path channels' scatteredness of W-CDMA having shorter chip duration and wider bandwidth is predominant over that of TD-SCDMA. It is also noted that three times higher time-domain resolution of W-CDMA leads to more richness of the multi-paths having diverse delay spreads.

Throughout a direct comparison of the time-domain multi-path resolution, the corresponding multi-path span and richness of the multi-path, we've investigated that the timing synchronization portrayed in Fig. 3 is determined as major ICS issue of all the CDMA families. Figs. 5 and 6 detailed four physical channel structures of W-CDMA DL systems

and a hierarchical radio-frame structure of TD-SCDMA DL systems, respectively, which are utilized for ICS procedures. We have also introduced that a generalization of TD-SCDMA configuration referred to as N-frequency network exhibits the current commercial network deployed in China as a mandatory feature. For the sake of delving into ICS procedures in two CDMA systems, at first Fig. 7 articulated a macroscopic view on ICS flow used in active-RAT mode of 2G, 3G, 4G, or 5G systems. Then, the details of the entire ICS procedure have been visualized in Figs. 8 and 9 for W-CDMA as well as in Figs. 10 and 11 for TD-SCDMA, respectively. As demystified in detailed taxonomy classification of Fig. 3, a realization of the hierarchical ICS procedure constituted timing synchronization, frequency synchronization, and finally code/cell identification. There existed a remarkable difference of the frequency offset estimations between W-CDMA and TD-SCDMA owing to the distinguishing synchronization sequence transmission. More specifically, the exploitation of continuous P-CPICH transmission in W-CDMA was to simplify the frequency offset compensation compared with sparseness of periodic synchronization preamble transmissions in TD-SCDMA. Deterioration of transmission resource made multi-step aided approach only guarantee reliable target performances. Moreover, timing synchronization and frequency offset estimation were processed in parallel as visualized in Fig. 11.

Entire search spaces and sequences adopted for ICS procedures as well as the essential ICS procedures for two CDMA systems have been compared in Tables 3, 4, and 5, respectively. Owing to inherently dissimilar channel structures influenced by both frequency and time division duplexes, the three step-aided ICS procedures of two CDMA systems became quite different and hence have been designed separately, which can be a distinct weakness compared with the corresponding LTE counterpart. It is also manifested that how the time-switched transmit diversity mode of two CDMA families has been leveraged for improving ICS performance gain. By our in-depth discussions of all the ICS flows and their relevant details, we have bestowed a potential on understanding systematic ICS flow of any hybrid CDMA related system to be designed in the future. It is worth noting that our TCS counterpart operating at two CDMA systems has been detailed in [9].

III. EVOLUTION OF INITIAL CELL SEARCH IN THE OFDMA SYSTEMS (LTE TO NR)

A. OVERVIEW OF INITIAL CELL SEARCH OPERATING OVER MULTI-MODE ENVIRONMENTS

The 3GPP is actively standardizing 5G systems referred to as NR [4]–[8], [19], [53]–[56]. From an overall evolution perspective, it is very beneficial for us to see how both the entire structures and key features of NR are specified in terms of cell search. One of the main objectives for NR is capable of providing a wider range of spectrum bands. Specifically, the NR access technology seeks to be flexible to support sub-6 GHz and above 6 GHz, which covers spectrum bands of up to 52.6 GHz, where the 3.5 GHz spectrum bands are exploited for early deployment of NR system. Three main categories of NR are commonly referred to as enhanced mobile broadband, ultra-reliable low latency communications, and massive machine type communications. The massive machine type communications are characterized by very narrow bandwidth of 200 kHz compared with the other two categories. For satisfying those diverse scenarios and their performance requirements, the NR systems support various numerologies [6]. Specifically, a variety of subcarrier spacing categories in the NR systems are applied in comparison with the LTE system supporting only one subcarrier spacing of 15 kHz. Owing to its bandwidth requirement, it is highly likely that dedicated Synchronization Signal (SS) design is required for this particular case. More explicitly, SSs having bandwidth of 200 kHz does not satisfy system requirements for the other two categories. Accordingly, a different type of SSs must be designed for its dedicated ICS scenario [57]. In this tutorial, we focus our attention on two particular NR ICS scenarios, which are typically considered in licensed sub-6 GHz and above 6 GHz bands, because their standardizations for NR systems have been discussed and agreed. The enhanced mobile broadband is capable of manifesting a main characteristic in NR operating at mmW bands. According to [4]–[7], [19], [53], [55], up to 300 GHz except for massive machine type communication services, Cyclic Prefix (CP) aided Orthogonal Frequency Division Multiplexing (OFDM) based waveform as used in LTE has also been adopted in NR.

Fig. 12 illustrates simultaneous multi-connectivity in 3G, 4G, and NR systems as well as NR ICS, where LTE-U, LAA, NPSS, and NSSS represent LTE-Unlicensed (LTE-U), Licensed-Assisted Access (LAA), New radio Primary Synchronization Signal (NPSS), and New radio Secondary Synchronization Signal (NSSS), respectively. For LTE operating at unlicensed spectrum bands, there are two ways of implementing LTE and its evolved versions in the unlicensed band, depending on whether the specification is modified or not, which correspond to LAA and LTE-U, respectively. The LTE-U can be deployed in regions such as the US, South Korea, China, and India. Without modifying Rel-10 protocols, a fair coexistence with unlicensed technologies such as WiFi systems becomes feasible only with additional software based functionality [58]–[62]. On the other hand, the LAA has been standardized in Rel-13 and it performs carrier aggregation in the DL to combine LTE signals in unlicensed spectrum bands operating at 5 GHz in conjunction with LTE ones in the licensed band. This approach has been chosen for the deployment in both EU and Japan [63]. Owing to inherent uncertainty issue of ZC sequences in case of occurring integer frequency offset, both NPSS and NSSS have newly been designed based on m-sequences [6], [64]. More explicitly, NPSS is frequency-domain based m-sequences having fixed time and frequency-domain ambiguities transmitted on pure Binary Phase Shift Keying and three cyclic shifts in the frequency-domain are able to generate three particular

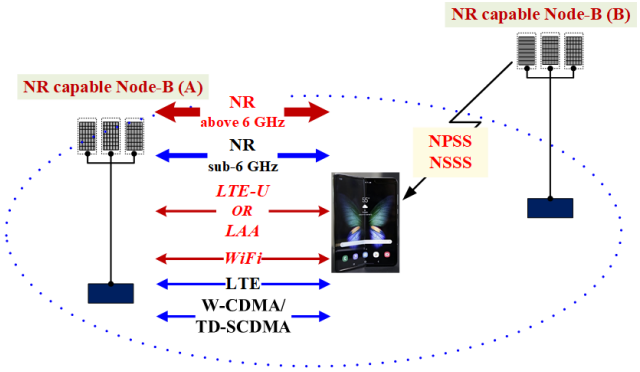

FIGURE 12. Simultaneous multiple connections in 3G, 4G, and NR systems as well as initial cell search in NR.

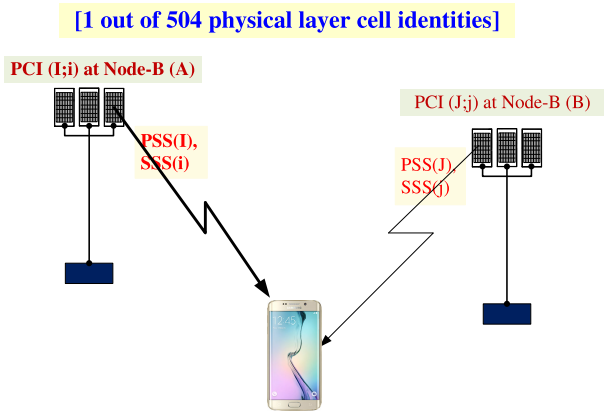

FIGURE 13. Synchronization signals and the corresponding target at each stage of initial cell search in LTE, where *I* and *J* represent physical layer identities assigned to two Node-Bs, respectively as well as *i* and *j* indicate physical layer identity group allocated to two Node-Bs, respectively. It is noted that Node-B (A) is assumed to be a serving cell and all related information is highlighted in bold type.

NPSS signals. NSSS is generated based on a combination of two generator polynomials having 127 and 9 cyclic shifts, respectively. Its resultant sequence becomes a kind of Gold-sequence [6], [65]–[70].

For the sake of supporting close inter-working between LTE and NR, aggregating signal flows between the two RATs to support dual connectivity and even multiple connectivity are widely considered in NR capable environment as portrayed in Fig. 12. More explicitly, it is under diverse heterogeneous deployments where macro and small cells having different sizes are overlapped as well as both cells are co-located or not, providing completely different cell coverages. It is noted that co-located cell represents that a small cell and a macro cell may be deployed at the same geographical location. For example, W-CDMA/TD-SCDMA, LTE, or NR (sub-6 GHz) may serve macro cells. On the other hand, WiFi, LTE-U, LAA, or NR (above 6 GHz) may serve small cells. Similar to Figs. 8, 10, and 13, NR ICS also follows exactly the same philosophy adopted in both 3G and 4G systems, namely hierarchical cell search strategy to reduce the complexity of the entire NR ICS and to acquire NR cell ID. The NR cell ID corresponds to the scrambling code in both W-CDMA and TD-SCDMA systems as well as PCI in LTE systems. The employment of both NPSS and NSSS will do similar procedures adopted in the LTE ICS with the aid of additionally utilizing beamformed SS in mmW communication systems operating at 28 GHz.

In the following three subsections, with the aid of Figs. 1, 2, and 3 as well as the corresponding cell search's hierarchical structure and detailed taxonomy classification manifesting three main targets of ICS scenarios in LTE-FDD, TD-LTE, and NR systems, we demonstrate the detailed physical channel structures exploited in the ICS scenarios of three OFDMA systems, followed by essential feature comparisons. Then, full details of the ICS scenarios are delineated, which are further visualized in Figs. 7 and 13 to 23 and elaborated in Tables 3 and 6 to 8. We also provide a contemplation in intelligence based multi-mode mobile station modem as visualized in Fig. 24 and future directions are summarized.

B. RADIO-FRAME STRUCTURE PERSPECTIVE

One noticeable characteristic of NR IA is the advent of scalability in the radio-frame structures in the NR system, which is beyond the widely deployed LTE system providing only scalable bandwidth. Specifically, additional support for multiple subcarrier spacings leads to further scalability in the radio-frame structures. Another salient point is the enhancement of synchronization sequences encompassing longer sequence length, which guarantees higher detection performance than the legacy system. Contemplating that the center of gravity shifts from the LTE system to NR system, we manifest the progress of the radio-frame structures more concretely in the following.

1) RADIO-FRAME STRUCTURE IN 4G

Figs. 14 and 15 illustrate the radio-frame structures of LTE-FDD and TD-LTE, respectively, (also referred to as frame structure Types 1 and 2, respectively) [3]. In the details of the radio-frame structures used here, the various fields expressed in the time-domain are based on sample time, which represents the amount of time dedicated to each time-domain OFDM sample and is considered as the basic unit of time for LTE, namely $T_s = 1/(15000 \cdot 2048)$ s, or about 32.55 ns. As portrayed in Figs. 14 and 15, both the DL and UL transmissions rely on radio-frames having a $T_f = 307200 \cdot T_s$ duration, equivalent to 10 ms. The radio-frame comprises 20 slots of a length $T_{slot} = 15360 \cdot T_s$ s, equivalent to 0.5 ms. A radio-frame is also represented by 10 subframes, where a single subframe is set to 1 ms. Each slot contains seven or six symbols, which corresponds to the normal or extended CP, respectively. One and two in dotted circles of the first trace in Fig. 14 represent the normal and extended CP modes, respectively. It is noted that in Fig. 14 the first symbol of the normal CP mode is slightly longer than others in order

TABLE 6. Synchronization resources for LTE and NR, where NPBCH represents NR physical broadcast channel.

	LTE	NR	Note
NPSS	Zadoff-Chu seq.	m-seq.	The Zadoff-Chu seq. is gravely influenced by an integer freq. offset.
NSSS	m-seq.	Gold seq.	The SSS in LTE is used for not only radio-frame boundary recovery but also cell identification. On the contrary, the NSSS in NR is employed only for the cell identification.
RS	Gold seq.	Gold seq.	New feature in NR for radio-frame boundary recovery
NPBCH	Not used	Used	New feature in NR for radio-frame boundary recovery

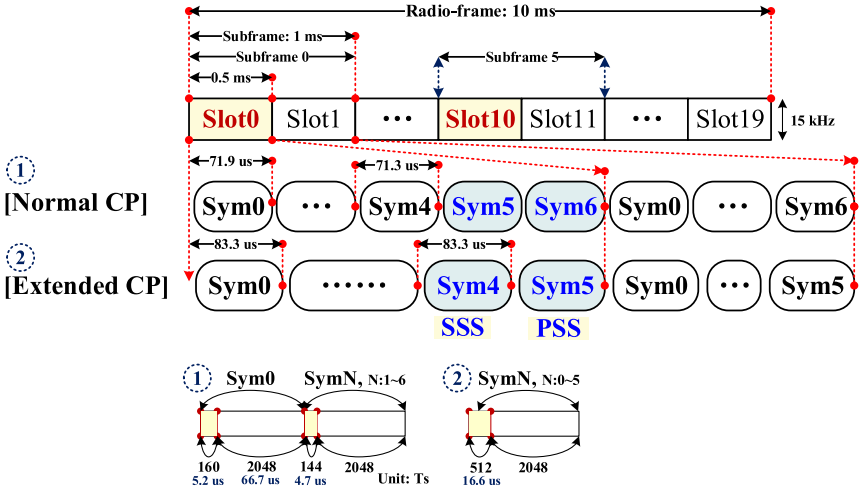

FIGURE 14. Radio-frame structure of LTE-FDD mode constituting both normal and extended CP modes.

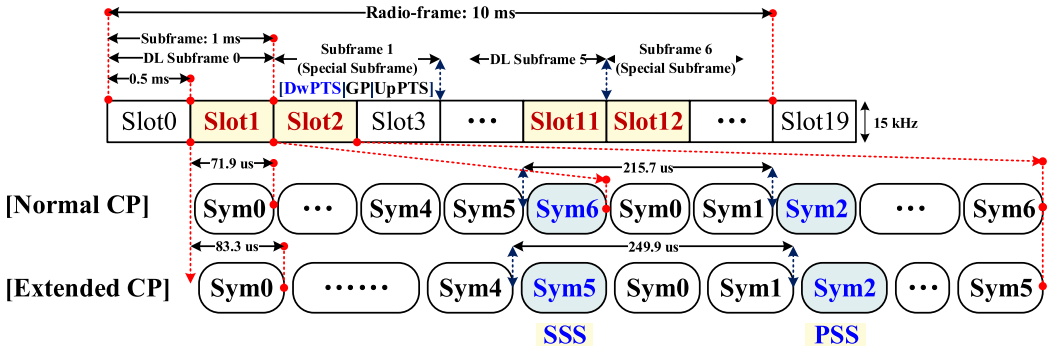

FIGURE 15. Radio-frame structure of TD-LTE mode constituting both normal and extended CP modes, where [DwPTS|GP|UpPTS] corresponds to a special subframe.

to make the entire slot length in terms of time units divisible by 15360. Hence, the first symbol constitutes a CP having a length T_{CP} of $160 \cdot T_s$ ($\cong 5.2\ \mu$s) plus the remaining length given by $T_R = 2048 \cdot T_s$ ($\cong 66.7\ \mu$s). The entire length of the first symbol becomes 71.9 μs. Similarly, other symbols have a CP having the length T_{CP} of $144 \cdot T_s$ ($\cong 4.7\ \mu$s) and their entire symbol length is about 71.3 μs. On the other hand, in the extended CP mode, the CP is set to $T_{CPe} = 512 \cdot T_s$ ($\cong 16.7\ \mu$s) and its entire symbol length is about 83.3 μs. The above-mentioned time-durations are visually illustrated in the second trace of Fig. 14. The normal CP mode is mainly employed in urban cell deployments, whereas the extended CP mode is exploited in both multi-cell broadcast and very large cell deployments.

Now, let us focus our attention on the locations of the Primary Synchronization Signal (PSS) and the Secondary Synchronization Signal (SSS) in LTE-FDD. Both PSS and SSS seen in Figs. 14 and 15 are transmitted every half radio-frame. The PSS is placed in the last OFDM symbol of the first and 11-th slots of each radio-frame. The PSS is also the same for any cell every half radio-frame. As observed in Figs. 14 and 15, the allocation of the SSS immediately precedes that of the PSS, namely it is placed at the second to last symbol of the first and 11-th slots of each radio-frame. Again, in Fig. 14, the PSS and SSS are situated at two consecutive symbol positions represented as symbols 5 and 6 in the normal CP mode, while as symbols 4 and 5 in the extended CP mode, respectively. The SSS alternates in a predefined pattern over a radio-frame duration.

Even though the details of the radio-frame structure in TD-LTE are similar to those in LTE-FDD, there are also several different features imposed by the time division duplex characteristics. According to [3], the UL-DL configuration in a cell may change between half radio-frames or between radio-frames. Either UL or DL subframe transmissions may occur in the current radio-frame. Specifically, the UL-DL

configuration in the current radio-frame is determined by Table 4.2-2 of [3]. The UL-DL configurations having both 5 ms and 10 ms DL-to-UL switch-point periodicity are used in TD-LTE. When the 5 ms DL-to-UL switch-point periodicity is in use, a special subframe exists in every half radio-frame, which is explained below and seen in Fig. 15. On the other hand, in case of the 10 ms DL-to-UL switch-point periodicity, a special subframe only exists in the first half radio-frame. More explicitly, if the switch time is set to 5 ms, the switch information occurs in every half radio-frame, namely a start point in subframe zero and again that in subframe five. Therefore, subframes zero and five as well as the DwPTS are always reserved for DL transmission. Similarly, the UpPTS and the subframe immediately following the UpPTS are also reserved for UL transmission. Fig. 15 illustrates the details of the radio-frame structure employed in TD-LTE, related to the 5 ms DL-to-UL switch-point periodicity.

Now, we would like to discuss the details of the special subframe of Fig. 15, which comprises the DwPTS, a GP, and the UpPTS. Subframe 1 of Fig. 15 is always a special subframe. If the 5 ms DL-to-UL switch-point periodicity is supported, subframe 6 also becomes another special subframe. The PSS of Fig. 15 is part of the DwPTS within the special subframe. The SSS of Fig. 15 is located at slots 1 and 11. It is also noted that the location of SSS is always within the normal DL subframe(s). More explicitly, as portrayed in Fig. 15 the PSS is located at the third symbol position of slots 2 and 12, which is three symbols away from the position of SSS. Accordingly, the location of SSS is situated at the last symbol position of slots 1 and 11. In Fig. 15, in case of the normal CP mode, its location is represented as symbol 6 in slot 1 and symbol 2 in slot 2. Similarly, in the extended CP mode of Fig. 15, the location of SSS is shown as symbol 5 in slot 1 and symbol 2 in slot 2. For the sake of preventing overlap between the UL and DL signaling, TD-LTE employs a GP in which a flexible blank period is allocated, as illustrated in Fig. 15. The GP represents the switching point between DL and UL transmission, as well as its length determines the maximum possible cell size, which has to be chosen for preventing the collision of UL and DL radio-frames. At the speed of light ($3{\cdot}10^8$ m/s), a maximum cell-radius would result in a GP of approximately 666.7 μs [3], [71]. The length of the GP has to consider both the size of the cell (or sector) and the potential interference generated by the adjacent cells. It is also noted that the special subframe of Fig. 15 encompasses a variable amount of DL information in both the DwPTS and the UpPTS as well as a flexible GP. Table 4.2-1 of [3] portrays the detailed configuration of the special subframe constituted by the DwPTS, GP, and UpPTS, where their entire length is equal to 1 ms.

Now, we shift our focus from the radio-frame structure in the time-domain to that in the frequency-domain [3]. The number N of subcarriers to be allocated varies from 128 to 2048, corresponding to channel bandwidth ranging from 1.25 to 20 MHz. Similarly, the size of FFT and sampling frequency also range from 128 to 2048 and from 1.92 to 30.72 MHz, respectively. Each individual subcarrier spacing Δ_f is $1/(2048 \cdot T_s)$, equivalent to 15 kHz. It leads to symbol duration of $1/15000 \cong 66.7$ μs after the inverse FFT operation. The sampling rate f_s becomes $\Delta_f \cdot N = 15000 \cdot N$. This relationship makes a sampling rate either multiple or sub-multiple of the W-CDMA chip rate having 3.84 Mcps. Accordingly, both FFT lengths and sampling rates are easily attained for all possible operation modes while a multi-mode modem having a common clock reference is readily implemented. It is noteworthy that not all the subcarriers are employed. More explicitly, a Direct Current (DC) subcarrier is not employed and located in the center of the DL band as well as guard subcarriers are also not available.

A Resource Block (RB) constitutes a group of 12 consecutive subcarriers ($12 \cdot 15 = 180$ kHz) over a single time slot (0.5 ms). This granularity is chosen for restricting signaling overhead. When a 20 MHz bandwidth is allocated, 1200 subcarriers are available, equivalent to 100 RBs over a single time slot. Hence, the RBs constitute two-dimensional units having a size of 12 subcarriers in the frequency-domain and a single slot in the time-domain. A Resource Element (RE) represents the smallest unit of resource consisting of a single subcarrier during a single OFDM symbol period. Accordingly, an RB comprises $12 \cdot 7 = 84$ and $12 \cdot 6 = 72$ REs corresponding to the normal and extended CP modes, respectively. However, the total number of subcarriers over a 20 MHz bandwidth is calculated as 20000 kHz / 15 kHz, which results in 1333 subcarriers. It is sufficiently higher than 1200. This fact manifests that all subcarriers are not exploited and some subcarriers act as guard subcarriers at the edges.

Figs. 16 and 17 represent both PSS and SSS mappings in the frequency-domain, respectively. The PSS and SSS are located at the central six consecutive RBs ranging from RB:47 to RB:52, irrespective of the LTE channel bandwidth configured. The fact allows the UE for synchronizing to the network without gaining a priori knowledge of the channel bandwidth allocated. After detecting both the PSS and SSS, the DL channel bandwidth is subsequently obtained from the MIB carried on the Physical Broadcast CHannel (PBCH). Only center 1.08 MHz bandwidth is used for both PSS and SSS mappings in the frequency-domain even though the corresponding channel bandwidth is set to 1.4 MHz. Both the PSS and SSS portrayed in Figs. 16 and 17 exploit 62 subcarriers constituting two 31 subcarriers mapped into each side of the DC subcarrier not utilized.[6] Two five subcarriers at each extremity of the central six consecutive RBs are reserved for a period of discontinuous transmission.

The PSS constitutes a sequence of complex symbols having a length of 62 symbols, generated based on a frequency-domain ZC sequence. The sequence $d_u(n)$

[6]The UE is capable of exploiting a 64 FFT and lower sampling rate. Furthermore, in case of TD-LTE, the employment of 62 subcarriers guarantees avoidance of correlation with the UL demodulation reference signals exploiting Zadoff-Chu (ZC) sequences [18].

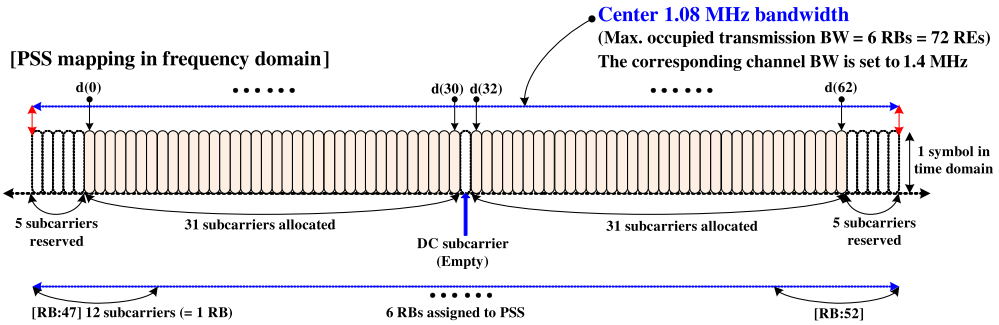

FIGURE 16. PSS mapping in the frequency-domain.

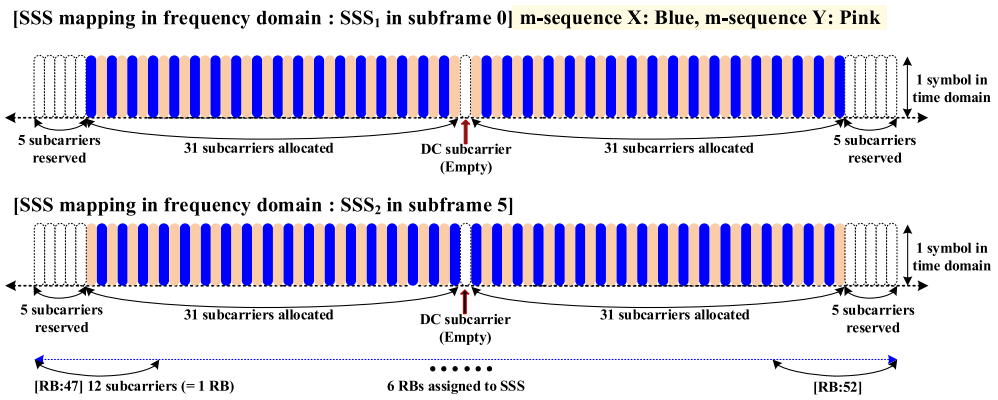

FIGURE 17. SSS mapping in the frequency-domain.

employed for generation of the PSS constitutes $d_u(n) = exp(-j\pi u{\cdot}n{\cdot}(n+1)/63)$ for $n = 0, 1, \ldots, 30$ and $d_u(n) = exp(-j\pi u{\cdot}(n+1){\cdot}(n+2)/63)$ for $n = 31, 32, \ldots, 61$, where u indicates the ZC Root Index (RI). As the DC subcarrier does not include any information in LTE DL, this leads to mapping into the middle 62 subcarriers within the central six consecutive RBs. Specifically, the PSS is mapped into two 31 subcarriers located on both sides of the DC subcarrier having five reserved subcarriers each side as illustrated in Fig. 16. Key properties of the ZC sequence are summarized in Appendix. RI is capable of determining a ZC sequence chosen from a set of ZC sequences having an entire period of N_{ZC}, where N_{ZC} is set to an odd prime. The RI root also determine the cell identity within the group $N_{ID}^{(1)}$, where $N_{ID}^{(1)} = 0, 1, 2$ represent the RI $= 25$, 29, and 34, respectively. When considering ZC sequence's root indices chosen for a generation of the PSS, by exploiting the two sequences 25 $(= N_1)$ and 29 $(= N_2)$, the third RI is derived by subtracting $(N_{ZC} - N_2)$, namely $63 - 29 = 34$. The RI set has been determined in terms of the best autocorrelation and crosscorrelation properties as well as frequency offset estimation error rate. More explicitly, under inter-cell site synchronous situation, interfering PSSs having the same sequence is capable of deteriorating the correct detection performance of the SSS based on coherent detection exploiting channel estimates obtained from the PSS detected. For the sake of avoiding the collision of the same PSSs from adjacent cells, three ZC sequences generated by the RI set are used in LTE systems [72]. Accordingly, the careful selection is able to improve ICS detection performances.

Fig. 17 portrays a visual illustration of the SSS in the frequency mapping, which is similar to the frequency-domain allocation of the PSS. However, the SSS is generated based on an m-sequence. The sequence exploited for generation of the SSS comprises an interleaved concatenation of two length-31 binary sequences, which is capable of alternating the sequence transmitted in subframes 0 and 5 every radio-frame. The feature allows the UE to achieve the radio-frame timing from observing only one of the two alternate sequences. The concatenated sequence is scrambled with a sequence related to the PSS with the physical-layer identity $N_{ID}^{(1)}$.

Let us see the details of each component sequence constituting the SSS in depth. The SSS is expressed by $d(2n) = s_0^{(m_0)}(n){\cdot}c_0(n)$ in subframe 0 and $s_1^{(m_1)}(n){\cdot}c_0(n)$ in subframe 5 as well as $d(2n+1) = s_1^{(m_1)}(n){\cdot}c_1(n){\cdot}z_1^{(m_0)}(n)$ in subframe 0 and $s_0^{(m_0)}(n){\cdot}c_1(n){\cdot}z_1^{(m_1)}(n)$ in subframe 5, where n represents 0, …, 30 and the indices m_0 and m_1 are derived from the Physical-layer Cell-Identity (PCI) group $N_{ID}^{(2)}$ as well as three pairs of sequences $(s_0^{(m_0)}, s_1^{(m_1)})$, $(c_0(n), c_1(n))$ and $(z_1^{(m_0)}(n), z_1^{(m_1)}(n))$ are generated by two different cyclic shifts of the three different m-sequences, respectively. In case of the

subframe 0, the sequences $s_0^{(m_0)}$ and $s_1^{(m_1)}$ map into the even and odd numbered subcarriers $d(2n)$ and $d(2n+1)$, respectively. On the contrary to the mapping, the reverse mapping is considered for the subframe 5. Their mappings are well described in Fig. 17, where m-sequences X and Y correspond to $s_0^{(m_0)}$ and $s_1^{(m_1)}$, respectively. The indices m_0 and m_1 indicate the PCI group $N_{ID}^{(2)}$, which provides totally 168 groups. A pair of the PSS-specific scrambling codes are denoted as $c_0(n)$ and $c_1(n)$, which are used to reduce the mutual interference between the same SSS sequences especially under the same cell site [72]. It is also noted that in case of transmission of $d(2n+1)$, a pair of scrambling code $(z_1^{(m_0)}(n), z_1^{(m_1)}(n))$ is exploited for enhancing cell search performance at cell edge. A mapping rule between PCI group $N_{ID}^{(2)}$ as well as the indices m_0 and m_1 is described in Table 6.11.2.1-1 of [3]. In the followings, operational scenario of LTE ICS is illustrated step-by-step.

2) RADIO-FRAME STRUCTURE IN NEW RADIO

As a distinguishing characteristic from LTE, a common radio-frame structure is utilized, irrelevant to any duplex mode in NR [73]. A numerology is specified by its subcarrier spacing representing the width of subcarrier in the frequency-domain and by its corresponding CP in the time-domain [6], [7]. Compared with LTE having only a single numerology corresponding to a particular subcarrier spacing in the frequency-domain in order to handle low to high carrier frequency bands to be supported by NR systems, diverse numerology options have been adopted in NR design by multiplying a basic subcarrier spacing with an integer N [4], [6], [7], [53]. The use of flexible subcarrier spacing plays a crucial role in designing NR systems based on CP aided OFDM. More explicitly, a shorter subcarrier spacing in the frequency-domain results in longer symbol duration and shorter CP overhead in the time-domain, which is capable of mitigating relatively longer delay spread. By contrast, a longer subcarrier spacing leads to shorter symbol duration and longer CP overhead. Therefore, the use of suitable subcarrier spacings is a critical issue relating to diverse carrier frequency bands ranging from 6 to 52.6 GHz. For instance, in case of carrier frequency bands operating at lower than 6 GHz, the use of 15 kHz is capable of guaranteeing large cell sizes employed in the current LTE systems having low CP overheads. Similarly, subcarrier spacings of 30 and 60 kHz are suitable for covering medium and small cell sizes, respectively. On the other hand, the exploitation of 120 kHz is able to provide tolerance to inherently high Doppler spread and carrier frequency offset when designing a particular NR system opted for small cells experiencing typically smaller delay spread values. When a UE experiences very high speed, the tolerance against carrier frequency offsets is directly proportional to bandwidth of the corresponding subcarrier and inversely proportional to the square root of the operational signal-to-noise ratio. High inter-carrier interference is also induced by high Doppler spread. Hence, the employment of higher subcarrier spacing appropriately chosen can be beneficial. Furthermore, at higher carrier frequency regime such as 28 GHz, adverse impacts on both frequency drift and phase noise deteriorate NR's performance substantially. By utilizing wider subcarrier spacing optimized, the negative impact can be minimized under a certain tolerance limit [57], [73], [75]–[77]. Accordingly, one of the major differences between LTE and NR is that multiple subcarrier spacings are defined in the NR design.

Essentially, the feasibility of multiple spacings in the NR comes from the support for an expanded maximum bandwidth. Specifically, the maximum allowable bandwidths in the NR are 100 and 400 MHz, corresponding to the Frequency Ranges (FRs) 1 and 2, respectively. Here, FR1 includes 3.7 and 4.5 GHz bands as well as FR2 indicates 28 GHz band. Accordingly, the NR systems are capable of managing diverse sizes of carrier frequency bands to cover up to mmW band regimes. It is also noted that subcarrier spacings depend upon the choice of a particular FR. Namely, a subcarrier spacing having either 15, 30, or 60 kHz operates under FR1. Similarly, that having either 60 or 120 kHz does under FR2 [73], [74]. In case of sub-6 GHz operations for NR, the minimum carrier bandwidths of subcarrier spacings 15 and 30 kHz can be set to 5 and 10 MHz, respectively. Especially, the subcarrier spacing of 30 kHz is the minimum carrier bandwidth for LTE and NR coexistence, which avoid potential collision with cell specific Reference Signal (RS) in LTE. Synchronization blocks for NR colliding with cell specific RS for LTE are not transmitted at gNB.[7] On the other hand, in case of above 6 GHz operation ranging from 6 to up to 52.6 GHz, the corresponding bandwidths of subcarrier spacings 120 and 240 kHz can be set to 50 and 100 MHz, respectively [4], [19].

Now, let us investigate the hierarchical NR radio-frame structure with SS/PBCH blocks in more detail. The NR radio-frame structures are capable of providing both fixed and flexible parts for the sake of facilitating both diverse numerologies and low latency operations. One of key features in the NR systems supports multiple numerologies for flexible NR radio-frame structures. Physical layers of NR systems are designed in a bandwidth agnostic manner, based on RBs in order to make the layers adapt to diverse spectrum allocations. A RB spans 12 contiguous subcarriers in the frequency-domain and is also based on a predetermined subcarrier spacing. Fig. 18 manifests a fixed overall NR radio-frame structure to define transmission timing when the subcarrier is 15 kHz as an example, where the first symbol indices of SS/PBCH blocks are determined depending on the subcarrier spacing [8]. It is worth noting that the subcarrier spacing for all SS/PBCH blocks cannot be provided by higher layer parameter. In this case, applicable cases for a cell are determined from a respective frequency band [78], [79]. In addition, the same subcarrier spacing is applied to all SS/PBCH blocks on the cell. NR radio-frame and subframe

[7] gNB represents NR Node-B having similar functionality as employed in evolved Node-B of LTE.

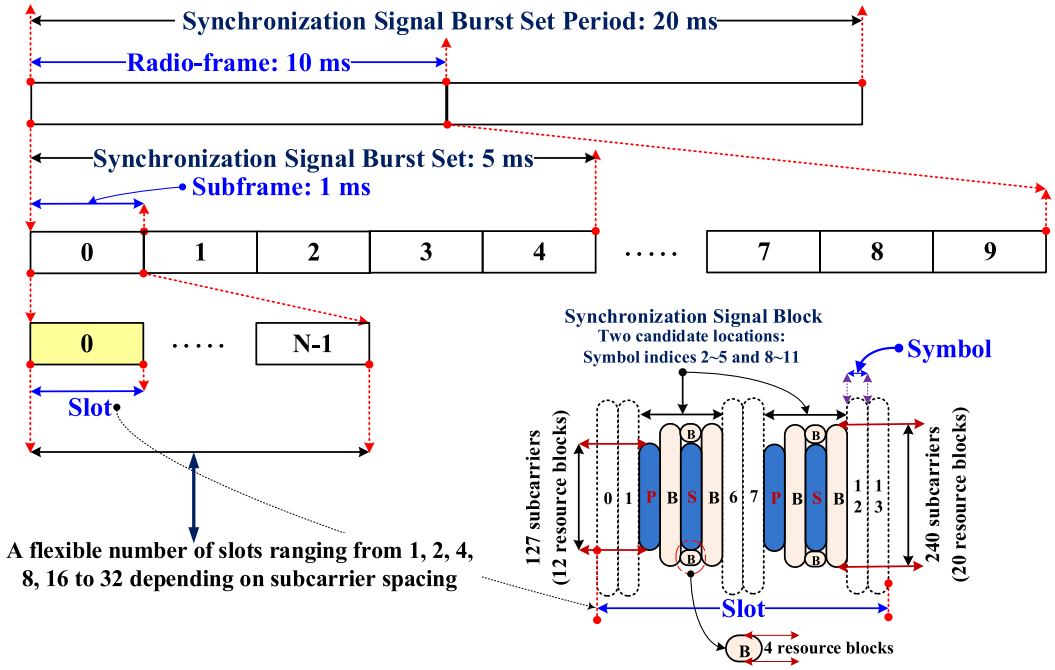

FIGURE 18. An example of hierarchical NR radio-frame structure with SS/PBCH blocks for the subcarrier spacing of 15 kHz.

have a fixed length in the time-domain. Both are selected to be the same as in LTE counterpart, which allows for efficient LTE and NR coexistence deployments. More explicitly, an NR radio-frame having a duration of 10 ms constitutes 10 subframes having a subframe duration of 1 ms each. A subframe is composed of one or multiple adjacent slots, each slot consisting of 14 consecutive symbols under normal CP mode. In NR system, there are two CP modes, i.e. normal CP and extended CP modes. In the extended CP mode, the number of OFDM symbols within a slot is 12 for securing longer CP length in comparison with the normal CP mode. It is noted that the extended CP mode is applied only to the case with the subcarrier spacing of 60 kHz, where the synchronization resources such as NPSS, NSSS, and NR Physical Broadcast CHannel (NPBCH) are not supported [80]. Each radio-frame is also considered as two half radio-frames having five subframes each. It is also noted that flexible numbers of slots within each subframe are determined by multiple numerologies ranging from 15, 30, 60, 120 to 240 kHz and hence the numbers depend entirely on subcarrier spacings having six scaling factors ranging from 1, 2, 4, 8 to 16. Accordingly, the number of symbols and slots in a single NR radio-frame will scale with the ratio of the corresponding subcarrier spacing with respect to the basic subcarrier spacing, i.e. 15 kHz, which is elucidated in Table 7, where a single slot constitutes 14 symbols [4]–[7], [19]. Furthermore, the subcarrier spacing of SS/PBCH blocks required for the ICS procedure depends on the feasible bandwidth, namely 15 kHz or 30 kHz for sub 6 GHz spectrum bands and 120 kHz or 240 kHz for above 6 GHz ones. Even though details on it are under manufacturers' implementation issue, both 15 kHz and 120 kHz options may be set to a default mode of UE's operation.

TABLE 7. Number of slots and symbols in NR radio-frame structure.

Subcarrier spacing	Num. of slots in 10 ms	Num. of symbols in 10 ms
15k (= LTE)	10 (= LTE)	140 (= LTE)
30k	20	280
60k	40	560
120k	80	1120
240k	160	2240

Compared with the existing LTE radio-frame structure, NR introduces new structures as follows. As visualized in Fig. 18, an SS burst set period constitutes two radio-frames, namely 20 ms. The SS burst set corresponds to half radio-frame duration of 5 ms. The SS/PBCH blocks in a half radio-frame are indexed in an ascending order in time ranging from 0 to $(L-1)$. NPSS, NSSS, and NPBCH are allocated within an SS/PBCH block in which symbols of NPSS, NPBCH, NSSS, and NPBCH are placed consecutively in the time-domain [6], [7], [68]. At least two symbols are preserved from the beginning from the SS/PBCH block for DL control. At least two symbols are also conserved at the end of the SS/PBCH block for guard period and UL control. The details of SS/PBCH block are also illustrated in Fig. 18, where P, B, and S represent NPSS, NPBCH, and NSSS, respectively [6], [7], [68]. For example, in case of the subcarrier spacing having 15 kHz, which requires 3.6 MHz transmission bandwidth of SS/PBCH block, there are two candidate locations representing symbol indices two to five

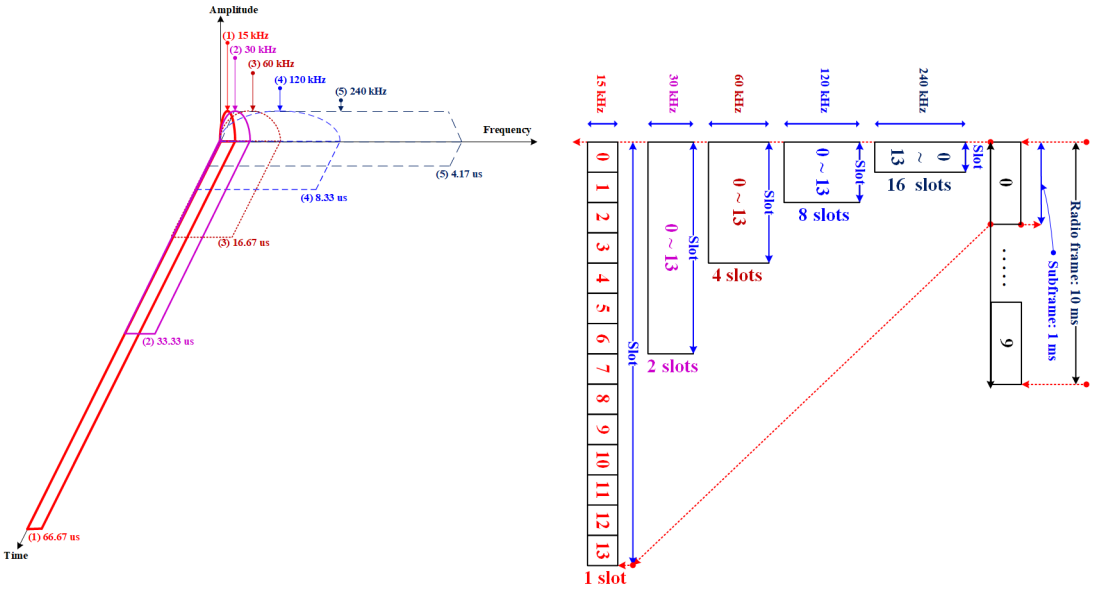

FIGURE 19. A diverse numerology of the NR system.

and eight to eleven, respectively [73]. A single SS/PBCH block corresponds to four OFDM symbols and is transmitted per slot at a fixed slot location.

In the light of the above-mentioned illustrating the diverse numerology of the NR system explicitly, the left hand side of Fig. 19 visualizes that the subcarrier spacings ranging from 15, 30, 60, 120 to 240 kHz correspond to the symbol durations ranging from 66.67, 33.33, 16.67, 8.33 to 4.17 μs, respectively, which is also analogous to the upper side of Fig. 4. As observed in Figs. 4 and 19, there exists an explicit inverse correlation relationship between the chip i(or symbol) duration and the corresponding bandwidth (or subcarrier spacing) in terms of each system of 3G and 4G as well as each mode in NR. Moreover, the right hand side of Fig. 19 illustrates how the number of slots in a single NR subframe duration of 1 ms scales with the subcarrier spacings having six scaling factors ranging from 1, 2, 4, 8 to 16, where a single slot comprises 14 symbols [4]–[7], [19]. In the perspective of the ICS, the support of the numerology implicitly means the followings. One is increased search space in the time-domain due to the scalable subcarrier spacing extension. The other is the feasibility of relatively long sequence for a boundary detection and channel estimation.

With the aid of Figs. 18 and 20, both figures visualize how both NPSS and NSSS sequences are allocated to 127 consecutive subcarriers in the frequency-domain, which range from the 8-th to 134-th positions. As portrayed in Fig. 20, eight and nine subcarriers at both extremities are void, which also range from the 0-th to 7-th positions and from the 135-th to 143-th ones, respectively. It is notable that NPSS and NSSS exploit the DC subcarrier, which is not used in LTE PSS and SSS mappings. Center frequency of both NPSS and NSSS is also aligned with that of NPBCH. Guard bands for both NPSS and NSSS sequences enable substantial reduction of interference. Therefore, both NPSS and NSSS are only occupied in 12 RBs constituting 127 subcarriers for SSs and 17 ones for empty spaces at both extremities. On the other hand, two NPBCHs of an SS/PBCH block occupy 20 consecutive RBs constituting 240 subcarriers [6], [7], [68]. Additional PBCH consisting of four RBs is allocated on each edge of NSSS as portrayed in Fig. 18. Bandwidth of an SS/PBCH block depends directly on its particular subcarrier spacing. More explicitly, a subcarrier spacing of the SS/PBCH block in FR1 is considered to be either 15 or 30 kHz corresponding to 3.6 and 7.2 MHz transmission bandwidths of the SS/PBCH block, respectively. On the other hand, for the sake of compensating for problematic phase noise at higher carrier frequencies of FR2, that of the SS/PBCH block is chosen as either 120 or 240 kHz corresponding to 28.8 and 57.6 MHz transmission bandwidths of the SS/PBCH block, respectively [73], [77]. UE postulates the same CP length and subcarrier spacing for both NPSS and NSSS in an allocated carrier frequency band [6], [7]. This is also true for NPBCH carrying basic cell configuration information. Furthermore, demodulation RS is used for NPBCH phase reference instead of using common RS in the LTE counterpart for decoding PBCH. Interestingly, the existence of multiple SS/PBCH blocks manifests that a variety of beamformed SSs can be feasible, which will be very effective for guaranteeing diverse NR coverages [5]–[8]. Based on the above-mentioned NR radio-frame structure, NR capable UE identifies at least OFDM symbol, slot, half radio-frame, and radio-frame timings by employing the SS/PBCH blocks. It is worth noting that NPSS, NSSS, and NPBCH are the only always-on three signals in NR.

C. INITIAL CELL SEARCH PROCEDURE PERSPECTIVE

The ICS procedure consists of timing recovery, frequency offset compensation, and finally cell ID detection. There is

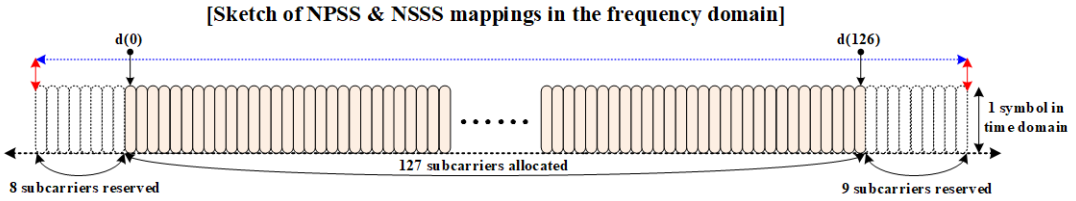

FIGURE 20. NPSS and NSSS mappings in the frequency-domain.

not much change in the cell identification in the sense that the hierarchical search for the cell ID is employed. For the frequency offset estimation, it is common with the legacy LTE system that the step-by-step estimation is invoked. One noticeable change is the radio-frame timing recovery exploiting DeModulation Reference Signal (DMRS) or NPBCH. This change implies a great deal of meaning because the NR system can come to overcome the inherent performance (i.e. detection performance) constraint of the legacy LTE system. Another remarkable feature is that the NR ICS procedure is in conjunction with beam sweeping, which is effective way to overcome the relatively insufficient link budget in the mmW spectrum bands.

LTE ICS only specifies that NPSS and NSSS from a serving cell can be broadcast with a particular antenna port chosen among ports 0 to 3, where the antenna ports are quasi co-located in terms of both associated Doppler shift and average time delay [42]. In comparison to two CDMA ICS operations, the LTE ICS does not assume a specific MIMO scheme such as the time-switched transmit diversity operation. Furthermore, NR ICS exploits SS/PBCH blocks so that analog beamforming becomes more feasible with higher flexibility compared with LTE ICS counterpart, which is an implementation issue in the perspective of a base station. More specifically, the number of antenna ports exploited for transmission of both NPSS and NSSS is set to 1, where the concept of antenna port has been introduced in LTE and is currently reused in NR. It is known as a logical abstraction of a physical resource, directly mapping to physical antenna elements. The number of the physical antenna elements being available is not necessarily the same as that of its logical counterpart [3], [6]. A single fixed number of antenna port(s) is allocated for NPBCH transmission. UE postulates that the numerology employed in transmission of both NPSS and NSSS is the same as that of NPBCH transmission [19]. In the followings, we describe the progress of IA by elaborating ICS procedures for the legacy LTE and NR systems.

1) INITIAL CELL SEARCH IN LTE

For the sake of reducing the complexity of the entire cell search, both W-CDMA and TD-SCDMA have adopted hierarchical cell search procedure [40], [41]. Similarly, LTE also follows the similar hierarchical cell search procedure to acquire PCI, which corresponds to the scrambling code employed to distinguish among Node-Bs in both W-CDMA and TD-SCDMA systems. A brief procedure of finding one out of 504 physical layer cell is portrayed in Fig. 13, where detection of the PSS indicates acquisitions of both slot and half radio-frame boundaries as well as finding one out of three physical layer identities. Similarly, detection of the SSS represents acquisition of radio-frame boundary as well as finding one out of 168 physical layer cell identity group. Then, the PCI can be obtained with proper serving cell timing information. Table 3 illustrates the entire search space of LTE ICS scenarios when W-CDMA, TD-SCDMA, LTE-FDD, TD-LTE, or NR is in active-RAT. To elaborate it a little bit further, the maximal time duration of the LTE-FDD and TD-LTE systems is set to 5 ms owing to its periodic PSS transmission. If original sampling rate of 30.72 MHz is down-sampled by 16,[8] the number of hypotheses in the time-domain becomes 9600. When considering three PSSs, the entire search space is determined as 28800 hypotheses. It is also noted that the attainable timing resolution is inversely proportional to bandwidth of the PSS. Hence, in case of the LTE DL, the timing resolution becomes just under $+/-$ 0.5 μs corresponding to roughly a fifth of the CP duration. Finding a start point of the peaky signal over the entire search space plays a pivotal role in the LTE ICS procedure. Now, let us investigate the details of the LTE ICS step-by-step.

Fig. 21 illustrates the details of the entire LTE ICS procedure in LTE systems, where the LTE ICS procedure may constitute three steps as a realization of its LTE ICS implementation [17], [18], [81]–[83]. Both steps 1 and 2 search are mandatory procedures, however the cell ID verification can be encompassed in the entire LTE ICS procedure to enhance the final cell search detection performance. It is noteworthy that cell-related information gained at each step may be changed depending on which detection schemes were chosen in the entire LTE ICS procedure. On each selected carrier achieved by carrier frequency search, which is portrayed in Figs. 7 and 21, the LTE ICS procedure moves into the step 1 search stage. During the step 1 search procedure of Fig. 21, symbol, slot, and half radio-frame timings as well as physical layer ID $N_{ID}^{(1)}$ ranging from 0 to 2 are acquired. By employing the received PSS, the coarse frequency offset

[8]The sampling rate of 30.72 MHz originates from the assumption that normal CP length is applied to each symbol having FFT size of 2048 for channel bandwidth of 20 MHz. The lengths of both the PSS and SSS are strictly less than or equivalent to 128. Therefore, down-sampled by 16 looks feasible rather than the original sampling rate, which induces higher processing speed and complexity to the following receiver design.

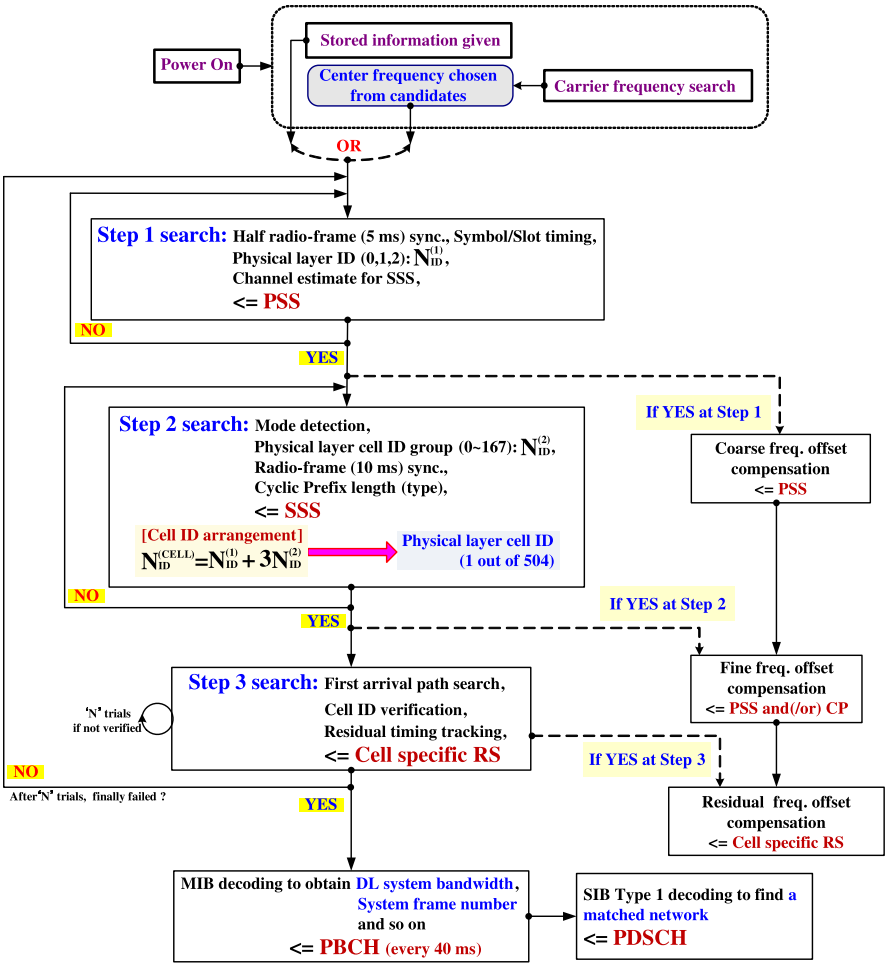

FIGURE 21. Detailed procedure of initial cell search in LTE constituting three steps and relevant frequency offset compensations, where PDSCH represents physical downlink shared channel.

compensation is also performed and is followed by channel estimation for detecting the SSS only if LTE-FDD mode is chosen. In case of TD-LTE, locations of both the PSS and SSS are not consecutively placed as visualized in Fig. 15. Therefore, UE may not guarantee reliable channel estimate for detecting the SSS at very high mobility situation due to the reduced coherence time. Accordingly, the non-coherent detection scheme without exploiting channel estimation may be a feasible solution. Then, during the step 2 search procedure of Fig. 21, radio-frame timing and physical layer cell ID group ranging from 0 to 167, $N_{ID}^{(2)}$ are achieved. The mode detection to choose either frequency division duplex or time division duplex as well as selection of CP type[9] are conducted. Subsequently, fine frequency offset compensation is further accomplished in order to reduce the remaining of frequency offset with the aid of PSS and(/or) CP. Finally, the physical layer cell ID is obtained by exploiting a relationship of $N_{ID}^{(CELL)} = N_{ID}^{(1)} + 3{\cdot}N_{ID}^{(2)}$. As an optional stage, the step 3 search procedure may be required for the UE to verify the serving cell ID by utilizing cell specific RSs. More explicitly, the procedure constitutes first arrival path search to align its FFT window with the first arrival path, followed by cell ID verification, where the entire 504 RSs correspond to 504 different cell IDs, respectively and hence a two-dimensional RS is capable of verifying a specific cell ID. After the step 3 search stage is finalized, residual frequency offset compensation should be activated to reduce still existing frequency offset by utilizing cell specific RS. Finally, the residual frequency offset becomes within the target range.

After the LTE ICS procedure has been completed, UE is capable of decoding the PBCH to read the MIB having DL system bandwidth, the system frame number and so on, where the PBCH is transmitted every 40 ms. Then, the acquisition of the system information can make the UE synchronized to both the time- and frequency-domains. In a realistic situation, a UE usually receive PSS/SSS/PBCH signals from several mobile network service providers. For the sake of identifying a predetermined mobile network, UE will proceed to acquire SIB Type 1 to find a matched network, where Physical Downlink Shared CHannel (PDSCH) having SIB Type 1 is transmitted

[9]In order to detect either of the CP type, two different CP lengths are exploited for distinguishing both the normal and extended CPs allocated in the SSS, respectively.

every 80 ms [18]. More explicitly, the UE may acquire multiple SIB Type 1's information from all nearby Node-Bs at both intra- and inter-carrier frequencies. According to the order of cell powers measured, the UE tries to check whether the identity gained from received SIB type 1 is matched to that stored in the USIM card of the UE until found. As opposed to traditional UE's connection only to one mobile network, it is noteworthy that Google Project Fi is able to intelligently link the UE to the best possible mobile network among multiple ones [84]. Accordingly, whenever LTE ICS is conducted, this approach may guarantee the highest-quality connection at the UE's position. Whenever normal communication starts, a UE moves into the connected mode. Depending on data services activated, a state of the UE moves back to the idle mode or keeps staying in the connected mode. In the connected mode, the compensation of the residual timing error and frequency offset estimations is required to maintain a best possible radio link continuously.

2) INITIAL CELL SEARCH IN NEW RADIO

For the sake of reducing the complexity of the entire cell search, W-CDMA, TD-SCDMA, and LTE have adopted hierarchical cell search procedure [40]–[42]. Similarly, NR also follows the similar hierarchical cell search procedure to acquire an NR cell ID. A brief procedure of finding one out of physical layer cells is portrayed in Fig. 12. Detection of both NPSS and NSSS is finally capable of obtaining the NR cell ID with an appropriate timing recovery of the serving cell, similar to the LTE counterpart [8], [27]. Table 3 also demonstrates entire search space of NR ICS scenario when NR is in active-RAT. During the NR ICS, the SS burst set period is fixed to 20 ms as a default value, which is four times longer than the transmission period of PSS and SSS in LTE in order to minimize a duty cycle of always-on SS transmission. Instead, in comparison to frequency channel raster[10] in LTE, a sparser raster in NR is necessary to mitigate the increased two-dimensional ICS burden induced by the sparser SS/PBCH block transmission periodicity. The transmission of SS/PBCH blocks within SS burst set is restricted to 5 ms [6]–[8], [65]. The maximum number of SS/PBCH blocks within the 5 ms duration denoted as L is determined according to the predetermined subcarrier spacing.[11] More explicitly, for carrier frequency ranges up to 3 GHz, from 3 to 6 GHz, and 6 to 52.6 GHz, values of L are set to four, eight, and 64, respectively [8], [65]. Basically, the search spaces of NR are scaled with the corresponding subcarrier spacings as portrayed in Table 7. First, let us ponder the case of basic subcarrier spacing, i.e. 15 kHz. When considering the lengths of NPSS and NSSS as well as their mappings in the frequency-domain [6], down-sampled by 16 from the original sample rate of 30.72 MHz can be utilized, which bestows us 1920 hypotheses for one subframe of 1 ms in the time-domain. Then, we have 38400 hypotheses from the default value of SS burst set period, i.e. 20 ms. Owing to the existence of three NPSSs, the resultant search space for the subcarrier spacing of 15 kHz becomes 115200. Finally, generalized search space is derived as $115200 \cdot N$, where the number of symbols is scaled based on the NR numerology with $N = 1, 2, 8,$ or 16 [8], [65].

From a selected carrier having the strongest signal power, NR ICS procedure commences by achieving a serving cell/sector's NR cell ID. Fig. 22 delineates detailed procedure of NR ICS constituting three steps operating at sub-6 GHz spectrum bands, i.e. 3.5 GHz and mmW spectrum bands, i.e. 28 GHz. As mentioned before, the overall NR ICS procedure is similar to that of the LTE system in a sense that the NR ICS procedure utilizes NPSS and NSSS. However, one noticeable feature of the NR ICS is the advent of new way of radio-frame timing recovery, which will be considered later. The NR ICS procedure is also composed of step 1 search, step 2 search, and step 3 search as well as NPBCH decoding to gain MIB as a final goal [8], [27].

As illustrated in Fig. 22, the first phase of the NR ICS encompasses a step 1 search as a timing recovery with a NPSS ID identification and coarse frequency offset estimation exploiting the NPSS. More explicitly, initial symbol and half-frame boundary timings to the NR cell can be acquired by detecting start position of the NPSS. Then, a coarse frequency offset estimation and compensation can be followed based on the specific NPSS having the detected NPSS ID. Here, the NPSS ID is denoted as $N_{ID}^{(1)}$, which ranges from 0 to 2. It is worth noting that the coarse frequency offset recovery is capable of reducing the existing frequency offset substantially, which makes the succedent step 2 search with more reliable detectability. Also, as a result of the NPSS ID detection, channel estimation of the NPSS becomes feasible so that the coherent detection of the NSSS can be utilized. The detection performance of NSSS is enhanced in comparison with that of NPSS, whose detection is performed via non-coherent detection. When contemplating beamforming aided NR ICS, the beamforming mode becomes optional at sub-6 GHz spectrum bands and mandatory at mmW spectrum bands, respectively. Beam sweeping is activated to obtain the most highly appropriate beam direction.

In the second phase of NR ICS, a cell identification as well as fine frequency offset estimation and compensation are accomplished as portrayed in Fig. 22. For the cell identification, step 2 search seeks for the NSSS ID. Here, the NSSS ID is denoted as $N_{ID}^{(2)}$, which ranges from 0 to 335. Consequently, the unique physical-layer cell identity is determined from an explicit relationship of $N_{ID}^{(CELL)} = N_{ID}^{(1)} + 3 \cdot N_{ID}^{(2)}$, which covers up to 1008 NR physical layer cells. In other words, their NR cell IDs range from 0 to 1007 [6], [7], [65]. Detection of

[10]Frequency channel raster represents a predetermined carrier frequency location exploited by UEs to detect SSs being present or absent when UEs initially camp on NR network.

[11]Within the 5 ms duration, multiple SS/PBCH blocks can be transmitted. Consequently, non-coherent combining of SS energy can be feasible for enhancing detection performance of SSs. Each SS/PBCH block can have a single beam or multi beams.

TABLE 8. Initial procedure comparisons for LTE and NR.

	LTE	NR
Step1	Symbol, slot, and half radio-frame (5 ms) boundaries	Symbol, slot, and SS burst set (5 ms) boundaries
Step2	Radio-frame (10 ms) boundary, mode detection, CP type, and cell identification	Only cell identification
Step3	First arrival path search and Cell ID verification	Radio-frame (10 ms) boundary, first arrival path search, and cell ID verification

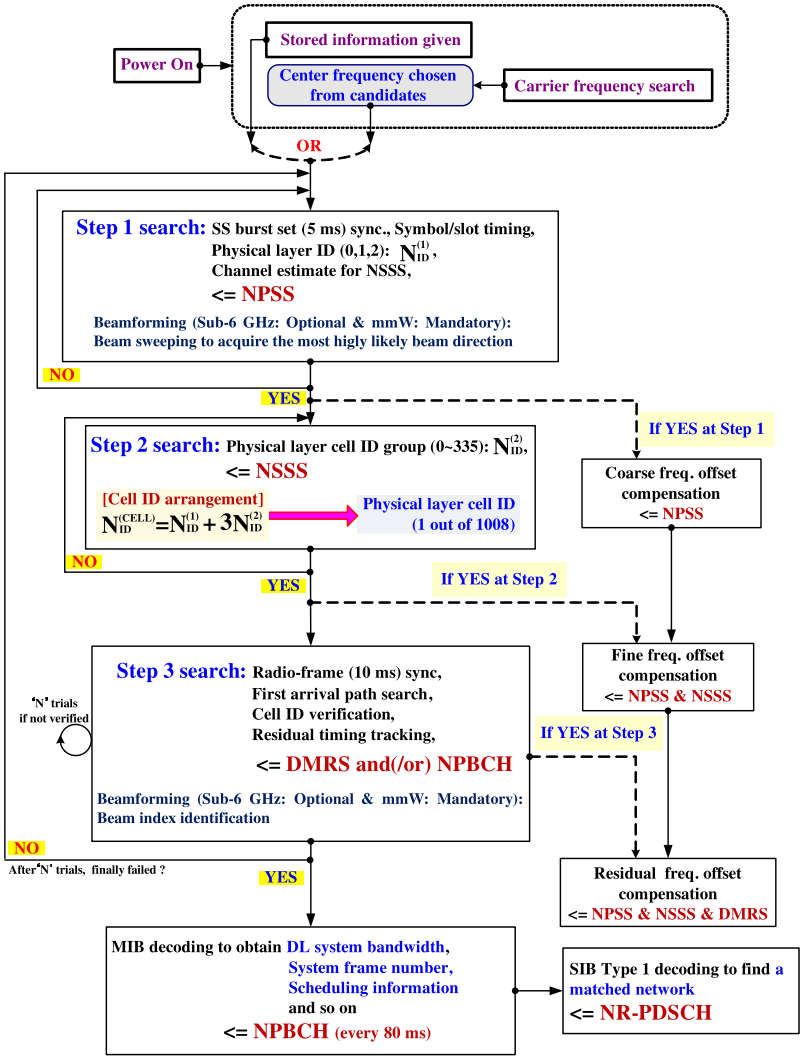

FIGURE 22. Detailed procedure of initial cell search in NR constituting three steps and relevant frequency offset compensations operating at sub-6 GHz and mmW spectrum bands.

received NSSS is also associated with a fixed relationship of SS/PBCH with NPSS location in terms of the time- and frequency-domains, irrelevant to specific conditions such as duplex mode and beam operation type. At the end of the successful step 2 search, the two SS sequences, namely NPSS and NSSS can be simultaneously employed to compensate the residual frequency offset more effectively, which we call as fine frequency offset estimation and compensation. It is worth noting that the NR ICS does not require integer frequency offset estimation and compensation procedure, which are required in the LTE ICS arisen by the inherent limitation of the ZC sequence.

For the sake of performing the NR ICS procedure, it is assumed that half radio-frames with SS/PBCH blocks in the serving cell occur with a periodicity of two radio-frames, namely 20 ms[12] [8]. From the fact that each SS/PBCH block has a periodicity of two radio-frames for the IA, it is

[12]A configurable periodicity ranges from 5 ms to 160 ms and a default period is set to 20 ms.

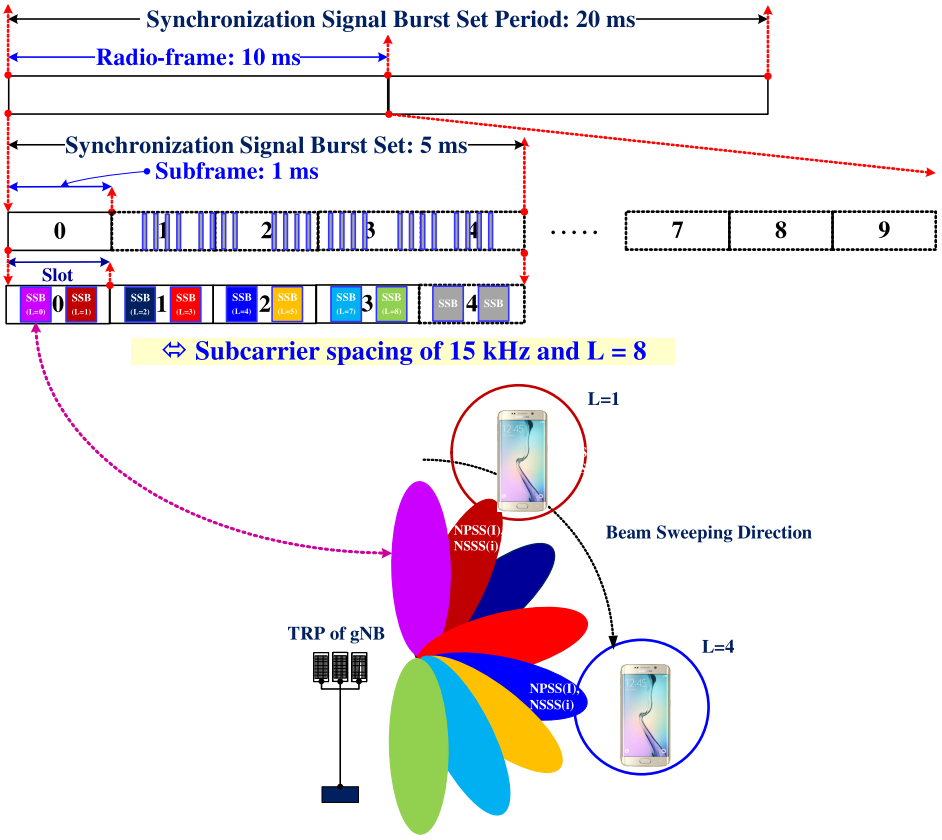

FIGURE 23. An exemplification of beam sweeping during initial cell search operating at mmW spectrum bands of a serving gNB when the subcarrier spacing is 15 kHz with $L = 8$ and two UEs are trying to gain a directionally aligned beam having the best possible strengths of both *NPSS*(I) and *NSSS*(i).

derived that the identification of SS/PBCH block index of l ($l = 1, 2, \cdots, L$) is equivalent to radio-frame timing identification. Accordingly, the SS/PBCH block index (a.k.a. beam index in Fig. 22) is provided to obtain NR radio-frame timing. It is worthy to note that each SS/PBCH block can be transmitted via a specific beam, which is a key functionality to overcome the insufficient link budget in the NR system [27], [85]–[89]. Specifically, the use of beamforming is an attractive way to solve cell coverage issue of NR ICS procedure in NR frequency bands possessing weak transmission characteristics of radio waves. DL sweeping time interval is required by one or multiple antenna array(s) configured at gNB for the sake of transmitting SSs directly related to the NR ICS procedure, where a DL sweeping time interval consists of multiple sweeping blocks. Fig. 23 illustrates an exemplification of the beam sweeping during ICS operating at mmW spectrum bands of a serving gNB when the subcarrier spacing is 15 kHz with $L = 8$. Here, L different beams are transmitted in the base station, which is called as beam sweeping [86] in the NR system.

For the successful NR frame timing, two plausible approaches to attain an SS/PBCH block index are feasible for the radio-frame synchronization. One way is to use a DMRS sequence index, where there is a one-to-one mapping between two least significant bits for $L = 4$ and three least significant bits for $L > 4$ as well as the DMRS sequence index. The other way transmits the SS/PBCH block index explicitly in NPBCH payload, where the NPBCH's bandwidth is set to 240 subcarriers over three default symbols [90], [91], where the part of the transmitted NPBCH payload bits forms the three most significant bits of the SS/PBCH block index when $L = 6$ [8]. Thus, only DMRS sequence index is sufficient to achieve radio-frame synchronization for sub-6 GHz band, which corresponds to $0 \leq L < 8$. On the contrary, both of the DMRS sequence index and NPBCH payload bit are required for radio-frame timing recovery when $8 < L \leq 63$, which covers above 6 GHz band. It is noted that the frame timing procedure in the NR ICS is different from that of the LTE ICS in the sense of utilizing the PBCH decoding. In other words, step 3 search and NPBCH decoding procedure are integrated especially for above 6 GHz band. In the perspective of the frequency offset estimation and compensation, more sophisticated estimation and compensation of the residual frequency offset become practicable due to the feasibility of the DMRS sequence after the step 3 search is completed. After getting through the whole NR ICS, the UE becomes ready for decoding the NPBCH to acquire the system information. Representative high layer parameters are SS/PBCH

indexes and a periodicity of SS/PBCH burst set through SIB Type 1. It is interesting to noting that the periodicity of SS/PBCH blocks may be assumed to be two radio-frames of 20 ms as a default value in the NR ICS [8], [53].

Beyond the progress of the ICS procedure in the NR system, there exist still technical issues to be settled in the evolution of NR system, which are overlapped with the present NR system. Among the constituent technologies based on the evolved NR standards, signal designs for both synchronization and channel estimation will be expected to be closely associated with high-speed mobile communication over 500 km/h. Basically, the common issue is that those synchronization and reference signals should guarantee robust detection performance by leveraging both autocorrelation and crosscorrelation characteristics. The robustness of the sequences should also be contemplated when the residual frequency offset exists, which is of critical importance in the high-speed Doppler channel environment. In order to address the issue, NPSS has replaced the conventional ZC sequence with newly defined m-sequence, because the problem of undesirable correlation characteristics disappears when the residual frequency offset leads to the detrimental integer frequency offset. Hence, optimal designs for the synchronization and reference signals will also be an open issue in the evolution of NR systems. Up to date, a class of m-sequence and gold sequence has been considered typically for guaranteeing stable autocorrelation and crosscorrelation properties. In a practical sense, there is another crucial issue that supports a sufficient number of code sequences, namely acquisition of adequate cell IDs to cover an entire NR network. For that, a pure gold sequence cannot be employed due to the limitation of the number of feasible sequences. Therefore, the novel sequence design based on a variation of two sequences can be expected to the evolution of NR systems.

Essentially, high speed environment resulting in high Doppler frequency becomes of critical importance as the carrier frequency increases, i.e. in case of operating at 28 GHz. Thus, it is inevitable to overcome an extremely shorter coherent time originating from very fast fading environment, which also arises the corresponding smaller symbol duration. A natural way to handle the very fast fading channel is two-dimensional resource allocation in time- and frequency-domains for the synchronization and reference signals. For the resource allocation, there is a trade-off between performance and resource overhead. Accordingly, a reasonable signal design should jointly be optimized with the signal allocation for satisfying the performance requirements, i.e. SS detection performance and NPBCH decoding capability. In addition, the set of more sophisticated DMRS to support high speed environments should further be investigated for coherent mobile communications such that the symbol duration is within the order of channel coherence time.

When postulating beamformed signals, every UE may not recognize the number of physical beam(s) to be transmitted at gNB and it is also not sure whether the UE experiences the same physical beam(s) across different SS/PBCH blocks within an SS burst set. Based on the amount of predetermined information, the detailed NR ICS procedure can be specified optimally. During the NR ICS procedure particularly operating at 28 GHz, for the sake of mitigating severe path loss, the exploitation of beamforming functionality is explicitly one of the essential capabilities [19]. Detection of beamformed SSs plays a crucial role in NR ICS procedure to achieve sufficient coverage extension [75]. NR should design both single-beam and multi-beam based ways to transmit SSs. When contemplating the multi-beam based operation, UEs are capable of receiving SSs for a shorter duration if gNB transmits SSs in a beamformed manner. Better orthogonality among adjacent cells results in significant reduction of inter-cell induced interference, which is quite beneficial under heterogeneous multi-cell environments [25], [92]. Single beam approach can be a special case of multi-beam approach. It is assumed that gNB does not support any prior information about preferred beam patterns for a UE during the NR ICS stage. UE must decide the best possible pair of transmitted and received beams [4], [19], [54], [73], [75]. If either analog or hybrid beamforming is contemplated for the NR ICS procedure, the SSs should be transmitted or received along only one or few beam direction(s) in one sweeping block due to the limited number of radio frequency chains [93]. The narrow beams in all the sweeping blocks of a sweeping time interval are able to cover the entire serving area. Therefore, with the help of the steering of phase shifter the multi-beam transmissions on a predetermined pattern of sweeping blocks are known as beam sweeping. In case of digital beamforming supporting higher flexibility, all the narrow beams can be transmitted or received simultaneously in a single sweeping block at a cost of increased number of radio frequency chains directly proportional to the entire number of multi-beams, which usually becomes unrealistic [25], [92], [92]–[95]. Here, the order of beam sweeping and the employment of single-beam or multi-beam at each SS/PBCH block are under an implementation issue [25], [92], [94], [95].

D. SUMMARY AND LESSONS LEARNED

In Section III, we have commenced by providing profound insight into the following nine key findings:

- With the aid of the diverse numerology in the time- and frequency domains as depicted in Fig. 19, flexibly allocated multiple subcarrier spacing categories in the NR system result in further scalability in the radio-frame structures in comparison with the LTE system providing only one subcarrier spacing of 15 kHz.
- As portrayed in Figs. 4 and 19, there exists an explicit inverse correlation relationship between the chip (or symbol) duration and the corresponding bandwidth (or subcarrier spacing) in terms of each system of 3G, 4G, and NR.
- Owing to inherent uncertainty issue of ZC sequences arising integer frequency offset, both NPSS and NSSS in NR have been devised based on m-sequences.

- Unlike LTE, a common radio-frame structure is exploited, irrelevant to any duplex mode in NR.
- Compared with LTE, three SSs represented as NPSS, NSSS, and NPBCH are the only always-on signals in NR.
- The frame synchronization acquisition method has changed completely from utilizing SSS in LTE to leveraging NPBCH decoding or DMRS index identification in NR.
- The existence of multiple SS/PBCH blocks is capable of supporting a variety of beamformed SSs, which becomes a key functionality to overcome the insufficient link budget and finally guarantee diverse NR coverages.
- An NR periodic SS transmission interval becomes four times longer than that of two SSs in LTE in order to minimize a duty cycle of always-on SS transmission while in comparison to frequency channel raster in LTE, a sparser raster in NR is to compensate for the increased two-dimensional search space burden.
- Complexity reduced hierarchical cell search procedure has been adopted in 3G, 4G, and NR to acquire cell IDs.

Figs. 14 and 15 visualized the radio-frame structures of LTE-FDD and TD-LTE, respectively, exploited for ICS procedures. Figs. 16 and 17 also portrayed both PSS and SSS mappings in the frequency-domain, respectively. The details of SS/PBCH block and the overall NR radio-frame structure have been illustrated in Fig. 18. With the aid of Fig. 20, both NPSS and NSSS mappings in the frequency-domain have been manifested. In order to dive into ICS procedures in three OFDMA systems, at first simultaneous multi-connectivity in 3G, 4G, and NR systems as well as a simplified NR ICS have been introduced in Fig. 12. Fig. 13 elucidated a macroscopic view on ICS flow exploited in active-RAT mode of LTE system. By utilizing the detailed taxonomy classification of Fig. 3 articulating timing synchronization, frequency synchronization, and finally code/cell identification, the details of the entire ICS procedure have been visualized in Fig. 21 for LTE as well as Figs. 22 and 23 for NR, respectively. Especially, Fig. 22 delineated exact procedures of NR ICS operating at both sub-6 GHz spectrum bands and mmW spectrum bands. An exemplification of the beam sweeping has also been delineated in Fig. 23. Sparseness of SSs' transmission resource led to multi-step aided approach for guaranteeing reliable target performances. More explicitly, timing synchronization and frequency offset estimation were processed in parallel as portrayed in Figs. 21 and 22.

Entire search spaces, sequences chosen for ICS procedures, and the core ICS procedures for three OFDMA systems have been compared in Tables 3, 6, and 8, respectively. In Table 8, similar algorithm design issues in Table 5 are applied essentially and therefore omitted. Table 7 has summarized the number of symbols and slots in a single NR radio-frame scaling with the ratio of the corresponding subcarrier spacing. Moreover, Tables 3 and 7 articulated that the search spaces of NR are also scaled with the corresponding subcarrier spacings. Due to inherently similar channel structures harmonized for both frequency and time division duplexes, the three step-aided ICS procedures of two LTE systems became overlapped and therefore have shared a substantial portion of constituting algorithms, which can be a distinct advantage over the corresponding CDMA counterpart. As an evolved OFDMA system to resolve frequency synchronization issue inherently arisen in ZC sequence, to reduce frequency domain search space, and to minimize synchronization resource transmission, the NR has substantiated a further optimized ICS procedure to satisfy multiple numerologies associated with diverse spectrum bands ranging from sub-6 GHz to 52.6 GHz. Both LTE and NR ICS procedures do not leverage any specific MIMO scheme compared with two CDMA families. Only a single antenna port is assigned for transmission of relevant synchronization signals. By our deep discussions of all the ICS flows and their relevant details, we manifested a potential on understanding systematic ICS flow of any hybrid OFDMA related system to be devised for beyond 5G configurations. It is worthy to note that our TCS counterpart working at three OFDMA systems has been guided in [9].

IV. A CONTEMPLATION IN INTELLIGENT WAYS OF DESIGNING MULTI-MODE MOBILE STATION MODEM AND FUTURE DIRECTIONS

A. ENTIRE CELL SEARCH OPERATIONS OVER DIVERSE SPECTRUM BANDS

Fig. 24 exemplifies a macroscopic view on entire cell search operations in conjunction with intelligent cell search system controller under heterogeneous cell environments, where numbers one to four inside the corresponding circle represent intelligence based carrier frequency searcher, ICS and TCS procedures in Radio Resource Control (RRC) states, and intelligent cell search system controller for UE, respectively. Let us take a look at diverse spectrum bands allocated for 2G, 3G, 4G, 5G, and possibly 6G systems. The bottom part at the right hand side of Fig. 24 articulates how spectrum bands are assigned for 2G, 3G, and 4G systems. Originally, sub-3 GHz spectrum bands had been assigned for 2G, 3G, and 4G systems. 3.5 GHz spectrum band has also been allocated for 4G system in order to improve user throughput significantly. By contrast, for the sake of operating 5G system, spectrum bands of the top part at the right hand side in Fig. 24 are classified into two categories, namely sub-6 GHz spectrum bands can constitute 600 MHz, 3.3 to 4.2 GHz, and 4.4 to 5.0 GHz bands as well as above 6 GHz spectrum bands may include 24.25 to 29.5 GHz, 37 to 56.2 GHz, 60 GHz, and 64 to 71 GHz [9], [74], [96]. Additionally, further higher spectrum bands for both 5G and 6G systems such as 100 to 300 GHz and 0.3 to 10 THz will be of very high interests.

The essential roles of the RRC protocol embrace mainly (1) RRC connection's establishment, (2) RRC connection's release, (3) reselection, and (4) system information broadcast. The fundamental operations of the RRC protocol are elucidated by a state diagram, which articulates specific states that a UE can stay in. Both RRC states and their transitions

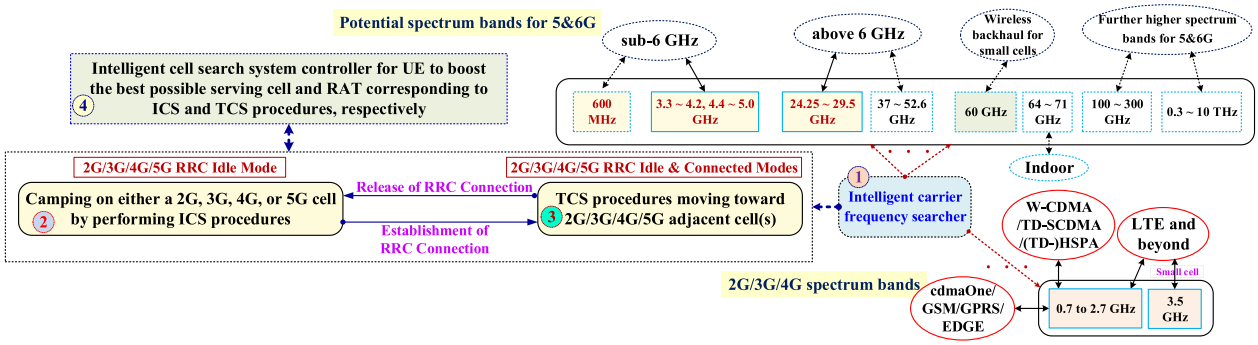

FIGURE 24. An exemplification of entire cell search operations amalgamated with intelligent cell search system controller under heterogeneous cell environments, where HSPA and TD-HSPA exhibit High Speed Packet Access and Time Division-High Speed Packet Access, respectively.

play a crucial role in allowing 3G, 4G, and 5G networks to balance radio resources among mobile users linked and to facilitate power-efficient operation during user data being not assigned. As portrayed in Figs. 7 and 24, entire states in 3G and 4G systems constitute RRC_CONNECTED and RRC_IDLE modes [9], [97]–[99]. Those in 5G NR consist of RRC_CONNECTED, RRC_INACTIVE, and RRC_IDLE modes [9], [100]. When UE is turned on, it enters RRC_IDLE mode and tries to camp on either a 3G, 4G, or 5G cell, which is directly associated with ICS procedure exploiting previously stored information. Then, the RRC connection becomes established between the UE and its serving radio network controller. The UE switches to the RRC_CONNECTED mode and the following TCS procedures commence [9]. Otherwise, as visualized in Figs. 7 and 24, carrier frequency search is activated to search all the existing spectrum bands involved in 2G, 3G, 4G, or 5G systems.

In order to boost overall performances of classic mobile station modem, the joint harmonization of the entire ICS and TCS performances over multi-RAT scenarios becomes crucial for guaranteeing the modem's always-on mobility. Intelligent systems leveraging deep learning's full potential on inherent data-driven characteristics have exhibited to outperform typical ones exploiting classic model assumptions and approximations. With the help of a huge volume of data gained from a composite network comprising 3G, 4G, and 5G systems as well as intelligent situational awareness system controller, big data aided deep learning techniques can be contemplated as one of cornerstones required for designing the future intelligent mobile network [9], [101]–[107]. More explicitly, the exploitation of deep learning methodologies is classified into three categories, namely network-level intelligent system controller, deep learning aided beam sweeping, and model-driven deep learning approaches for detection schemes of selected communication blocks. The optimum design of the intelligent cell search system controller manifests the most important open challenge in order for UE to determine the best possible serving cell in terms of reliable communication and the best possible RAT with respect to (1) Seamless handover, (2) Overall system performance, and (3) Scarce resource management. It is noted that the intelligent beam sweeping strategy is capable of reducing initial beam establishment time substantially, which will be detailed in the followings. Furthermore, deep learning based signal detection schemes are capable of substantially enhancing the achievable performance of each separate module in an entire transceiver, particularly when contemplating (1) the joint optimization of the classically operating modules and (2) the corresponding communication channels being hard to be attained by analytical models [108]–[110]. To elaborate it a little bit further, a data-driven joint channel estimation and signal detection algorithms have been devised in [108] and even a deep learning aided MIMO detection schemes have been proposed in [110]. By leveraging the above-mentioned detection approaches, detection schemes optimal for the existing cell search framework can be viewed as deep learning assisted classification, which may articulate a great potential for exploring systematically designed intelligence aided cell search constituting a hierarchical structure.

B. INTELLIGENT ICS SYSTEM CONTROLLER AND DEEP LEARNING DRIVEN BEAM SWEEPING APPROACH

With the adoption and further evolution of NR system, a set of the intelligent controllers is flexibly to balance the total network throughput under all the existing 2G, 3G, and 4G networks as well as novel 5G one in a systematic manner. Banal ways of harmonizing many key parameters in a classic manner are incapable of guaranteeing a timely effective optimization through adaptively established heterogeneous networks. By leveraging the enormous volume of data gained from NR network and the relevant intelligent decision making system controller, big data boosted deep learning assisted approaches enable to be contemplated as a cornerstone of NR network design. More explicitly, deep learning aided method processes the gigantic volume of data and extracts latent critical features. With the help of the attained essence, intelligent decision-making role enables to optimize the NR network. From the UE perspective, a set of intelligent controllers in Fig. 25 consists of (1) Intelligent system performance controller, (2) Intelligent resource management controller, and (3) Intelligent cell search system controller, each of which

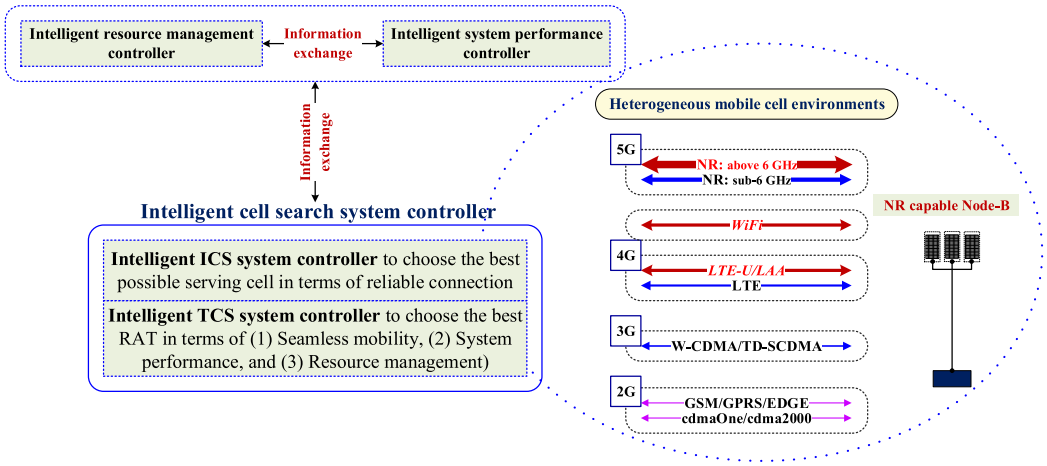

FIGURE 25. A visual diagram of integrated intelligent cell search system controller leveraging deep learning's potential, where the system controller constitutes (1) Intelligent ICS system controller and (2) Intelligent TCS system controller.

may exploit its own deep learning aided method and attained information can be shared and reused among three intelligent controllers [9].

For the sake of leveraging full potential on data-rich NR network, the best possible design of the intelligent cell search system controller becomes the most crucial open challenge, because UE must explore the best possible RAT and serving cell under complicated and unexpected network environment. It is worth noting that the realization of the intelligent controllers is under manufacturers' design issue and our main objective is only to introduce basic tasks of the intelligent cell search system controller portrayed in Fig. 25. Even though our companion paper has fully detailed the role of intelligent TCS system controller as evidence by [9], from the integrated system controller perspective, the system controller constitutes (1) Intelligent ICS system controller and (2) Intelligent TCS system controller. The ICS system controller can intelligently aid in timely decision making of reliable serving cell selection and guaranteeing the seamless transition to normal communication operations of individual user, where the system controller operates under heterogeneous mobile cell environment being composed of 2G (cdmaOne/GSM/GPRS/EDGE), 3G (W-CDMA/TD-SCDMA), 4G (LTE/LTE-U/LAA), 5G (NR: sub-6 GHz and above 6 GHz), and WiFi systems. To elaborate its role a little bit further, by leveraging the intelligence aided ICS system controller utilizing all the given information, the initially formidable search space arisen by the sub-6 GHz and mmW spectrum bands may be decreased efficiently. Furthermore, the system controller may benefit from a reduced set of spectrum bands to be searched. If ICS trials are not successfully conducted on a particular RAT such as NR mode, the system controller activates another ICS trial in a suggested RAT as visualized by Fig. 7. Therefore, the strategic exploitation of the substantial volume of relevant data and its associated deep learning technics enables to pave a pivotal way of optimizing the efficient intelligent ICS system controller meeting complicated control requests under intricately heterogeneous mobile cell environment.

As illustrated in Fig. 23, ICS operating at mmW spectrum bands performs beam sweeping to overcome severely deteriorated path loss. Based on the existing 5G specification, the employment of any conventional beam sweeping approaches may take time overhead of a half radio-frame (5 ms) for the sake of completing initial beam configuration [6]. In literature, deep learning algorithm aided beam selection approaches, compatible with the 5G specification, have been investigated [111]–[113]. Interesting results of the deep learning driven methods shed light on a critical issue arisen by a conventional scheme such as exhaustive search assisted beam sweeping method under specified mobile assumptions and environments. As visualized in Fig. 26, performance criteria can be classified into three categories, namely (1) Search space reduction approach, (2) Reduced use of reference signals, and (3) Detection theory related approach. To elaborate it a little bit further, according to [111]–[113], the search space reduction approach is directly related to beam search space reduction and beam sweep time reduction.[13] The reduced use of reference signals is associated with both efficient transmission of resources at transmitter and sophisticated signal acquisition algorithms at receiver. Finally, the detection theory based algorithms should strike a balance among high beam detection probability and low beam misdetection probability.[14] Possible inputs of the deep learning driven beam sweeping algorithms are considered as (1) Signal to interference plus noise ratio, (2) Received signal strength, (3) Power delay profiles,

[13] Beam sweep time is defined as a time duration taken to sweep a specified number of beams. The time is linearly proportional to the number of beams swept and dominates mean ICS time.

[14] If maximum likelihood detection scheme is assumed, a summation of detection probability, misdetection probability, and false alarm probability goes to 1 [22].

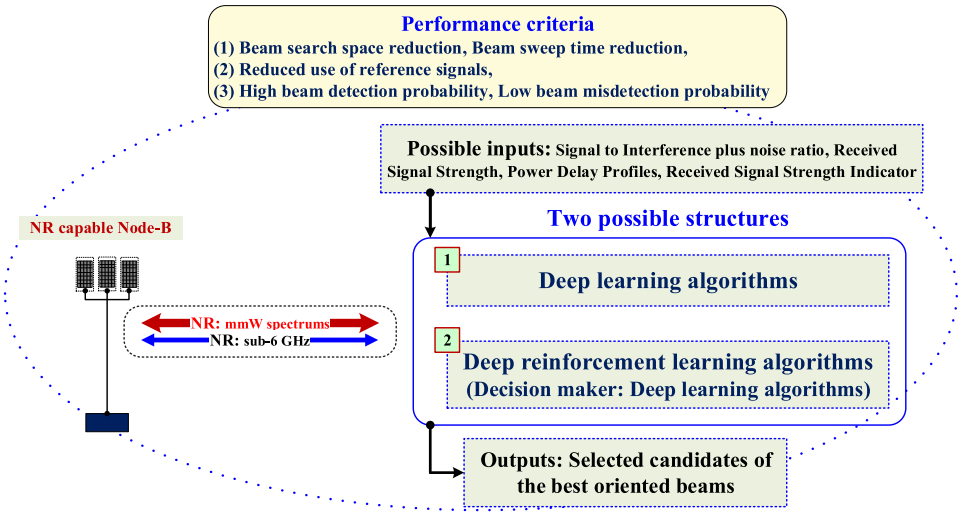

FIGURE 26. A visualization of deep learning driven beam selection approaches under mmW spectrum bands proposed for beyond 5G systems.

(4) Received signal strength indicator.[15] Results of [111] has manifested the exploitation of sub-6 GHz channel information to acquire candidates of the best oriented beams required for mmW spectrum bands. As a main input of the deep learning algorithms in [111], multi-path channel's power delay profiles under sub-6 GHz spectrum band have been chosen to estimate key channel characteristics as fingerprint of UE position. Two possible structures can constitute (1) Typical deep learning algorithms and (2) Deep reinforcement learning algorithms having a typical deep learning algorithm as a decision maker.[16] Then, outputs of the above-mentioned deep learning algorithms suggest selected candidates of the best oriented beams having their own probabilities. Accordingly, by leveraging the best possible combination of the above-mentioned demonstrated in Fig. 26, feasible deep learning driven beam selection approach enables to resolve the critical issue in beyond 5G systems operating over mmW and further higher spectrum bands.

C. INTELLIGENT MULTI-MODE MOBILE STATION MODEM AND FUTURE DIRECTIONS

When considering extremely wide bandwidth boosted beyond 5G communications operating at both mmW and THz spectrum bands, low resolution based signal processing becomes a vital power efficient approach. More specifically, the exploitation of one-bit resolution is to reduce the target system's complexity substantially. Furthermore, convolutional neural network and its variant such as deep residual learning have been well suitable for a design of robust and efficient carrier frequency estimator, where a single bit carrier frequency estimation problem was contemplated as a learning problem and hence the corresponding nonlinear function has been accurately approximated to beat conventional benchmarks in terms of performance metric [115]. The classic detection approach can be formulated as a multi-class classification problem with the aid of diverse levels of situational awareness gaining particular features. The situational awareness aided detection scheme leveraging a potential on deep learning is possible to provide meaningful side information and therefore to result in considerably enhanced detection performance under well-structured knowledge of the surrounding environment. Accordingly, we are required to approximate a certain function linking the situational awareness to the optimal solution [116], [117].

For the sake of meeting the requirement, we would provide a key summary on the model-driven deep learning approaches to be substituted for classic detection schemes [118]. The exploitation of an entirely data-driven deep learning methodology becomes the most attractive approach to enhance important fields such as computer vision and natural language processing, which does not employ both exact mathematical model and specific domain knowledge. Similarly, each individual processing block of the entire wireless communication system is based on the deep neural network structure, represented as a black box. Therefore, the most existing endeavors focus its main attentions on the utilization of a gigantic volume of labeled data arising enormous computing resources and extensive processing time, which are scarcely gained in typical communication systems. On the other hand, the model-driven approaches incorporating the known physical behavior and prior domain knowledge of the wireless communication system, for example, accurately designed channel models and information theoretic features, are capable of reducing the number of parameters to be learned, decreasing the considerable requests for computation

[15]Received signal strength indicator stands for linearly averaged entire received power measured only in specified OFDM symbols inside the measurement bandwidth over a predetermined number of resource blocks [114]. The information can be exploited for enhancing detection performance further.

[16]Further details on a basic principle of the deep reinforcement learning and how it has been used for TCS scenarios are well provided in [9].

resources during training phase, and hence enhancing the training efficiency of selected processing blocks. Such efforts enable to leverage the wireless communication system topology based on analyzed physical layer mechanisms and the corresponding domain knowledge. Accordingly, only a limited number of critical parameters are necessary to optimize a chosen deep neural network in a supervised learning manner, which guarantees both a shorter period of training phase and even less training data set compared with a regular training process of the deep neural network. The model-driven deep learning strategy becomes a promising approach for intelligent physical layer communications, because at least approximated or simplified results of the mathematical analyses have been sufficiently verified and are available in literature. Therefore, the specific domain knowledge accumulated through high intensive research endeavors conducted in wireless communications society can be employed in an efficient manner. Moreover, unknown non-linear function approximation capability of deep learning can also be leveraged in designing of the physical layer of future wireless communication systems in order to attain substantial enhancements compared with classic approaches. Presumably, a crucial use case of exploiting deep learning in beyond 5G communications is capable of approximating well-known however computationally formidable algorithms. Namely, there are quite a few exemplifications of iterative algorithms asymptotically exploring a local (or global) optimum point in terms of an optimization problem however requiring a high number of iterations for their convergences with complicated operations in each iteration. Accordingly, successful leverage of deep learning can be achieved by identifying each task in beyond 5G communication systems manifesting a distinct lack of an optimal approach, which articulates a highly-likely opportunity to defeat the state of the art. Furthermore, from the complexity reduction perspective, the existing algorithms and complicated hardware structures can be designed in an efficient parallel processing manner [119].

A great potential on the model-driven deep learning enables to leverage the advantages of the model-driven approaches and evade the high requests for precise modeling, which substantially compensate for degenerated system performance induced by the inaccuracy of the model and predefined parameters [118]. Parts of the communication processing blocks can be preserved and the model-driven deep learning approaches can also be adopted for chosen blocks. Then, a careful design of the system enables to strike a balance between overall system performance and training efficiency [108], [120]. By adding always-on intelligence to well-designed cell search flows and sophisticated deep learning based detection schemes, their harmonization will play an essential role in realizing the best possible intelligent cell search modules and its corresponding system controller operating on the multi-mode mobile station modem.[17]

To elaborate it a little bit further, as visualized in Fig. 24, the intelligent system controller covering carrier frequency search, ICS procedures, and all the TCS scenarios must be designed for the future intelligent multi-mode modem. It is worth noting that a design of the intelligent system controller is under implementation issue, however its realization will lead to maximizing the proposed modem's capability.

With proliferation of artificial intelligence induced applications, the commercial modem design must encompass a dedicated hardware accelerator to foster ultra low latency on power-efficient artificial intelligence assisted inferences, where the accelerator becomes crucial for pursuing a high degree of parallelism and is referred to as different names such as neural processing unit, tensor processing unit, or others [121]–[123]. The intelligent multi-mode mobile station modem can comprise (a) application-specific integrated circuit, (b) specific purpose digital signal processor, (c) ARM chip, and (d) dedicated hardware accelerator for artificial intelligence boosted inferences, indicated as alphabetical characters a to d inside the corresponding circle, respectively in Fig. 27. Constituent components of the modem are further illustrated as follows:

Component (a)'s role is aiming for classic hardware accelerator to implement key components working continuously at chip (or half-chip) level for CDMA systems or symbol level for OFDMA systems. Hence, the examples of satisfying the objective are a bank of matched filters, a set of FFTs, and so on. Component (b)'s role aims at realizing most of cell search detection algorithms in conjunction with the corresponding component (a). Component (c) is required for designing a role of classic cell search scheduler covering both signal controls at physical layer and those at higher layers. Finally, component (d) is a dedicated hardware accelerator to facilitate an ultra low latency on power-efficient artificial intelligence boosted inferences. Accordingly, core algorithms of the intelligent system controller are mainly implemented on the component (d). The intelligence aided cell search operating on the multi-mode modem of Fig. 27 are also categorized as model-driven deep learning based signal detection schemes and intelligent system control. The signal detection scheme for each communication module can constitute both classic communication algorithm as initialization and the following refined neural net [118], where the former and the latter represent a combination of (a) and (b) as well as that of (d) and (b), respectively.[18] More specifically, each novel module is capable of initializing the classic algorithm chosen for the module and then amalgamating it with a refined neural network to boost the model-driven deep learning capability.

An enormous volume of data related to hundreds of billions of wirelessly linked devices, machines and human beings is required to be gained and exploited in beyond 5G systems [124]. As advocated by diverse daily life applications and even wireless communication society, an explicitly

[17]Our companion paper has exhibited full details of intelligence based TCS system controller [9].

[18]It is also noted that the intelligent cell search system controller can be a harmonization of (d), (b), and (c).

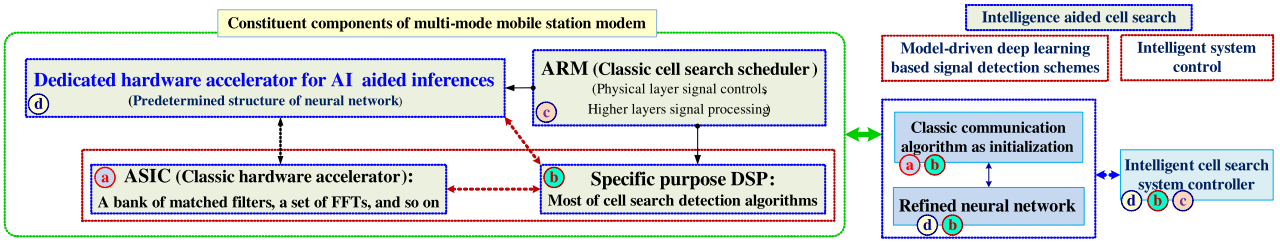

FIGURE 27. An exemplification of multi-mode mobile station modem and intelligence aided cell search algorithms constituting two stages, where AI, ASIC, and DSP represent Artificial Intelligence, Application-Specific Integrated Circuit, and Digital Signal Processor, respectively.

powerful booster leveraged for future wireless communications is surely artificial intelligence. Our proposed systematic approach maximizing full intelligence will lead to the greatest way of clarifying the forthcoming beyond 5G systems in terms of cell search. The commercial multi-mode modem is capable of functioning on virtually all 2G to 5G commercial mobile networks. To elaborate it a little bit further, the modem can constitute (1) cdmaOne (Interim Standard-95) and its evolutions, (2) GSM, GPRS, and EDGE, (3) W-CDMA and High Speed Packet Access, (4) TD-SCDMA and Time Division-High Speed Packet Access, (5) LTE-FDD, TD-LTE, and their derivatives, as well as (6) NR and its enhancements.

In order to realize feasible evolutions of the IA, the following three research directions may be of high interests.

(1) It is more effective that the exploitation of the beamforming technology is in conjunction with positioning [125]. More explicitly, the core essence is that the energy efficient beamforming becomes feasible when additional but beneficial location information gained by NR capable UE is even available at the stage of the IA. To illustrate it a little bit further, the availability of the UE's location might be guaranteed since the ranging information from non-negligible multiple cells can be acquired to accomplish a localization based on a specific approach such as triangulation method [126]. One typical exemplification is the one-dimensional high mobility support for high speed train, whose route is predetermined [127]. Specifically, with the aid of the predetermined mobility pattern of the high speed train, in the perspective of implementations, the analog beamforming pattern can be predesigned and optimized. Then, the analog beamforming can be applied to the maintenance of robust wireless links between gNB and UEs on a high speed train [128].

(2) Systematic design for a further interesting evolution of the IA should be handled for more sensitive frequency uncertainty in the evolution of NR system, which comes mainly from the support for ultra high speed mobility such as Hyperloop transportation system, traveling at top speeds of 1200 km/h [129]–[132]. The critical design issue involves the determination of the coherent length of the synchronization sequence and the accuracy of the commercial crystal oscillator experiencing both the very high carrier frequency and its residual frequency offset. In addition, based on the numerology in NR, a longer synchronization sequence can be contemplated so that cell identification is capable of being more flexible beyond the present three step-aided cell identification employed in both LTE and NR ICSs. It is worthy noting that the detection performance for the synchronization signal is affected by not only the aggregated frequency offset but also the coherent length relating to correlation properties of the delicately designed synchronization sequence. For the sake of further enhancing the detection performance, the coherent detection should be devised based on the estimated channel state information at the ICS stage. Even though powerful benefits of the coherent detection have been widely utilized since adopted in the 2^{nd} stage of ICS operating in the two 3G CDMA systems, under line-of-sight dominant propagation environments, this technique is still expected to be attractive and be further extended at the cost of high computational complexity arisen by estimating the channel state information.

(3) In addition to our discussions involved in the intelligence based cell search design and the corresponding intelligent system controller, overall ICS process can be interpreted as a state transition diagram [29]. Not only improving the detection performance itself but also optimizing a penalty time due to false detection are crucial for minimizing a mean acquisition time in terms of the diagram, which manifests the ultimate total synchronization performance. Consequently, more intelligent and sophisticated system designs associated with big data aided deep learning techniques should be required for achieving a particular synchronization performance requirement such as a harmonization of detection probability, false alarm probability, miss-detection probability, and mean acquisition time [14], [133].

D. SUMMARY AND LESSONS LEARNED

In Section IV, with the aid of Fig. 24, we have investigated the following four key factors.

- Various spectrum bands allocated for 2G, 3G, 4G, 5G, and possibly 6G systems.
- A macroscopic view on the entire cell search operations under heterogeneous cell environments.
- The key roles of the RRC protocol embracing four essential purposes and a summarized illustration of how UE operates through RRC states to perform both ICS and TCS.
- The optimal design of the intelligent cell search system controller covering carrier frequency search,

ICS procedures to select the most reliable serving cell, and all the TCS scenarios to choose the best possible RAT.

Then, Figs. 25 and 26 have conceptualized both intelligent ICS system controller and deep learning driven beam sweeping approach as follows.

- Sketch of the integrated intelligent cell search system controller leveraging deep learning's potential, consisting of both intelligent ICS and TCS system controllers.
- A potential on deep learning driven beam selection approaches under mmW spectrum bands proposed for beyond 5G systems.

Thirdly, Fig. 27 has visualized the two key design elements of the intelligent multi-mode mobile station modem as follows.

- Structure of the commercial intelligent modem having a dedicated hardware accelerator proposed for artificial intelligence boosted inferences.
- A potential on the intelligence based cell search algorithms constituting two stages, namely model-driven deep learning based signal detection schemes and intelligent cell search control.

Moreover, for the sake of clarifying feasible evolutions of NR with respect to ICS, we contemplated some imperative features, which are categorized into three challenges as follows:

- Specialized ICS by benefiting from synergy effect on both beamforming and positioning in order to optimize the one-dimensional high mobility support for high speed train.
- Systematic design for an ultra high speed mobility under Hyperloop transportation system by conducting the exploration of the delicately designed synchronization sequences and devising the robust coherent detection schemes optimized for line-of-sight dominant propagation environments.
- Deep learning boosted essential cell search parameter optimization by achieving the best-possible trade-off point among detection probability, false alarm probability, miss-detection probability, and mean acquisition time.

Based on our aforementioned details of the future modem design philosophy, we articulated a potential on realizing systematic structure of trendy intelligent modem operating on any beyond 5G communication systems.

V. CONCLUSION

In this paper, we have provided a comprehensive tutorial of the associated open literature that is related to the entire aspects of the ICS employed in commercial multi-mode mobile station modem operating under 3G, 4G, and 5G 3GPP standard specifications. Furthermore, we also focused our attention to the latest contributions of 5G system exploiting the fundamental characteristics of mmW spectrum.

Firstly, with the help of the proposed taxonomy diagram to summarize a hierarchical structure of the entire ICS flow and three main targets comprising essential ICS procedures in 3G, 4G, and 5G systems as portrayed in Fig. 3, the importance of ICS, contributions of this tutorial, a hierarchical structure of cell search, and an entire IA process of 3GPP systems have been underlined in Section I.

Secondly, we have commenced our discourse by considering evolution of ICS in CDMA systems in Section II. Specifically, in light of the evolution of cdmaOne to WCDMA and TD-SCDMA, we have highlighted the details of the frame structures in both W-CDMA and TD-SCDMA. Subsequently, we proceeded by providing a profound insight on the ICS procedures in these two CDMA systems, which are visualized in Figs. 7 to 11.

Thirdly, in Section III, we proceeded to provide the further evolution of ICS in OFDMA systems, which is the progress from LTE to NR. Then, we analyzed the corresponding synchronization resources and their ICS procedures, which are demystified in Figs. 12 to 23 with comparative analysis of Tables 6 and 7.

Lastly, with the aid of Figs. 24 to 27, Section IV has elucidated that how both ICS and TCS on intelligent modem operate under various spectrum bands. More explicitly, we have articulated that how deep learning aided approaches have been leveraged in three distinct manners, namely (1) the exploitation of intelligent ICS system controller, (2) the use of deep learning driven beam sweeping approach, and (3) suggestion of a feasible structure of the modem aligned with great potentials on the model-driven deep learning aided signal detection schemes. In order to realize further evolutions of NR in terms of ICS, we pondered some interesting factors and challenges, which are classified into three objectives, namely (1) Enhanced ICS by leveraging both beamforming and positioning, (2) Systematic design for an ultra high speed mobility under Hyperloop transportation system, and (3) Deep learning boosted essential cell search parameter optimization.

We have articulated a deeper perception into IA from a system engineering perspective by comparison analysis between multiple RATs. Specifically, we demonstrated direct comparisons for the entire search spaces of the ICS scenarios encompassing W-CDMA, TD-SCDMA, LTE-FDD, TD-LTE, and NR in order to see further in-depth essence on the ICS implementation complexity in Table 3. Subsequently, Tables 4 and 6 condensed the type of sequences exploited in W-CDMA, TD-SCDMA, LTE, and NR, which are closely associated with Sections II and III. Tables 5 and 8 manifested the ICS procedure comparisons utilized in W-CDMA, TD-SCDMA, LTE, and NR, which are detailed in Sections II and III. Table 7 manifested the number of slots and symbols employed in NR radio-frame structure. Throughout a direct comparison of all the ICS flows and their relevant details, we provided a potential on comprehending novel ICS flow of any hybrid system to be pondered in beyond 5G systems. Interestingly, a concrete illustration of the intelligent modem further conjectured artificial intelligence boosted modem's feasibility and its realized case.

Finally, with the aid of Figs. 28 and 29, we have also outlined the main characteristics of all the sequences used

in 3G, 4G, and 5G DL systems in Appendix. Based on our elaborations regarding the above-mentioned, the in-depth understanding of all the ICS scenarios in 3G, 4G, and 5G systems will play a pivotal role in designing the key essence on intelligence based IA optimized for the future multi-mode mobile station modem. By providing the tutorial through two decades of a journey for 3GPP ICS in the perspectives of theory, standard, and implementation, we pave the way for deeper comprehension of intelligence based IA designs, which will become the primary drivers for the forthcoming evolutions of NR and even beyond 5G systems.

APPENDIX
SEQUENCES EXPLOITED IN 3G, 4G, AND 5G DOWNLINK SYSTEMS

In this Appendix, we introduce the key features of the five sequences employed in the 3G, 4G, and 5G DL systems, namely OVSF codes, m-sequence, Gold-sequence, Golay-sequence, and finally ZC sequence. Those sequences exploited for W-CDMA and TD-SCDMA as well as for LTE and NR were summarized in Tables 4 and 6, respectively.

A. SEQUENCES EXPLOITED IN W-CDMA, TD-SCDMA, AND NR

1) OVSF CODE

The OVSF codes are generated from a set of orthogonal Walsh-Hadamard codes, which are defined recursively by a tree structure [28]. These spreading codes have been introduced in 3G systems [40], [41]. An individual code depends on two parameters, namely on the spreading factor representing the length of the code and the code index, which is an integer ranging from 0, 1, …, N-1, where N indicates the spreading factor. The exploitation of the OVSF codes allows the spreading factor to be adapted, while the orthogonality among multiple OVSF codes having different lengths is still preserved. Accordingly, the use of the OVSF codes maintains the orthogonality among the different DL data and control channels allocated to both the same UE and different UEs. Hence, it is also often referred to as a channelization code. In W-CDMA, the lengths of the OVSF code range from 4 to 512. On the other hand, those in TD-SCDMA range from 1 to 16 for accommodating its unique time slot structure [40], [41].

2) M-SEQUENCE

Even though the sets of m-sequences have been adopted by the pan-American 2G mobile communication systems known as cdmaOne (Interim Standard-95), the use of the m-sequences is quite widespread also in 3G and 4G mobile communication systems. According to [64], the m-sequences have also been exploited for the design of NR sequences. Here, we would like to highlight three of their key features as follows:

- Balanced property: The number of ones is only one higher than that of zeros in each m-sequence. Explicitly, when the length of an m-sequence is set to $2^n - 1$, there are $2^{(n-1)}$ ones and $2^{(n-1)} - 1$ zeros in it.
- Shift-and-add property: The modulo-2 operation of an m-sequence and any phase-shifted version of it generates another phase shifted version of the same m-sequence.
- Correlation property: If an m-sequence is compared to any shifted version of the m-sequence chip-by-chip, the number of identical chips minus that of the different ones always leads to -1. This unique property of m-sequences is beneficial for designing direct sequence spread spectrum systems [29], [36], [134], because the property allows for suppressing unsynchronized sequences sufficiently.

3) GOLD-SEQUENCE

Gold-sequences have been utilized in the 3G mobile communication systems for supporting asynchronous W-CDMA systems and later in the 4G systems as well. In asynchronous code division multiple access systems, where the links among UEs and Node-B are not aligned in time, the sum of a large number of Gold sequences leads to multiple access interference, which is near-Gaussian. Under such environments the crosscorrelation peaks in the set are not higher than the minimum possible crosscorrelation peaks between any pair of m-sequences having the same length. The maximum crosscorrelation value is bounded by $2^{(N+1)/2} + 1$, where N represents the length of the linear feedback shift registers used for generating the sequences. Accordingly, the above-mentioned attractive crosscorrelation property is widely exploited in mobile communication systems [36], [134]. Fig. 28 visualizes how the resultant Gold sequence is generated by exploiting a preferred pair of two linear feedback shift registers and their own initial seed values.

4) GENERALIZED HIERARCHICAL GOLAY SEQUENCE

The generalized hierarchical Golay sequence approach adopted in W-CDMA constitutes a combination of the hierarchical structure and the Golay sequence[19] proposed in [31], [40], [135], which leads to an efficient correlator design, while guaranteeing beneficial synchronization properties and detection performance even under high initial frequency offset values spread over the range of $\pm$ 10 kHz [31], [135].

B. A SEQUENCE UTILIZED IN BOTH LTE-FDD AND TD-LTE

1) ZC SEQUENCE

According to [3], ZC sequences have been used in various parts of the LTE systems. In this tutorial, the key features of the ZC sequences have been exploited for detecting the so-called PSS. Their main features are portrayed in Fig. 29, where the characteristics are classified into items 1 to 9 in the dotted circles.

[19]Golay sequences have a low aperiodic autocorrelation sidelobes and there exists a large number of the sequences for a particular code length [30].

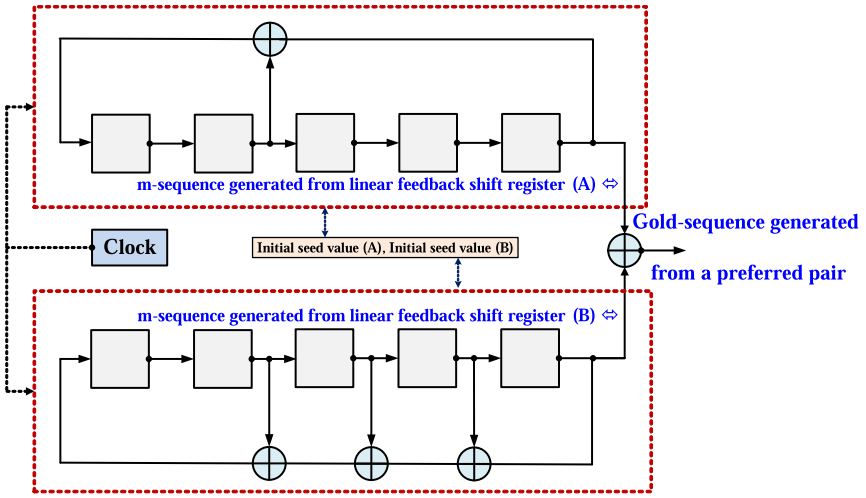

FIGURE 28. A visualization of how Gold sequence is generated, where a preferred pair of two linear feedback shift registers having their own initial seed values becomes core essence on the circuit.

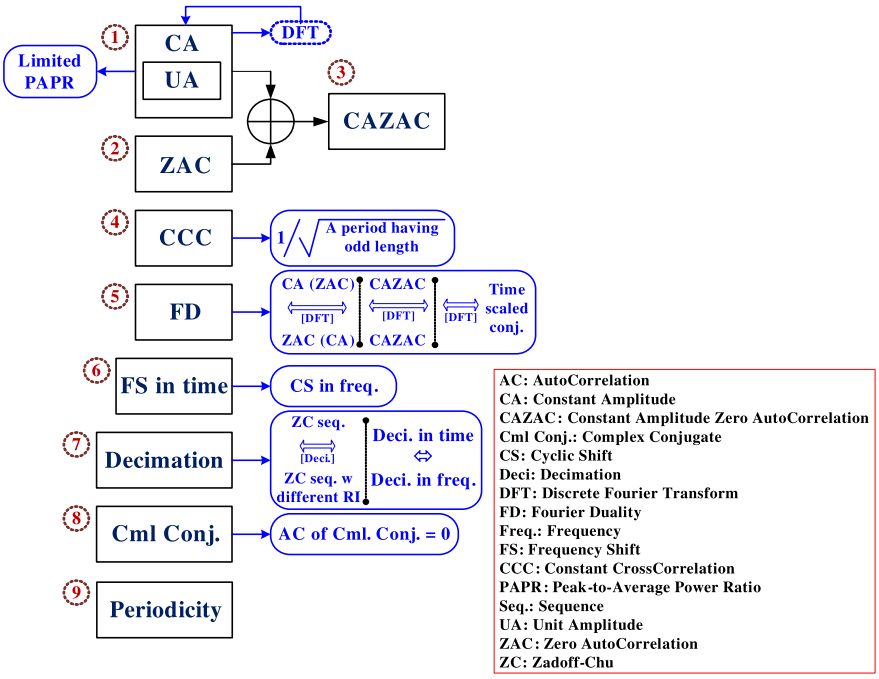

FIGURE 29. Nine main characteristics of Zadoff-Chu sequences being employed for initial cell search procedures.

- Constant amplitude (① in Fig. 29): One of the ZC sequence's beneficial features is that they exhibit constant amplitude, where the ZC sequence may be expressed in an exponential form. The values of the ZC sequence are placed into a circle having unit amplitude. Furthermore, its N_{ZC}-point discrete Fourier Transform also maintains constant amplitude, where N_{ZC} represents an entire period of the ZC sequence. Accordingly, a low peak-to-average power ratio is obtained as a benefit of the constant amplitude property, which leads detector only using phase information and a radio frequency power amplifier [11], [18].
- Zero-autocorrelation (② in Fig. 29): The correlation between a ZC sequence and another sequence generated by arbitrary N shifts of the original sequence leads to a zero value. Explicitly, any cyclic shifted versions of the original sequence are orthogonal to each other. Hence, the simple shift operation of a ZC sequence is capable of generating a sufficiently high number of orthogonal sequences to be exploited. The

sequences have zero-autocorrelation at all non-zero lags [18], [32]–[34].

- Constant-amplitude zero-autocorrelation (③ in Fig. 29): Any sequences exhibiting both the constant amplitude and the zero-autocorrelation properties portrayed above are referred to as constant-amplitude zero-autocorrelation sequences [11], [33], [34]. The ZC sequence is the most popular constant-amplitude zero-autocorrelation sequence used in wireless communication systems.
- Constant crosscorrelation (④ in Fig. 29): The crosscorrelation of two arbitrary ZC sequences based on different root indices is bounded by $1/\sqrt{N_{ZC}}$, where the difference of any two indices is relative prime to N_{ZC}. Therefore, the resultant crosscorrelation value at all lags becomes constant [34].
- Fourier transform duality (⑤ in Fig. 29): It is noteworthy that the zero-autocorrelation found in the time-domain corresponds to having a constant frequency-domain representation. Therefore, the discrete Fourier transformed pair of a constant-amplitude zero-autocorrelation sequence is another constant-amplitude zero-autocorrelation sequence [34], [35]. The discrete Fourier transformed pair of a ZC sequence is a time-scaled conjugate version of the sequence multiplied by a constant factor of N_{ZC}, where N_{ZC} is set to an odd prime [35]. This property is also often referred to as Fourier transform duality, which is exploited for devising efficient PSS detection in the time-domain.
- Frequency shift (⑥ in Fig. 29): An integer amount of frequency shift in the time-domain corresponds to a cyclic shift in the frequency domain. In this situation, the constant-amplitude zero-autocorrelation property is retained, where N_{ZC} is set to an odd prime [34].
- Decimation (⑦ in Fig. 29): The decimated version of a ZC sequence is another ZC sequence [33]. Furthermore, decimation in the time domain leads to that in the frequency domain [34].
- Complex conjugation (⑧ in Fig. 29): The autocorrelation of a complex conjugate version of a ZC sequence also exhibits a zero-autocorrelation value [34].
- Periodicity (⑨ in Fig. 29): If the sequence-length N is set to an odd value, the ZC sequence having the period of N_{ZC} is periodic, where N_{ZC} is set to an odd prime [32].

REFERENCES

[1] *Physical Channels and Mapping of Transport Channels onto Physical Channels (FDD)*, Standard 3GPP TS 25.211 v12.0.0, 2014.
[2] *Physical Channels and Mapping of Transport Channels onto Physical Channels (TDD)*, Standard 3GPP TS 25.221 v14.0.0, 2017.
[3] *Physical Channels and Modulation*, Standard 3GPP TS 36.211 v12.6.0, 2015.
[4] *Study on New Radio (NR) Access Technology; Physical Layer Aspects*, Standard 3GPP TR 38.802 v2.0.0, 2017.
[5] *NR; Physical Layer; General Description*, Standard 3GPP TS 38.201 v15.0.0, 2017.
[6] *NR; Physical Channels and Modulation*, Standard 3GPP TS 38.211 v15.5.0, 2019.
[7] *Making 5G NR a Reality*, Qualcomm Research Document, Qualcomm Incorporated, San Diego, CA, USA, Dec. 2016, pp. 1–26.
[8] *NR; Physical Layer Procedures for Control*, Standard 3GPP TS 38.213 v15.5.0, 2019.
[9] S. Won and S. W. Choi, "Three decades of 3GPP target cell search through 3G, 4G, and 5G," *IEEE Access*, vol. 8, pp. 116914–116960, 2020.
[10] S. Won and L. Hanzo, "Initial synchronisation of wideband and UWB direct sequence systems: Single- and multiple-antenna aided solutions," *IEEE Commun. Surveys Tuts.*, vol. 14, no. 1, pp. 87–108, 1st Quart., 2012.
[11] Y. Tsai, G. Zhang, D. Grieco, F. Ozluturk, and X. Wang, "Cell search in 3GPP long term evolution systems," *IEEE Veh. Technol. Mag.*, vol. 2, no. 2, pp. 23–29, Jun. 2007.
[12] S. H. Won and L. Hanzo, "Initial and post-initial code acquisition in the noncoherent multiple-input/multiple-output-Aided DS-CDMA downlink," *IEEE Trans. Veh. Technol.*, vol. 58, no. 5, pp. 2322–2330, Oct. 2009.
[13] S. Won and L. Hanzo, "Synchronization of noncoherent MIMO systems: Synchronization issues," *IEEE Veh. Technol. Mag.*, vol. 7, no. 4, pp. 95–103, Dec. 2012.
[14] S. Won and L. Hanzo, "Synchronization issues in relay-aided cooperative MIMO networks," *IEEE Wireless Commun.*, vol. 21, no. 5, pp. 41–51, Oct. 2014.
[15] *Physical Layer Procedures (FDD)*, Standard 3GPP TS 25.214 v12.3.0, 2015.
[16] *Physical Layer Procedures (TDD)*, Standard 3GPP TS 25.224 v13.0.0, 2015.
[17] K. Manolakis, D. M. G. Estevez, V. Jungnickel, W. Xu, and C. Drewes, "A closed concept for synchronization and cell search in 3GPP LTE systems," in *Proc. IEEE Wireless Commun. Netw. Conf.*, Apr. 2009, pp. 1–6, doi: 10.1109/WCNC.2009.4917491.
[18] *1MA150: Cell Search and Cell Selection in UMTS LTE*, Rohde & Schwarz Application Note, Rohde & Schwarz, Munich, Germany, 2009, pp. 1–40.
[19] *Study on New Radio (NR) Access Technology*, Standard 3GPP TR 38.912 v16.0.0, 2020.
[20] Y. Shen, T. Luo, and M. Z. Win, "Neighboring cell search for LTE systems," *IEEE Trans. Wireless Commun.*, vol. 11, no. 3, pp. 908–919, Mar. 2012.
[21] Y.-P.-E. Wang and T. Ottosson, "Cell search in W-CDMA," *IEEE J. Sel. Areas Commun.*, vol. 18, no. 8, pp. 1470–1482, Aug. 2000.
[22] M. K. Song and V. K. Bhargava, "Performance analysis of cell search in W-CDMA systems over Rayleigh fading channels," *IEEE Trans. Veh. Technol.*, vol. 51, no. 4, pp. 749–759, Jul. 2002.
[23] R.-M. Peng, Z.-T. Hao, and Y. Mei, "A frequency estimation for TD-SCDMA UE based on phase difference," *Int. J. Comput. Netw. Inf. Secur.*, vol. 3, no. 3, pp. 55–61, Apr. 2011.
[24] Z. Jiang, L. Tian, J. Liu, and W. Xu, "Practical carrier frequency offset estimation schemes for TD-SCDMA scanning receiver," in *Proc. Int. Conf. Microw. Millim. Wave Technol. (ICMMT)*, May 2012, pp. 1–4, doi: 10.1109/ICMMT.2012.6230052.
[25] V. Raghavan, J. Cezanne, S. Subramanian, A. Sampath, and O. Koymen, "Beamforming tradeoffs for initial UE discovery in millimeter-wave MIMO systems," *IEEE J. Sel. Topics Signal Process.*, vol. 10, no. 3, pp. 543–559, Apr. 2016.
[26] H. Soleimani, R. Parada, S. Tomasin, and M. Zorzi, "Fast initial access for mmWave 5G systems with hybrid beamforming using online statistics learning," *IEEE Commun. Mag.*, vol. 57, no. 9, pp. 132–137, Sep. 2019.
[27] A. Omri, M. Shaqfeh, A. Ali, and H. Alnuweiri, "Synchronization procedure in 5G NR systems," *IEEE Access*, vol. 7, pp. 41286–41295, 2019.
[28] F. Adachi, M. Sawahashi, and K. Okawa, "Tree-structured generation of orthogonal spreading codes with different lengths for forward link of DS-CDMA mobile radio," *Electron. Lett.*, vol. 33, no. 1, pp. 27–28, Jan. 1997.
[29] A. Viterbi, *CDMA: Principles of Spread Spectrum Communication: Chapter 3*. Reading, MA, USA: Addison-Wesley, 1995.
[30] *Reduced Complexity Primary and Secondary Synchronisation Codes With Good Aperiodic Correlation Properties for the WCDMA System*, document R1-99373, Texas Instruments, 1999, pp. 1–14.
[31] *Generalised Hierarchical Golay Sequence for PSC With Low Complexity Correlation Using Pruned Efficient Golay Correlators*, document R1-99567, Siemens and Texas Instruments, 1999, pp. 1–6.

[32] B. M. Popovic, "Generalized chirp-like polyphase sequences with optimum correlation properties," *IEEE Trans. Inf. Theory*, vol. 38, no. 4, pp. 1406–1409, Jul. 1992.
[33] S. Budišin, "Decimation generator of Zadoff-Chu sequences," in *Proc. Int. Conf. Sequences Appl.*, 2010, pp. 30–40.
[34] S. Budišin and P. Spasojević, "Björck sequence sets," *Electron. Lett.*, vol. 47, no. 8, pp. 491–493, 2011.
[35] S. Beyme and C. Leung, "Efficient computation of DFT of Zadoff-Chu sequences," *Electron. Lett.*, vol. 45, no. 9, pp. 461–463, Apr. 2009.
[36] J. Lee and L. Miller, *CDMA Systems Engineering Handbook: Chapters 4, 5, and 6*. London, U.K.: Artect House, 1998.
[37] *Radio Frequency (RF) System Scenarios*, Standard 3GPP TR 25.942 v9.0.0, 2009.
[38] *User Equipment (UE) Radio Transmission and Reception (FDD)*, Standard 3GPP TS 25.101 v16.1.0, 2019.
[39] *User Equipment (UE) Radio Transmission and Reception (TDD)*, Standard 3GPP TS 25.102 v15.0.0, 2018.
[40] *Spreading and Modulation (FDD)*, Standard 3GPP TS 25.213 v12.0.0, 2014.
[41] *Spreading and Modulation (TDD)*, Standard 3GPP TS 25.223 v12.0.0, 2014.
[42] *Physical Layer Procedures*, Standard 3GPP TS 36.213 v16.5.0, 2021.
[43] *Physical Channels and Mapping of Transport Channels onto Physical Channels (TDD)*, Standard 3GPP TS 25.221 v9.0.0, 2009.
[44] J. Dong and X. Wu, "Research on TD-SCDMA network planning for data services based on HSDPA," in *Proc. IEEE Int. Conf. Commun. Technol. Appl.*, Oct. 2009, pp. 251–254.
[45] S. Won and L. Hanzo, "Non-coherent and differentially coherent code acquisition in MIMO assisted DS-CDMA multi-path downlink scenarios," *IEEE Trans. Wireless Commun.*, vol. 7, no. 5, pp. 1585–1593, May 2008.
[46] S. Won and L. Hanzo, "Non-coherent code acquisition in the multiple transmit/multiple receive antenna aided single- and multi-carrier DS-CDMA downlink," *IEEE Trans. Wireless Commun.*, vol. 6, no. 11, pp. 3864–3869, Nov. 2007.
[47] *Radio Resource Control (RRC)*, Standard 3GPP TS 25.331 v12.6.0, 2015.
[48] L. Meng, J. Bao, H. Xu, J. Hua, and X. Xu, "A coarse cell search scheme of TD-SCDMA systems," in *Proc. 11th IEEE Int. Conf. Commun. Technol.*, Nov. 2008, pp. 1196–1199.
[49] X. Wang, T. Song, and L. Shen, "A novel power ratio detection for frame synchronization in TD-SCDMA systems," in *Proc. IEEE 12th Int. Conf. Commun. Technol.*, Nov. 2010, pp. 5–8.
[50] M. Shim, S. Won, S. W. Choi, J. Moon and J. Hwang, *Method and Apparatus for Acquiring Synchronization in Code Division Multiple Access System*, document 20140254580, 2014.
[51] S. W. Choi, S. Won, M. Shim, J. Moon and J. Hwang, *Multi-Path Search Apparatus and Method in a Wireless Communication System*, document 20150029878, 2015.
[52] M. Shim, S. Won, S. W. Choi, J. Moon and J. Hwang, *Method and Apparatus for Acquiring Synchronization in Code Division Multiple Access System*, document 20140254562, 2014.
[53] emphStudy on New Radio (NR) Access Technology; Radio Interface Protocol Aspects, Standard 3GPP TR 38.804 v14.0.0, 2017.
[54] *Study on Scenarios and Requirements for Next Generation Access Technologies*, Standard 3GPP TR 38.913 v0.4.0, 2016.
[55] 5G Americas, "Wireless technology evolution towards 5G: 3GPP release 13 to release 15 and beyond, chap 5.1. 5G RAN," White Paper, Feb. 2017, pp. 137–152.
[56] *Study on Channel Model for Frequency Spectrum Above 6 GHz*, Standard 3GPP TR 38.900 v14.2.0, 2016.
[57] *On System Design for Multiple Numerologies—Initial Access*, document R1-167258, Nokia and Alcatel-Lucent Shanghai Bell, 2016, pp. 1–6.
[58] *Extending LTE Advanced to Unlicensed Spectrum*, Qualcomm Research Document, Qualcomm Incorporated, San Diego, CA, USA, 2013, pp. 1–12.
[59] Nokia Networks, "LTE for unlicensed spectrum," White Paper, 2014, pp. 1–12.
[60] *LTE in Unlicensed Spectrum: Harmonious Coexistence with Wi-Fi*, Qualcomm Research Document, Qualcomm Incorporated, San Diego, CA, USA, 2014, pp. 1–19.
[61] *LTE-U Technical Report Coexistence Study for LTE-U SDL*, document LTE-U Forum, v(1.0.0), 2015, pp. 1–52.
[62] *LTE-U CSAT Procedure*, document LTE-U Forum, v(1.0.0), 2015, pp. 1–7.
[63] *Study on Licensed-Assisted Access to Unlicensed Spectrum*, Standard 3GPP TR 36.889 v13.0.0, 2015.
[64] *NR PSS and SSS Design*, document R1-1710501, Intel Corporation, 2017, pp. 1–4.
[65] *3GPP TSG RAN WG1 Meeting #89: RAN1 Chairman's Notes*, Standard 3GPP, 2017, pp. 1–73.
[66] *Evaluation Results for NR-SSS Sequences*, document R1-1709595, Samsung, 2017, pp. 1–4.
[67] *WF on NR-SS Sequence Design*, document R1-1709220, NTT Docomo, Inc. and ZTE, 2017, pp. 1–6.
[68] *SS Block Composition and SS Burst Set Composition*, document R1-1708720, Ericsson, 2017, pp. 1–8.
[69] *Remaining Details for Synchronization Signals*, document R1-1708160, Huawei and HiSilicon, 2017, pp. 1–16.
[70] P. Wang and F. Berggren, "Secondary synchronization signal in 5G new radio," in *Proc. IEEE Int. Conf. Commun. (ICC)*, May 2018, pp. 1–6, doi: 10.1109/ICC.2018.8422145.
[71] Motorola, "TD-LTE: Exciting alternative, global momentum," White Paper, 2010, pp. 1–12.
[72] N. Noguchi, S. Nagata, and M. Sawahashi, "Fast cell search method using PSS and SSS based on frequency offset estimation for heterogeneous networks with separate frequency spectrum," in *Proc. IEEE 81st Veh. Technol. Conf. (VTC Spring)*, May 2015, pp. 1–6, doi: 10.1109/VTC-Spring.2015.7145838.
[73] K. Takeda, H. Harada, R. Osawa, Y. Kakishima, L. Wang, and R. Wang, "NR physical layer specifications in 5G," *NTT Docomo Tech. J.*, vol. 20, no. 3, pp. 49–61, Jan. 2019.
[74] Y. Sano, S. Okuyama, N. Iizasa, T. Takada, K. Ando, and N. Fujimura, "5G radio performance and radio resource management specifications," *NTT Docomo Tech. J.*, vol. 20, no. 3, pp. 79–84, Jan. 2019.
[75] *Discussion on Initial Access and Mobility for NR*, document R1-167379, NTT Docomo, Inc., 2016, pp. 1–10.
[76] *Numerology for New Radio Interface*, document R1-162386, Intel Corporation, 2016, pp. 1–6.
[77] A. Zaidi, R. Baldemair, M. Andersson, S. Faxér, V. Molés-Cases, and Z. Wang, "5G new radio: Designing for the future," *Ericsson Techn. Rev.*, vol. 7, no. 1, Jun. 2017, pp. 1–14.
[78] *User Equipment (UE) Radio Transmission and Reception; Part 1: Range 1 Standalone*, Standard 3GPP TS 38.101-1 v15.5.0, 2019.
[79] *User Equipment (UE) Radio Transmission and Reception; Part 2: Range 2 Standalone*, Standard 3GPP TS 38.101-2 v15.5.0, 2019.
[80] *NR; NR and NG-RAN Overall Description*, Standard 3GPP TS 38.300 v15.5.0, 2019.
[81] J.-I. Kim, J.-S. Han, H.-J. Roh, and H.-J. Choi, "SSS detection method for initial cell search in 3GPP LTE FDD/TDD dual mode receiver," in *Proc. 9th Int. Symp. Commun. Inf. Technol.*, Sep. 2009, pp. 199–203.
[82] A. Golnari, M. Shabany, A. Nezamalhosseini, and G. Gulak, "Design and implementation of time and frequency synchronization in LTE," *IEEE Trans. Very Large Scale Integr. (VLSI) Syst.*, vol. 23, no. 12, pp. 2970–2982, Dec. 2015.
[83] M. Morelli and M. Moretti, "A robust maximum likelihood scheme for PSS detection and integer frequency offset recovery in LTE systems," *IEEE Trans. Wireless Commun.*, vol. 15, no. 2, pp. 1353–1363, Feb. 2016.
[84] Google. (2015). *Project Fi Automatically Connects to the Best Network*. [Online] Available: https://fi.google.com/about/network/
[85] M. Giordani, M. Mezzavilla, and M. Zorzi, "Initial access in 5G mmWave cellular networks," *IEEE Commun. Mag.*, vol. 54, no. 11, pp. 40–47, Nov. 2016.
[86] M. Giordani, M. Polese, A. Roy, D. Castor, and M. Zorzi, "A tutorial on beam management for 3GPP NR at mmWave frequencies," *IEEE Commun. Surveys Tuts.*, vol. 21, no. 1, pp. 173–196, 1st Quart., 2019.
[87] C. Jeong, J. Park, and H. Yu, "Random access in millimeter-wave beamforming cellular networks: Issues and approaches," *IEEE Commun. Mag.*, vol. 53, no. 1, pp. 180–815, Jan. 2015.

[88] I. Aykin and M. Krunz, "Efficient beam sweeping algorithms and initial access protocols for millimeter-wave networks," *IEEE Trans. Wireless Commun.*, vol. 19, no. 4, pp. 2504–2514, Apr. 2020.
[89] A. Abdelreheem, E. M. Mohamed, and H. Esmaiel, "Location-based millimeter wave multi-level beamforming using compressive sensing," *IEEE Commun. Lett.*, vol. 22, no. 1, pp. 185–188, Jan. 2018.
[90] *Reply LS on NR Minimum Carrier Bandwidth*, document R4-1709187, Dish, 2017, pp. 1–2.
[91] *Reply LS on NR Minimum Carrier Bandwidth and SS Block Numerology*, document R1-1719165, Ericsson, 2017, p. 1.
[92] *Initial Access Consideration for Millimeter Wave Systems*, document R1-166384, Qualcomm Incorporated, 2016, pp. 1–4.
[93] S. Han, C.-L. I, Z. Xu, and C. Rowell, "Large-scale antenna systems with hybrid analog and digital beamforming for millimeter wave 5G," *IEEE Commun. Mag.*, vol. 53, no. 1, pp. 186–194, Jan. 2015.
[94] *Initial Access Consideration for Millimeter Wave Systems*, document R1-166384, ZTE, 2016, pp. 1–4.
[95] *Beam Sweeping for Initial Access*, document R1-166947, ETRI, 2016, pp. 1–4.
[96] *Spectrum for 4G and 5G*, Qualcomm Research Document, Qualcomm Incorporated, San Diego, CA, USA, 2017, pp. 1–32.
[97] S.-R. Yang and Y.-B. Lin, "Modeling UMTS discontinuous reception mechanism," *IEEE Trans. Wireless Commun.*, vol. 4, no. 1, pp. 312–319, Jan. 2005.
[98] P. H. J. Perala, A. Barbuzzi, G. Boggia, and K. Pentikousis, "Theory and practice of RRC state transitions in UMTS networks," in *Proc. IEEE Globecom Workshops*, Nov. 2009, pp. 1–6, doi: 10.1109/GLOCOMW.2009.5360763.
[99] *Radio Resource Control (RRC)*, Standard 3GPP TS 36.331 v12.6.0, 2015.
[100] *NR-Radio Resource Control (RRC) Protocol Specification*, Standard 3GPP TS 38.331 v15.5.0, 2019.
[101] C. Jiang, H. Zhang, Y. Ren, Z. Han, K.-C. Chen, and L. Hanzo, "Machine learning paradigms for next-generation wireless networks," *IEEE Wireless Commun.*, vol. 24, no. 2, pp. 98–105, Apr. 2017.
[102] C. Zhang, P. Patras, and H. Haddadi, "Deep learning in mobile and wireless networking: A survey," *IEEE Commun. Surveys Tuts.*, vol. 21, no. 3, pp. 2224–2287, 3rd Quart., 2019.
[103] M. Chen, U. Challita, W. Saad, C. Yin, and M. Debbah, "Artificial neural networks-based machine learning for wireless networks: A tutorial," *IEEE Commun. Surveys Tuts.*, vol. 21, no. 4, pp. 3039–3071, 4th Quart., 2019.
[104] N. C. Luong, D. T. Hoang, S. Gong, D. Niyato, P. Wang, Y.-C. Liang, and D. I. Kim, "Applications of deep reinforcement learning in communications and networking: A survey," *IEEE Commun. Surveys Tuts.*, vol. 21, no. 4, pp. 3133–3174, 4th Quart., 2019.
[105] Z. Xiong, Y. Zhang, D. Niyato, R. Deng, P. Wang, and L.-C. Wang, "Deep reinforcement learning for mobile 5G and beyond: Fundamentals, applications, and challenges," *IEEE Veh. Technol. Mag.*, vol. 14, no. 2, pp. 44–52, Jun. 2019.
[106] H. Song, J. Bai, Y. Yi, J. Wu, and L. Liu, "Artificial intelligence enabled Internet of Things: Network architecture and spectrum access," *IEEE Comput. Intell. Mag.*, vol. 15, no. 1, pp. 44–51, Feb. 2020.
[107] J. Wang, C. Jiang, H. Zhang, Y. Ren, K.-C. Chen, and L. Hanzo, "Thirty years of machine learning: The road to Pareto-optimal wireless networks," *IEEE Commun. Surveys Tuts.*, vol. 22, no. 3, pp. 1472–1514, 3rd Quart., 2020.
[108] Z. Qin, H. Ye, G. Y. Li, and B.-H.-F. Juang, "Deep learning in physical layer communications," *IEEE Wireless Commun.*, vol. 26, no. 2, pp. 93–99, Apr. 2019.
[109] D. Gunduz, P. de Kerret, N. Sidiroupoulos, D. Gesbert, C. Murthy, and M. van der Schaar, "Machine learning in the air," *IEEE J. Sel. Areas Commun.*, vol. 37, no. 10, pp. 2184–2199, Oct. 2019.
[110] H. He, C.-K. Wen, S. Jin, and G. Y. Li, "Model-driven deep learning for MIMO detection," *IEEE Trans. Signal Process.*, vol. 68, pp. 1702–1715, Feb. 2020.
[111] M. S. Sim, Y.-G. Lim, S. H. Park, L. Dai, and C.-B. Chae, "Deep learning-based mmWave beam selection for 5G NR/6G with sub-6 GHz channel information: Algorithms and prototype validation," *IEEE Access*, vol. 8, pp. 51634–51646, 2020.
[112] T. S. Cousik, V. K. Shah, T. Erpek, Y. E. Sagduyu, and J. H. Reed, "Deep learning for fast and reliable initial access in AI-driven 6G mmWave networks," 2021, *arXiv:2101.01847*. [Online]. Available: http://arxiv.org/abs/2101.01847
[113] I. Ismath, K. B. S. Manosha, S. Ali, N. Rajatheva, and M. Latva-Aho, "Deep contextual bandits for fast initial access in mmWave based user-centric ultra-dense networks," 2020, *arXiv:2009.06974*. [Online]. Available: http://arxiv.org/abs/2009.06974
[114] *NR; Physical Measurements*, Standard 3GPP TS 38.215 v16.4.0, 2020.
[115] R. M. Dreifuerst, R. W. Heath, M. N. Kulkarni, and J. Charlie, "Deep learning-based carrier frequency offset estimation with one-bit ADCs," in *Proc. IEEE 21st Int. Workshop Signal Process. Adv. Wireless Commun. (SPAWC)*, May 2020, pp. 1–5, doi: 10.1109/SPAWC48557.2020.9154214.
[116] Y. Wang, A. Klautau, M. Ribero, A. C. K. Soong, and R. W. Heath, "MmWave vehicular beam selection with situational awareness using machine learning," *IEEE Access*, vol. 7, pp. 87479–87493, 2019.
[117] N. J. Myers, Y. Wang, N. Gonzalez-Prelcic, and R. W. Heath, "Deep learning-based beam alignment in mmwave vehicular networks," in *Proc. IEEE Int. Conf. Acoust., Speech Signal Process. (ICASSP)*, May 2020, pp. 8569–8573.
[118] H. He, S. Jin, C.-K. Wen, F. Gao, G. Y. Li, and Z. Xu, "Model-driven deep learning for physical layer communications," *IEEE Wireless Commun.*, vol. 26, no. 5, pp. 77–83, Oct. 2019.
[119] E. Bjornson and P. Giselsson, "Two applications of deep learning in the physical layer of communication systems [lecture notes]," *IEEE Signal Process. Mag.*, vol. 37, no. 5, pp. 134–140, Sep. 2020.
[120] H. Huang, S. Guo, G. Gui, Z. Yang, J. Zhang, H. Sari, and F. Adachi, "Deep learning for physical-layer 5G wireless techniques: Opportunities, challenges and solutions," *IEEE Wireless Commun.*, vol. 27, no. 1, pp. 214–222, Feb. 2020.
[121] Samsung. (2020). *BLOG: Create Your World With the Exynos 990 Processor*. [Online]. Available: https://www.samsung.com/semiconductor/minisite/exynos/newsroom/blog/create-your-world-with-the-exynos-990-processor/
[122] Qualcomm Incorporated. (2020). *Qualcomm Developer Network: Artificial Intelligence*. [Online]. Available: https://https://developer.qualcomm.com/solutions/artificial-intelligence
[123] Google Cloud. (2017). *An in-Depth Look at Google's First Tensor Processing Unit (TPU)*. [Online]. Available: https://cloud.google.com/blog/products/gcp/an-in-depth-look-at-googles-first-tensor-processing-unit-tpu
[124] *6G The Next Hyper-Connected Experiences for All*, Samsung Research White Paper, Samsung Research, Bengaluru, India, 2020, pp. 1–42.
[125] *Stage 2 Functional Specification of User Equipment (UE) Positioning in NG-RAN*, Standard 3GPP TS 38.305 v15.3.0, 2019.
[126] K. Radnosrati, C. Fritsche, F. Gunnarsson, F. Gustafsson, and G. Hendeby, "Localization in 3GPP LTE based on one RTT and one TDOA observation," *IEEE Trans. Veh. Technol.*, vol. 69, no. 3, pp. 3399–3411, Mar. 2020.
[127] K. Xu, Z. Shen, Y. Wang, and X. Xia, "Location-aided mMIMO channel tracking and hybrid beamforming for high-speed railway communications: An angle-domain approach," *IEEE Syst. J.*, vol. 14, no. 1, pp. 93–104, Mar. 2020.
[128] *Study on Performance Enhancements for High Speed Scenario in LTE*, Standard 3GPP TR 36.878 v13.0.0, 2016.
[129] A. S. Abdelrahman, J. Sayeed, and M. Z. Youssef, "Hyperloop transportation system: Analysis, design, control, and implementation," *IEEE Trans. Ind. Electron.*, vol. 65, no. 9, pp. 7427–7436, Sep. 2018.
[130] S. Choi, C. Lee, J. Jo, J. Choe, Y. Oh, K. Lee, and J. Lim, "Subsonic linear synchronous motors using superconducting magnets for the hyperloop," *Energies*, vol. 12, no. 24, pp. 1–18, Dec. 2019.
[131] J.-M. Jo, S. Y. Lee, K. Lee, Y. J. Oh, S. Y. Choi, C.-Y. Lee, and K. Lee, "A position estimator using Kalman filter with a data rejection filter for a long-stator linear synchronous motor of maglev," *IEEE Access*, vol. 8, pp. 52443–52451, 2020.
[132] R. Walker, "Hyperloop: Cutting through the hype," White Paper, Jun. 2018, pp. 1–19.
[133] K. S. Kim, S. W. Kim, Y. S. Cho, and J. Y. Ahn, "Synchronization and cell-search technique using preamble for OFDM cellular systems," *IEEE Trans. Veh. Technol.*, vol. 56, no. 6, pp. 3469–3485, Nov. 2007.
[134] R. Ziemer, R. Peterson, and D. Borth, *CDMA Systems Engineering Handbook: Chapter 3*. Upper Saddle River, NJ, USA: Prentice-Hall, 1995.
[135] *Text Proposal for Generalised Hierarchical Golay Sequence for PSC With Low Complexity Correlation Using Pruned Efficient Golay Correlators*, document R1-99568, Siemens and Texas Instruments, 1999, pp. 1–2.

SEUNGHWAN WON (Senior Member, IEEE) received the B.S. and M.S. degrees in radio science and engineering from Korea University, Seoul, Republic of Korea, in 1999 and 2001, respectively, and the Ph.D. degree from the Communications Research Group, School of Electronics and Computer Science, University of Southampton, U.K. Upon completing his Ph.D. degree, he returned to his native Republic of Korea and joined Samsung. Then, he was involved in designing commercial mobile station modem. He was a Research Engineer with the Mobile Communication Technology Research Laboratory, LG Electronics Research and Development, from January 2001 to September 2004. In 2013, he was appointed as an Associate Professor. He is currently teaching and conducting research with the University of Southampton Malaysia in Johor, Malaysia. He published a host of articles in these research fields and secured 20 U.S. and lots of Korean patents. His major research interests include encompass diverse deep learning aided mobile communications based on synchronization, multi-user MIMO and hybrid beamforming in mmW mobile communications, the IoT and UAV mobile communications, and intelligent multi-copter design. He was a recipient of the 2004 State Scholarship of the Information and Telecommunication National Scholarship Program, Ministry of Information and Communication (MIC), Republic of Korea.

SANG WON CHOI (Member, IEEE) received the M.S. and Ph.D. degrees in electric and electrical engineering and computer science from KAIST, Daejeon, South Korea, in 2004 and 2010, respectively. He was a Senior Research Engineer involved in the development of multimode modem chips, from 2010 to 2014. From 2014 to 2020, he was a Senior Researcher with the Train Control and Communication Research Team, Korea Railroad Research Institute. Since September 2020, he is currently an Assistant Professor with the Department of Electronic Engineering, Kyonggi University, South Korea. His research interests include mission-critical communications, mobile communication, communication signal processing, multi-user information theory, and machine learning. He was a recipient of the Silver Prize with the Samsung Humantech Paper Contest, in 2010.